LA-UR-97-4620

TITLE: PYROCLASTIC SURGES AND COMPRESSIBLE TWO-PHASE FLOW

AUTHORS: Kenneth H. Wohletz

SUBMITTED TO: The Physics of Explosive Volcanism
Elsevier Science Publications

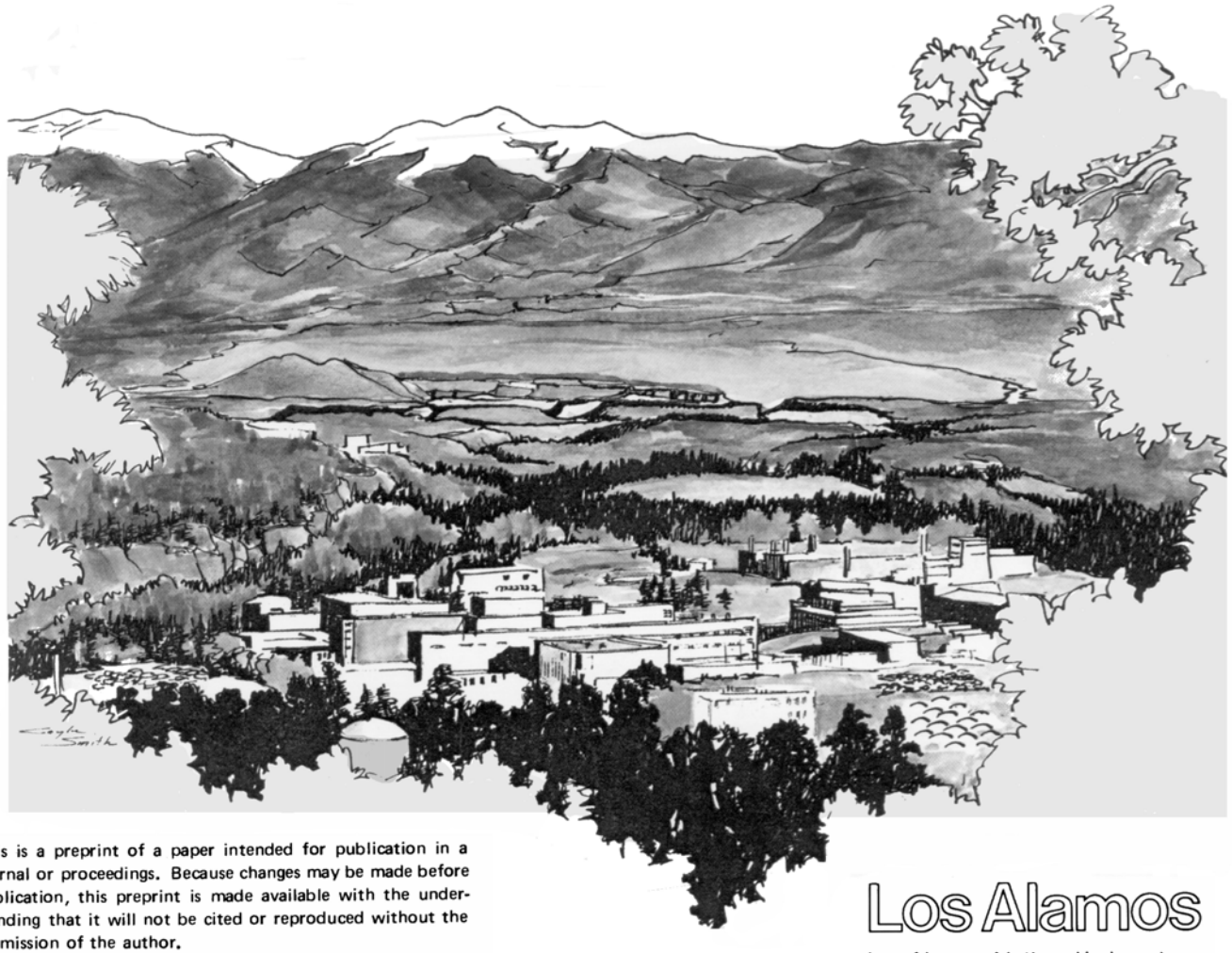

Los Alamos
Los Alamos National Laboratory
Los Alamos, New Mexico 87545

Pyroclastic Surges and Compressible Two-Phase Flow

Kenneth H. Wohletz
Los Alamos National Laboratory
Los Alamos, New Mexico USA

Abstract

Although constituting little of the geological record, pyroclastic surges are now recognized as products of some of the most hazardous eruptive manifestations. They were initially defined by analogy to the base surge that accompanies large surface explosions, common to the atmospheric testing of nuclear weapons in the 1950s. Their textural similarity to high-flow-regime aqueous sediments led early workers to interpret their origins by analogy to submarine density currents and fluvial sedimentation. However recognition of the same deposits left around the craters of large nuclear and non-nuclear explosions attests to their origin by the high-speed flow of a gas and particulate mixture under the influence of propagating shock waves. Such a two-phase compressible flow regime is similar to conventional sediments only to the extent that one can make an analogy between the Froude and Mach numbers. In survey of recent terminology, pyroclastic surges are defined as lean, turbulent gas and particulate flows as opposed to dense, laminar transport displayed by pyroclastic flows. This conventional jargon is incorrect, considering the wide range of bedforms left by pyroclastic surges, notwithstanding the problem of distinguishing between transport and depositional regimes, phenomena that have never been monitored nor closely observed. Considering shock-tube and wind-tunnel experiments with dusty gases and the ever developing theory of multiphase compressible flow, surges are predicted to both modify and be modified by the substrate over which they travel, a hypothesis that field work readily supports. However great their complexity, the careful mapping and analysis of pyroclastic surges is paramount in evaluating volcanic risk as well as understanding the formation of economic ore deposits and geothermal systems.

Notation

A	particle surface area
a	surge acceleration
a_0	gas sound speed
C_d	interphase drag coefficient
C_p	constant pressure heat capacity
C_{pg}	gas constant pressure heat capacity
C_s	particle heat capacity
C_{vg}	gas constant volume heat capacity
c_0	pure gas reference sound speed
c^*	bulk sound speed
c_0^*	bulk sound speed at rest
c_1^*	bulk sound speed while moving
d	total thickness of surge cloud
E	internal energy
E_0	unshocked internal energy
E_1	shocked internal energy
F	interphase momentum exchange
g	gravitational acceleration
h	height
h_c	column collapse height
J_d	density source/sink
J_e	latent heat source/sink
K	perturbation solution constant
K_1	dispersion coefficient
K_2	attenuation coefficient
k	von Kármán constant
k_t	thermal conductivity coefficient
L	characteristic length scale
ℓ	particle diameter
M	Mach number
$\mathbf{M}$	Total mass per size interval
M^*	particle to gas mass ratio
m	mass
m_g	mass of gas
m_p	mass of particles
m_1	reference particle mass
m'	parental particle mass
N	Brunt-Väisälä frequency
N_T	total number of particles
$n(m)$	number of particles of mass m
P_a	particle cross-sectional perimeter
p	pressure
p_0	unshocked pressure
p_1	shocked pressure
Pn	average Rouse number
Q	particle-to-gas heat exchange
Q_g	interphase heat transfer coefficient
R_g	gas constant
R_m	water/magma mass ratio
R^*	bulk gas constant
r	surge radial distance
r_f	final surge runout distance
Re	Reynolds number
Re^*	bulk Reynolds number
Re^{**}	effective bulk Reynolds number
S	particle shape factor = $P_a^2/(4\pi A)$
T	temperature
T_0	unshocked temperature
T_1	shocked temperature
T_g	gas temperature
T_p	particle temperature
t	time
t_t	thermal relaxation time
t_v	velocity relaxation time
U	shock velocity
$\mathbf{u}$	velocity vector
u	velocity
u_g	gas velocity
u_p	particle velocity
u_x	velocity parallel to substrate
u_y	velocity perpendicular to substrate
u^*	shear velocity
V	surge volume
V_p	particle volume
V_g	gas volume
v_0	surge initial velocity
w_i	particle class settling velocity
W	SFT normalization constant
W_S	SFT shape normalization constant
W_ρ	SFT density normalization constant
x	distance
x'	source location
Y	shock strength
y_h	obstacle height scale or depth of specified density increment

β	isentropic coefficient
β*	bulk isentropic coefficient
δ	boundary layer thickness
ϕ	logarithmic grain-size = $-\log_2$(mm)
γ	SFT fragmentation exponent
γ_S	SFT shape exponent
γ_ρ	SFT density exponent
κ	thermodynamic constant = pV^β
λ	characteristic topographic wavelength
λ_t	thermal relaxation wavelength (distance)
λ_v	velocity relaxation wavelength (distance)
η	dimensionless height
η_0	reference level dimensionless height
μ	dynamic viscosity
μ*	collision viscosity
μ**	effective bulk dynamic viscosity
ν	kinematic viscosity
ν*	bulk kinematic viscosity
ν**	effective bulk kinematic viscosity
ρ	density
ρ_0	unshocked density
ρ_1	shocked density
ρ_b	surge bulk density
ρ_g	gas density
ρ_{max}	fixed bed density
ρ_p	particle density
ρ*	bulk density
θ	volume fraction
θ_g	gas volume fraction
θ_p	particle volume fraction
θ_{pi}	particle volume fraction for each w_i
θ_{pa}	average particle volume fraction
θ_{p0}	reference level particle volume fraction
τ	viscous stress tensor
τ_s	shear stress
ω	perturbation wave number
ξ	SFT transport coefficient
ξ_0	SFT source transport coefficient
ψ	isentropic expansion limit

1. Introduction

Richard Fisher vividly and graphically introduced me to the subject of base surge with his wealth of experience. His analogies to more commonly observed sedimentary processes helped me appreciate the importance of field relationships and textures. Michael Sheridan enthusiastically guided me in quantitative methods applied to study of base surges and suggested possible facies relationships in surge deposits and quantitative methods of studying them. This early training was further strengthened by my colleagues in Los Alamos, Grant Heiken and Bruce Crowe, both of whom had considerable field experience with surge deposits. I have received considerable help from discussions with other researchers, all of whom rank among the early students of pyroclastic surge, including Aaron Waters, Steve Self, Volker Lorenz, Juergen Kienle, Hans Schmincke, and Jim Moore. In addition, my colleagues at Los Alamos National Laboratory generously shared their knowledge of the effects of large man-made explosions, observations of which first defined the concept of base surge. I feel that recognition of these pioneers is an appropriate preamble to this manuscript.

This manuscript is in two parts: observational and theoretical. In discussions below, I focus on the following 9 topics: observational topics include (1) history and terminology; (2) field characteristics; (3) facies interpretation; and (4) laboratory analysis; and theoretical topics include: (5) compressible two-phase flow; (6) bedform interpretation; (7) sequential fragmentation/transport; (8) thermodynamics of wet and dry surges; and (9) volcanological models. To be sure, I do not cover these topics in entirety but discuss what I consider to be salient aspects. I only ask the reader to be forgiving if some aspect is not mentioned, for in compressing the vast amount of pertinent literature into a manuscript, much had to be left out.

2. Observations

The pyroclastic surge has been recognized as a common and violent component of explosive volcanic activity for over 30 years. To understand the concepts of the volcanic phenomenon, one must trace their history back to when the base surge was first studied for large, manmade explosions. Atmospheric nuclear explosion tests started in the 1940s and continued into the early 1960s. During this period of time, the base surge was intensely studied to understand its damage potential. Later in the mid 1960s, the base surge phenomena was recognized during volcanic eruptions. From that time when it was first recognized, the concept of volcanic base surge has been widely studied, and the term *pyroclastic surge* was formalized to include the base surge other volcanic phenomena that produced similar effects. The next four sections review important field and laboratory observations that have shaped our understanding.

2.1. History of the base surge concept and the development of terminology

When the underwater nuclear test (BAKER) was exploded in Bikini Lagoon on July 25, 1946, among the various surface phenomena that this 20 kt bomb produced, the ***base surge*** (Wilkes 1946; Brinkley et al. 1950) caused the greatest concern. Young (1965) described the phenomena:

> "This was a dense toroidal cloud which emerged from the base of the cylindrical column of spray that was formed by the explosion. As the column settled back, it apparently fed material into the base surge, which spread rapidly along the surface of the lagoon. The exact nature of the process was not understood. However, the collapse of the column and growth of the surge was believed to be an example of "bulk subsidence," in which a falling suspension of water drops in air behaves like a homogeneous fluid with a density greater than that of the surrounding atmosphere."

Young (1965), used 570 s of photographic records to document the following primary observations.

- Initial formation of the ***primary surge*** (Figs. 1 and 2) occurred 11 seconds after the burst. It formed as a spillout of seawater jets, driven by shock wave propagation, that emerged at an angle of ~60° from horizontal and later broke into a spray, forming a dense toroidal

cloud. The cloud moved laterally at an average of ~33 m/s for the first 20 s after which it slowed to 20 m/s (Fig. 2).

- Multiple shock waves were generated in the air, and behind each, a rarefaction (suction) zone caused adiabatic cooling and condensation of moisture.
- A modified lognormal distribution of water drop sizes constituted the surge; drops had an initial maximum size of 0.27 mm that increased to 1.2 mm as drops coalesced over a period of about 1 s.
- The primary surge aerosol flowed as a density current until 50 s after the burst at which point the large drops began to fall out.
- A ***secondary surge*** formed by subsidence of mist in the column (column collapse) 20 s after the primary surge and was eventually swamped by fallout.
- After fallout of the large drops, the surge density was approximately ambient with remaining droplets <0.030 mm in size.
- The top surface of the surge turbulently mixed with the atmosphere, and the resulting mixture rose vertically off of the surge.
- The surge front was characterized by bulges and pockets and moved preferentially with wind direction.

Young's observations along with his laboratory simulations (Fig. 3) allowed him to analyze the flow history of the base surge from observational data. The surge decelerated from its initial peak velocity during flow dominated by four principle stages (Fig. 4). The initial spillout stage showed high flow speed driven by shock wave propagation and reflection. After ~20 s the secondary surge contributed to flow, resulting in dominantly gravitational acceleration (Stage 1). After ~1 min, and some 1.5 km of runout, gravitational acceleration began to be balanced by atmospheric drag, and the surge moved just by its velocity potential (Stage 2). At a distance of ~3 km significant turbulent mixing of the surge cloud with the atmosphere produced vertical convection of the surge's energy, causing it to rapidly decelerate (Stage 3). Similar observations have been made at other underwater and underground explosions, and it is my belief that the flow history of the BAKER surge described by Young (1965) is applicable to volcanic base (pyroclastic) surge as well.

Observations of base surge in explosive tests: Perhaps one of the most widely cited books describing the base surge and related phenomena created by man-made explosion (Fig. 5) is that by Glasstone and Dolan (1977). These authors make a comprehensive assessment of damage phenomena related to the surge and show that propagation of shock waves (air blast) and their interaction with the ground surface are a primary component of base surge. In reading other literature on explosive testing and crater formation (*e.g.*, Nordyke, 1961; Carlson and Roberts, 1963; Johnson, 1971), one finds that explosive crater formation is almost always accompanied by base surge. For example, Carlson and Roberts (1963) found that the SEDAN nuclear event in 1962 formed a crater 370 m wide and 100 m deep with base surge deposits extending out for over 1 km. These authors found the base surge deposits to be bedded and contain dune-like structures. Other pertinent observations are listed here.

- High explosives and nuclear cratering tests produce a base surge by (1) the ballistic overturn of rock/sediment near the surface (producing inverted stratigraphy), (2) the

interaction of low-angle ejecta with the substrate, (3) column (stem) fallback, and (4) propagation of multiple shock waves.
- The ejecta blanket within one to two crater radii of the crater rim is dominated by surge ejecta and surge-reworked ballistic ejecta.
- Surge ejecta shows fine-scale (mm to cm) bedding planes, and for large explosions, surge deposits show dune bedding.

Wohletz and Raymond (1993) observed and studied base surge phenomena in the MISERS GOLD high-explosive test. One of the most impressive features of this ~5 kt-equivalent blast was the damage caused by shock waves accompanying the base surge (Fig. 6). Within several hundred meters of the crater, trees were incinerated almost instantaneously as the leading shock wave passed. Although the surge left only several centimeters of deposit at distances over 100 m from the crater, the surge had completely removed the turf. Granulometric analyses of the surge deposits showed a very systematic behavior, which I will discuss later in this paper.

Some mention should also be made regarding base surge and impact cratering. When NASA first considered landing man on the moon, a great debate about the nature of lunar craters fired up. As understanding of the differences between impact and volcanic craters developed, one class of volcanic craters (maars and tuff rings) were found to have similar profiles as impact craters. Since these volcanic craters have ejecta blankets consisting of base surge materials, workers considered the possibility that impact craters also produced base surge. However, at that time volcanic base surges were thought to require steam. The anhydrous nature of the lunar surface seemed to preclude base surge formation. This debate still continues to this day, with laboratory simulations of impact cratering showing ejecta moving in orderly ballistic trajectories. But Viking observations of Martian craters showed ejecta deposits with structures typical of lateral flow, difficult to explain by ballistic transport (Fig. 7). Since the surface of Mars was likely wet during much of its impact history, Wohletz and Sheridan (1983) suggested that base surge can be a part of impact cratering.

Early observations of volcanic base surge: In searching the pre-1960 literature about thinly bedded volcaniclastic deposits around vents, I found that geologists often recognized these deposits as fluvial sediments or wind reworked ejecta (*e.g.*, Hack, 1942; Shoemaker, 1957). Those volcanologists first documenting base-surge events in volcanic eruptions drew upon experience gained from explosives testing (Moore, 1967; Fisher and Waters, 1970). Below, I summarize some pertinent milestones in early work on volcanic base surge.

- Richards (1959) first suggested that volcanoes show base-surge-like activity, based on his observations of Volcán Bárcena eruptions.
- R.V. Fisher was the first volcanologist to witness the base surge from a nuclear test while stationed at Bikini. His observations led him to apply the concept to the 1957 Capelinhos volcano and the 1965 Taal volcano eruptions (Fisher and Waters, 1969, 1970; Waters and Fisher, 1971).
- Moore (1967) formalized the concept of volcanic base surge from his field studies at Taal. He found that the Taal base surge moved at speeds > 50 m/s, obliterated all trees within 1 km of the vent, sandblasted objects out to 8 km, and had temperatures near 373 K. The

deposits included ballistic blocks and fallout ash along with the lapilli and ash carried by the surge, much of which formed sticky mud coatings on trees and the substrate. Within 3 km of the vent, the deposits show a crude dune-type bedding, the dunes being largest adjacent to the vent. Moore (1967) suggested that volcanic base surges should have many of the same characteristics as those from nuclear explosions.

- Fisher and Waters (1970) greatly extended the characterization of base surge deposits, recognizing in over 30 studied localities, their thinly bedded, alternating coarse and fine ash and lapilli character, the occurrence of antidune structures, and planar beds that are distinct from fallout materials.
- Fisher and Waters (1970) first suggested that the transport and deposition of base surge deposits must be governed by a set of variables similar to bedforms produced by debris-laden water in alluvial channels, wind-driven sand, and subaqueous turbidity currents; surge bedforms are similar to those of upper flow regime fluvial sediments.
- Fisher and Waters (1970) further recognized that surges have high (50 m/s) initial velocities, are turbulent and cohesive, that gravity plays a role in adding energy to the surge, and that they must have a high particle concentration leading to an increase in effective viscosity from particle collisions.
- Waters and Fisher (1971) continued study of surges by detailed descriptions of base surge deposits at Capelinhos and Taal volcanoes, furthering the concept of high flow regime deposition.
- Crowe and Fisher (1973) studied the many varieties of cross bedding in surge deposits, demonstrating their similarity to antidunes formed in a high flow regime, while noting the importance of soft-sediment deformation indicative of ash cohesiveness.
- Sheridan and Updike (1975) studied a rhyolitic surge deposit and were first to promote a fluidization model where bedforms resulted from the gradual deflation of the surge. They supported this hypothesis by a novel approach to grain-size data analysis that indicated the varying interplay of inertial and viscous forces.
- Sparks (1976) suggested usage of the term *pyroclastic surge* to include deposits such as the ground surge and base surge so that pyroclastic deposits could be classified in a tripartite scheme (fall, flow, and surge).
- Wohletz and Sheridan (1979) first introduced the concept of a facies model for surge deposits, using a detailed Markovian statistical analysis of measured bedforms in surge deposits from many volcanoes. The facies model supported the concept of gradual deflation of the surge as it moved away from the volcano, making it a highly unsteady flow compared to the more homogeneous steady movement of pyroclastic flows.

Over the last 20 years since these early studies numerous authors have furthered the documentation of base-surge deposits, offering many insights and interpretations. However, with renewed study after the 1980 Mount St. Helens eruption, a much broader recognition of the importance of the base surge in volcanic hazards evolved. The concept of base surge has been extensively questioned and redefined. Many new workers unfamiliar with surges have asked the same questions answered many years before, attempting to redefine the phenomena and pose new classifications that have troubled researchers since (*e.g.*, surges are turbulent--flows are laminar, can one distinguish a pyroclastic flow from a surge, analogy to water-laid sediments became fashionable again). In a recent review of pyroclastic surges and flows,

Carey (1990) details some observations and arguments surrounding the issue of pyroclastic surge transport and depositional processes.

2.2. Field characteristics of pyroclastic surges

Over recent years most new research efforts have been devoted to understanding the mechanism of pyroclastic surge and the term has taken on quite a genetic context. Nevertheless, pyroclastic surges are defined by their field characteristics, and it is these general characteristics that distinguish them from other volcaniclastic deposits such as pyroclastic flows, debris avalanches, and volcaniclastic sediments. I list below some general field characteristic of surges, but from my point of view, their most distinguishing feature is multiple thin (cm-scale) laminations.

- Surges form apron-like deposits around the vent, generally extending only a few crater radii (< 10 km with notable exception of ground and ash-cloud surges) from the crater rim (Table 1).
- They are associated with volcanoes of most compositions, but commonly found where hydrovolcanism has occurred (Table 2).
- Their thickness is extremely variable with location from a few mm to over 10 m (Fig. 8).
- They are composed of dominantly coarse ash and lapilli-sized fragments (fines depleted) (Fig. 9).
- Surge deposit volumes are generally << 1 km^3.
- Surge deposits show both erosional and depositional features with marked unconformities.
- The deposits are generally well stratified and poorly sorted, surges can show a multiplicity of bedforms, most notably a variety of dune-like forms, termed sandwaves (Table 3; Fig. 10 and 11).
- Surge deposits from blast eruptions are easily eroded, but those produced by hydrovolcanism commonly lithify by glass alteration.

Given these general field characteristics, pyroclastic surges fall within a tripartite classification scheme (Table 1) of pyroclastic material that include fallout (fall), flow (ash flow), and surge. The term ***pyroclastic surge*** is general in context. It first derived from the term ***base surge***, but later *pyroclastic surge* was defined to include the ***ash-cloud surge*** and ***ground surge***, discussed below. With new types of surges now recognized, the *base surge* is generally taken to connote origin from hydrovolcanic-types of eruptions, most commonly recognized at basaltic vents (Table 2), but certainly an important factor in the evolution of more silicic composite volcanoes and domes.

The ground surge and ash cloud surge. Three types of pyroclastic surge deposits are now commonly recognized and discriminated based upon their field relationships. These types include the base surge, ground surge, and ash-cloud surge (Figs. 12 and 13).

Sparks and Walker (1973) recognized the ***ground surge*** as a separate pyroclastic rock type (now called pyroclastic surge) to include *base surge* deposits commonly found around

maar volcanoes and tuff rings and cones. Whereas *pyroclastic flow* deposits are in general relatively homogeneous, lacking internal stratification, and accumulating in topographic depressions (absent from steep slopes), Sparks and Walker (1973) contrasted ground surge by their deposits, which mantle topography with non-uniform thickness, have internal stratification, and extend only limited distance (5 - 10 km) from the vent; however, Valentine et al. (1989) identified ground surge deposits up to an estimated 100 km from the vent of the Peach Springs tuff. The common usage for ground surge is now limited to those stratified and graded beds (other than fall deposits) mantling the ground below ignimbrite flow units (Fig. 12). Those authors suggested that ground surges formed by segregation of dilute, turbulent clouds from a pyroclastic flow that moved ahead of the denser body of the flow and are subsequently overridden by the flow (Fig. 13). Fisher (1979) attributed ground surges to the initial collapse of fine-grained, outer portions of an eruption column, while Wohletz et al. (1984) modeled them as originating from the initial blast waves moving ahead of a pyroclastic flow. Other theories include formation by turbulence at the base (Valentine and Fisher, 1986) and at the front (Valentine and Wohletz, 1989) of moving pyroclastic flows.

More recently, Fisher (1979) distinguished ***ash-cloud*** surge deposits from those of ground surge, because they are emplaced on top of pyroclastic flow units, showing evidence of originating by eleutriation from the top of moving pyroclastic flows. Having textures very similar to those of ground surge, ash-cloud surges are mainly distinguished by their stratigraphic position. If they exist between successive pyroclastic flow units, then their classification becomes problematic, for which cross-cutting relationships must be exactly determined to associate them with the flow unit below them. If they are genetically associated with the pyroclastic flow above them, then they are better termed ground surge. The discrimination of ash cloud surges by stratigraphic position is well illustrated by Fisher (1979), but more recent observations of pyroclastic flows at Unzen volcano document ash cloud surges that have outrun their associated flow only to be over-topped by that flow, giving them the appearance of ground surges (Yamamoto et al., 1993).

In practice, ground and ash-cloud surges are generally found to exist at distances from the vent much greater than is expected for base surges. Whereas base surge deposits are rarely found beyond 10 km from the vent, ground and ash-cloud surges may deposit up to several tens of km from the vent. Ground- and ash-cloud surge deposits are rarely thicker than a meter or so, and in many cases are only a few cm thick, consisting of a dozen or fewer individual laminations. With exceptions of ground surge deposits underlying large ash flow, they crop out in very discontinuous patterns. It is common to find ground- and ash-cloud surge deposits that pinch and swell considerably with outcrop location, being readily visible in some and only indicated by a narrow rock parting in others. Pyroclastic flows that encounter topographic obstacles often shed ground surges with deposits that can be several meters thick but of only limited lateral extent.

Kieffer(1981) formalized the concept of a volcanic blast, and those well bedded pyroclastic deposits that form during blast-type eruptions, such as during the 18 May 1980, have come to be known as ***blast surge***. Having all the typical features described for pyroclastic surge above, blast surge deposits generally show only limited thicknesses (< 1m) and a limited number of beds owing to the short duration of the eruption that produces them.

2.3. The development of facies interpretations

Perhaps the most distinguishing feature of pyroclastic surge deposits are their various dune-like (sandwave) bedforms (Fig. 11). Without the presence of dunes, many workers still fail to recognize a surge deposit. However, as mentioned above, surges present a multiplicity of bedforms, from planar, inversely graded beds, to massive beds, to massive beds with faint internal stratification, to dune-like beds. Because of their similarity to the Bouma (1962) and Lowe (1982) sequence of turbidite-related sediments, the concept of bedform facies distribution became an important means for classification and interpretation of surge deposits. This concept involves recognition of the relative accumulation rate of tephra within the deposit as a function of flow steadiness (temporal variation in emplacement speed) and flow uniformity (spatial variation of emplacement speed), a subject recently reviewed by Kneller (1995). In Kneller's analysis, local topography combined with waxing and waning flow results in variations of flow steadiness and uniformity, the combination of which determines the sequence of bedforms deposited at any given location. Although facies models related to turbidity currents may address a greatly different fluid dynamical system, they have nonetheless inspired studies of pyroclastic surge deposits. Wohletz and Sheridan (1979) attempted the first facies discrimination for surge deposits surrounding a variety of vent types, based on the lateral variation in bedform transitions away from the vent (Table 4).

The main problem of defining surge facies by bedform is that at any one location, a wide range of bedforms may be represented in a surge deposit, and for thick deposits it is difficult to recognize a predominant bedform. Fisher recognized that surge beds often cropped out in what he called *bedding sets* of several layers that appear with a common sequence of bedforms from bottom to top. This observation led Wohletz and Sheridan (1979) to suggest that the vertical sequence of bedforms in a surge deposit is Markovian, that there is a statistical signature of the probability that a surge bed of one form will be overlain by a surge bed of another form. Accordingly, instead of defining a surge deposit solely by the abundance of various bedforms, Wohletz and Sheridan (1979) studied the vertical sequences of bedforms. The Markovian sequencing idea involves the assumption that the surge depositional regime is responsible for the nature of bedforms emplaced and furthermore, that a given state of a surge depositional regime statistically determines the next likely state of that regime. The Markovian sequence at any location in a surge deposit can then be represented by a matrix of bedform transitions observed on a fixed vertical scale (Fig. 14). This approach led Wohletz and Sheridan (1979) to define three common surge facies types: a sandwave type where vertical transitions from any bedform to a sandwave bedform are most common; a massive type where all vertical transitions are nearly the same in abundance, and a planar facies type in which planar bed to planar bed vertical transitions are most common. Further work showed that surge facies are strongly controlled by vent type, eruption mechanism, and depositional slope (Table 4).

Analysis of surge facies distributions (Fig. 15) by Wohletz and Sheridan (1979) showed a pattern suggesting a gradual deflation (loss of gas and increase of overall bulk density) of pyroclastic surges as they move away from the vent (Fig. 16). This interpretation,

which shows sandwave facies more likely to be deposited near the vent, massive facies at intermediate distances, and planar facies in distal reaches of surge deposits, is based upon the concentration of particles in a surge cloud necessary for saltation and deposition of dune-like bedforms in comparison to that required for traction flowage and deposition of planar bedforms. While this general facies distribution is common around many types of volcanoes where depositional slopes are low (*e.g.*, Crisci et al., 1981), other distributions may show the opposite trend (Fig. 17) in which sandwave facies become prominent at distal reaches of a surge deposit. This situation can result from the gradual inflation of a surge as it moves away from a volcano. Examples of this gradual inflation include those where surges move downslope on a dome (*e.g.*, Unzen volcano; Yamamoto, 1993) or composite cone (*e.g.*, Vulcano, Frazzetta et al., 1983) or during the movement of an ash-cloud surge (Fig. 18). I note that theoretical and laboratory studies by Woods and Bursik (1994) show inflation by atmospheric entrainment as a pyroclastic density current moves downslope.

Sohn and Chough (1989; 1992) took a different approach to recognizing depositional facies in surge deposits. These authors characterized more than a dozen facies, which were related more to bedding-set textures at finite locations than statistical sequencing (Fig. 19). Their facies showed lateral variations (Fig. 20) that they related to progressive decreases in particle concentration and increases in turbulence as pyroclastic surges moved from the vent (Fig. 21).

It is apparent that facies analysis of pyroclastic surge deposits holds some promise in unraveling the complex nature of these texturally diverse tephra. The relationship of bedform distributions to emplacement mechanisms of pyroclastic surges is a topic to be further explored later in this manuscript.

2.4. Laboratory analysis of surge samples

Pyroclastic surge deposits comprise a wide range of tephra compositions, sizes, and shapes, as well as a variety of lithification states and secondary minerals. Laboratory analysis of samples taken from surge deposits constitutes an important approach to classification and interpretation.

Granulometry (grain-size analysis) has been the most widely applied laboratory technique in analysis of pyroclastic surge samples. Although surge deposits show a range of median grain size [mostly in the range of coarse ash (0.125 to 1.0 mm)] similar to matrix materials of pyroclastic flow, they are generally better sorted than pyroclastic flow deposits. Pyroclastic surge deposits are often characterized as *fines depleted*, meaning that they lack fine ash components when compared to fallout or flow products from the same volcano. Generally following methods developed in sedimentology for characterization, classification, and interpretation, early studies (*e.g.*, Fisher and Waters, 1970; Sheridan and Updike, 1971; Crowe and Fisher, 1973) found that samples from different bedforms had distinctive grain-size attributes, the most notable being that of median grain size. This attribute is well illustrated by Fig. 22. Sheridan and Updike (1971) applied factor-analysis to the multivariate data set of surge grain sizes and found that in general two factors could explain 95% of the

observed variance; these two factors were attributed to relative importance of laminar and turbulent flow during the deposition of surge beds.

Wohletz (1983) showed how the grain-size variations of surges produced by hydrovolcanism might be related to eruption energy, based on surface area control of heat transfer rates. Accordingly, sandwave beds, which typically show median grain diameters of <0.5 mm resulted from hydrovolcanic eruptions in which heat transfer times are over an order of magnitude shorter than those eruptions producing planar beds (median diameter > 0.5 mm); hence, one conclusion is that surges producing sandwave beds originate from more energetic eruptions than those that produce planar beds. In contrast, Walker (1984) concluded that dune-bedded surges from the May 1980 Mount St. Helens blast were emplaced by relatively weak surges, based on the assumption that coarser grained deposits reflect higher velocity emplacement.

While base surge deposits show a wide range of component compositions, including glass, crystals, and lithic fragments, ground surge and ash-cloud surges are often dominated by crystals and crystal fragments, especially where fines depletion is noted. One consequence of this unique component composition can be found where ground/ash-cloud surges are intercalated in a welded ignimbrite. Such surges show little or no welding effects whereas the tuff below or on top is strongly welded; a result attributable to the fact that the surge layers have few glass shards that can be influenced by welding deformation. In base surge deposits, the variations in component abundances can be related to the wetness of the emplacement environment (Fig. 23). Tuff cone deposits characteristically form from wetter surges than do tuff ring deposits. Consequently palagonitized glass is typically more abundant in surge deposits from young tuff cones. But surges in tuff rings generally show greater abundances of lithic fragments than do those of tuff cones, perhaps as a consequence of depth of eruption. The abundance of lithic fragments in surges is also a useful indicator of host rock stratigraphy below a vent area. Wohletz and Heiken (1992) demonstrate that lithic fragment type and abundance follow a pattern in surge deposits, depending upon the depth and abundance of external water sources around a vent conduit during hydrovolcanic eruptions. This pattern of type and abundance can be useful in reconstructing the progression of hydrovolcanic eruptions and even in characterization of aquifer rocks.

Grain shape analysis is a laboratory method that has received little development in contrast to those of size and constituent analysis. Glass fragments show a wide range of morphologies largely due to their mode of formation during fragmentation and eruption (Fig. 24). Still, transport within pyroclastic surges has the potential to modify shapes of individual particles by particle abrasion caused by grain-to-grain and grain-to-substrate collisions. Wohletz and Krinsley (1982) studied glass fragments from numerous samples of surge deposits of various origins and noted a number of grain morphology characteristics that they classified as indicative of eruptive mechanism, transport, and grain alteration (Table 5). Using a point counting technique and qualitative morphology descriptors, they found that grain rounding and abrasion features increased in abundance with increased particle size and that sandwave beds possessed fewer grain abrasion features than did massive beds and planar beds, the latter of which have grains showing the greatest abundance of these features. One possible explanation of these results is that grains deposited in planar beds suffered more

collisions than those deposited in sandwave beds. This kind of interpretation has significance for estimating the importance of grain collisions as a mechanism of kinetic energy transfer and dissipation during surge emplacement. Wohletz (1987) used these morphologies help understand the origin of surge tephra from various kinds of hydrovolcanic eruptions, but quantitative morphology analysis applied solely to understanding surge emplacement has yet to be realized; however, such a study may benefit could draw upon textural studies of sand grains from wind-tunnel experiments (*e.g.*, Krinsley et al., 1979).

3. Theory

Theoretical considerations can help in analysis of pyroclastic surge transport and depositional mechanics. To be sure, pyroclastic surges involve complex physical phenomena that arise from the flow of particles and gases from slow to high speeds, and there is to my knowledge, yet to be a comprehensive theoretical approach that can adequately predict this complexity.

In the next sections I summarize some rather basic aspects of compressible two-phase flow, methods for predicting some dynamical properties of surges, how bedforms can be understood from simple dynamic properties, theoretical differences between pyroclastic flows and surges, how granulometry is useful for interpreting surge deposits, the effects of moisture carried by pyroclastic surges, and the importance of blast wave propagation in surges.

3.1. Two-phase flow

Perhaps the best way to start this discussion is presentation of the mathematical relationships, which express fundamental relationships among characteristic flow parameters (Fig. 25) with conservation of mass, momentum, and energy. These equations are often referred to as the *Navier-Stokes* equations. In their full expression, they are nonlinear and require simplification for analytical solution. As a convenient simplification, one can assume that the mixture of gases and particles of varying sizes, shapes, and densities can be adequately idealized as a two-phase system consisting of an ideal gas and spherical solid particles of uniform density and size. This approach yields six coupled, nonlinear differential equations for which full analytical solutions have not been achieved, but numerical techniques (see Valentine, this volume) hold promise. A problem in application of numerical simulation stems from the lack of an adequate base of measured dynamic properties of surges, properties that are difficult if not impossible at this time to measure because of the hazardous nature of surges. However, it is likely that carefully designed laboratory experiments might yield scalable properties. Examples of such experiments might include wind-tunnel (*e.g.*, Greeley et al., 1984) and shock-tube experiments (*e.g.*, Hwang, 1986) or cleverly tailored tank experiments (*e.g.*, Carey et al., 1988).

In order to fully apply the Navier-Stokes equations to a mixture of solid particles and gas, one must write the equations for each phase separately. Recognizing that solid particles are not a contiguous phase, the continuum approach allows for spatial averaging of physical

properties, such that over a specified control volume, which must me much larger than the size of individual solid particles (Travis et al., 1975), the properties of each phase are homogeneous. These averaged properties define the particulate phase, occupying a volume fraction expressed as θ_p, the solid volume fraction, and the gas phase that occupies a volume fraction θ_g, often termed the *void* fraction. The following formulation for two-phase flow is based on that originally presented by Harlow and Amsden (1975), and it has been applied successfully to wide variety of flows.

During flow of a pyroclastic surge, mass is conserved among the phases and the environment. For a given phase, considering a control volume, this continuity can be expressed as the sum of temporal and spatial density variations (left-hand side) equal to the sources and/or sinks mass in that volume (right-hand side) of Eq. (1):

$$\frac{\partial\left(\theta\rho\right)}{\partial t}+\nabla\cdot\left(\theta\rho\ \mathbf{u}\right)=\pm J_d \quad . \tag{1}$$

For this equation, θ expresses the volume fraction of the phase, ρ its density, $\mathbf{u}$ its velocity vector, and t is time. J_d represents the sum of density source and sinks; for example, gas exsolved/condensed, particles sedimented and/or eleutriated, or particles incorporated by substrate erosion.

Likewise, flow momentum is conserved in Eq. (2) below, for which the left-hand side sum of temporal and spatial variations of momentum is equal to the right-hand side sum of terms accounting for the pressure (p) gradient, exchange of momentum between phases by interphase drag (C_d), momentum source/sinks (J_d), gravitational (g) forces, and viscous/deviatoric stresses ($\boldsymbol{\tau}$), respectively.

$$\frac{\partial\left(\theta\rho\,\mathbf{u}\right)}{\partial t}+\nabla\cdot\left(\theta\rho\ \mathbf{uu}\right)=-\theta\ \nabla p+C_d\left|\Delta\ \mathbf{u}\right|\pm J_d\ \mathbf{u}+\theta\rho g-\nabla\cdot\left(\theta\boldsymbol{\tau}\right) \tag{2}$$

Note that Eq. (2) is very similar to Eq. (1) for terms multiplied by a velocity vector to express momentum transfer. The viscous/deviatoric stresses are expressed as a tensor term $\boldsymbol{\tau}$, which can take on different forms depending on the phase under consideration. For example, the gas-phase viscous stresses can range from its molecular viscosity to much greater values where momentum is dissipated by turbulent eddies, or for the particulate phase where an effective viscosity may develop from particle collisions analogous to kinetic theory of gases. Deviatoric stresses might also include significant shear stress near the substrate boundary.

For conservation of energy, expressed in Eq. (3) below, the temporal and spatial variation of heat (or internal energy, E) is equal to the sum of terms on the right-hand side expressing the thermodynamic work (with subscripts for the volume fraction and velocity vector for the two phases considered), interphase drag-induced heat dissipation, interphase heat transfer (Q_g), latent heat source/sinks due to phase change (J_e), and heat produced by viscous dissipation, respectively [note the scalar product of the stress tensor $\boldsymbol{\tau}$ and velocity

vector gradient in the last term of Eq. (3), which is known as the *dyadic* and denoted by a colon].

$$\frac{\partial\left(\theta\rho E\right)}{\partial t}+\nabla\cdot\left(\theta\rho I\,\mathbf{u}\right)=-p\nabla\cdot\left[\theta_1\,\mathbf{u}_1+\theta_2\,\mathbf{u}_2\right]+\left|C_d\right|\left(\Delta\,\mathbf{u}\right)^2+Q_g+J_e-\theta\boldsymbol{\tau}:\nabla\,\mathbf{u}\quad . \tag{3}$$

The solution of these equations is complex and requires additional closure equations, stipulating constitutive relationships and interphase coupling that can simplify the task. Below I show some of these simplifications that aid analysis. A major consideration that can simplify analysis is that these equations are coupled by interphase momentum and heat exchange, which in idealized analysis dominates the character of the solutions. Another set of simplifications addresses the bulk behavior of two-phase systems, which help in understanding flow character with respect to the concentration of the particulate phase. The compressibility of the gas phase can be an important complicating factor when surge velocities are high, but simplification is also aided by considering bulk behavior. Finally, I summarize some insight gained by simplifying these equations in light of stratified flow theory.

Simplifications arising from momentum and energy coupling. The solutions of the Navier-Stokes equations for the gas and particulate phases show an interdependency due to their coupling by momentum and energy exchange between the phases. This interdependency is greatest over a period of time during which the phases *relax* to an equilibrium of velocity and temperature, after which the mixture behaves more or less like a single-phased fluid or *pseudogas*. Any subsequent perturbation of the flow such as a change in flow regime (*e.g.*, laminar to turbulent, supersonic to subsonic, topographic irregularity) or interaction with an obstacle can upset this equilibrium, after which a period of relaxation is re-established. The *relaxation time* is typically expressed as the time during which the slip velocity (the difference between particle and gas velocity) or particle-gas temperature difference decays by 1/e. It is through analysis of this relaxation time that some bulk flow properties can be approximated without detailed solutions of the Navier-Stokes equations.

For example, consider the Stokes flow regime where there is no convective heat transfer (*e.g.*, Marble, 1970). The relaxation times for particle and gas equilibrium are:

$$t_v=\frac{m}{6\pi\,\ell\mu}\quad , \tag{Velocity Relaxation - 4}$$

$$t_t=\frac{mC_p}{4\pi\,\ell k_t}\quad , \tag{Thermal Relaxation - 5}$$

where m is the particle mass, ℓ is particle diameter, μ is viscosity, C_p is constant pressure heat capacity, and k_t is thermal conductivity. Accordingly, drag force and heat exchanged between the particles and gas are respectively proportional to the rates of change of momentum and thermal energy, which are sensitive to the relaxation times:

$$F = \frac{\rho_p\left(u_p - u_g\right)}{t_v} \quad , \qquad \text{(Force - 6)}$$

$$Q = \frac{\rho_p C_p\left(T_p - T_g\right)}{t_t} \quad , \qquad \text{(Heat - 7)}$$

where ρ_p is particle density, u_p and u_g are the particle and gas velocities, and T_p and T_g are the particle and gas temperatures. The distance (or wavelength) a two-phase mixture moves during its relaxation is simply the product of t and the mixture's velocity, and this distance is λ_v for velocity equilibrium and λ_t for thermal equilibrium. However, the Stokes flow regime is best suited for low Reynolds number flows and gives relaxation times that are less than those predicted by quadratic or hypersonic models better suited for higher *Re* flow regimes. The preceding illustration is shown only to introduce the relaxation concept discussed later, but first, a few other bulk flow parameter simplifications should be introduced.

Bulk behavior simplifications. For a lean mixture of gas and solid particles (*e.g.*, *dusty gas*; Marble, 1970), one can define the mass ratio $M^* \equiv m_p/m_g$, or $M^* = (\rho_p\ \theta_p) / (\rho_g\ \theta_g)$ where $\theta_p + \theta_g = 1$, such that the solid fraction of the flow is $\theta_p = M^*\ \rho_g / (\rho_p + M^*\ \rho_g)$, and the *bulk density* ρ^* is:

$$\rho^* = \theta_p\rho_p + \left(1-\theta_p\right)\rho_p = \left(1+ M^*\right)\left(1-\theta_p\right)\rho_g \approx \left(1+ M^*\right)\rho_g \,. \qquad (8)$$

This bulk density is shown in Fig. 26, but its approximate value, given on the right-hand-side of Eq. (8), is only appropriate for dilute mixtures where $\theta_p < 0.01$ ($M^* < 35$ for saturated steam and particles at 0.1 MPa*)*.

Marble (1970) defines the *bulk kinematic viscosity* ν^* for a dusty gas by $\nu^* \equiv \mu/(1 + M^*)\rho_g = \nu/(1 + M^*)$, for which μ is the dynamic (Newtonian) viscosity. This definition essentially accounts for the increased density of the bulk fluid. However, the dynamic viscosity is affected by particle collisions that result from particles of different sizes having different λ_v values, leading to particles crossing pathlines. The effect of these grain collisions produces a dispersive pressure (Bagnold, 1954) and an effective (collision) viscosity, inversely proportional to the particle mean-free path (particle separation or free distance) and analogous to kinetic theory of gases (*e.g.*, Savage, 1979; Haff, 1986). Bagnold (1954) defined the particle linear concentration as the ratio of particle diameter to the free distance, and it is a nearly linear function of M^* (linear correlation coefficient > 0.97). Many authors (*e.g.*, Walton and Bruan, 1986; Haaf, 1986; Hui and Haff, 1986; Campbell and Brennen, 1985; Bagnold, 1954) have theoretically and empirically shown the *collision viscosity* μ^* to be directly proportional to the particle linear concentration, for which an approximation is $\mu^* = \mu (1+ M^*)$. With increasing M^* particles become more closely spaced, collisions become more frequent, and the collision viscosity increases. Accordingly the *effective bulk kinematic viscosity* ν^{**} reflects the contributions bulk density increase and collision viscosity, the

importance of each greatly dependent on the degree of particle concentration in the mixture. As such, I propose that the effective bulk kinematic viscosity can be approximated as $\nu^{**} \approx \nu^* + \mu^*/\rho_g \approx \mu(1 + M^*)^2/\rho^* = \nu^*(1 + M^*)^2$. The *effective bulk dynamic viscosity* μ^{**}, which takes into account the contributions to the viscous stresses by both the gas viscosity and the collision viscosity, is given by:

$$\mu^{**} = \nu^{**}\rho^* \approx \mu\left(1 + M^*\right)^2 \quad . \tag{9}$$

Eq. (9) is plotted in Fig. 27, and it shows the effect of increasing θ_p, resulting in a higher effective bulk viscosity, whereas at low values of θ_p, μ^{**} is approximately equal to the Newtonian viscosity of the gas (steam).

The bulk Reynolds number was also defined by Marble (1970) as $Re^* = uL/\nu^*$, for which u is the average flow velocity and L is the characteristic dimension of gas flow around a particle, taken as the particle diameter. In order to take into account the collisional viscosity, the *effective bulk Reynolds number* Re^{**} is given by:

$$Re^{**} = \frac{uL}{\nu^{**}} = \frac{\rho^* uL}{\mu^{**}} \quad . \tag{10}$$

Fig. 28 is a plot of Re** versus θ_p, showing that for very dense surges of high θ_p, Re^{**} is low in a range typical for laminar flow, but with decreasing particle concentration Re^{**} rises to values characteristic of turbulent flow.

The preceding estimates of two-phase flow parameters are very model dependent and one could add further considerations to modify these results. Nonetheless, the effects of solid particle concentration show that with increasing θ_p, a surge's dynamic pressure ($\rho^* u^2$) greatly increases as do the drag forces the substrate or an obstacle can exert upon it (a function of viscosity). By analogy, surges with $\theta_p > 0.01$ have a similar destructive force as a rapidly moving flood of water. One may also conclude that, depending upon the solid fraction, a surge might range from laminar to fully turbulent flow. As discussed below, consideration of the bedforms deposited and likely density stratification present in a surge, there is no reason to believe that surges are always turbulent or always laminar.

With the simplified expressions for interphase exchange of momentum and heat as well as those of bulk density and viscosity, one must consider the compressibility of the gas phase. Compressibility is important for high-speed flows in which thermodynamic equilibrium lags velocity equilibrium. In these situations, the flow may behave over a range from isothermal to isentropic, which greatly affects the gas pressure as a function of its temperature, how fast it dissipates its kinetic energy with distance traveled, and the transition from subsonic to supersonic flow.

Compressible flow: added complexity. An important two-phase compressible flow thermodynamic property is its polytropic exponent $\beta = C_{pg}/C_{vg}$; gas behaves isothermally

when β is near unity and adiabatically when it approaches a value of $(7R/2) / (5R/2) \approx 1.4$ for ideal diatomic gases ($\beta_{steam} = 1.3$). For a surge (Fig. 29):

$$\beta^* = \frac{C_{pg} + M^* C_s}{C_{vg} + M^* C_s} \ , \tag{11}$$

where C_{pg} and C_{vg} denote the constant pressure and constant volume heat capacities of the gas, M^* is the particle/gas mass ratio, and C_s is the heat capacity of the particles (*e.g.*, Kieffer, 1981).

Flow of a gas and particulate mixture may reach speeds where thermodynamic properties cannot adjust in a continuous fashion to changes in flow velocity, leading to formation of shock discontinuities. Such is the case where a surge moves at speeds greater than its internal sound speed, the speed at which pressure signals propagate through the flow and promote local changes in the gas-phase thermodynamic state.

The bulk sound speed c^* of a homogeneous two-phase mixture (Kieffer, 1982) is dependent upon the bulk isentropic exponent β^* and has a value at rest of

$$c_0^* = \left(\frac{\beta^* p}{\rho^*} \right)^{1/2} = \left(\beta^* R^* T \right)^{1/2} \ , \tag{12}$$

where p is pressure, R^* is the bulk gas constant [$R^* = R_g /(1+M^*)$], and T is temperature. While moving in a homogeneous flow the bulk sound speed is

$$c_1^* = c_0 \left(\frac{2}{\beta^* + 1} \right)^n \ , \tag{13}$$

where the exponent n is 1 for unsteady flow and 1/2 for steady flow. The values of c^* calculated for surges (Fig. 30) indicate that at typical flow speeds of 20 to 50 m/s, surges can be internally supersonic where they have dense particle concentrations.

An important result of finite relaxation times and lower effective sound speed for the mixture is that pressure signals propagating within this mixture are dispersed and attenuated. These are the signals that *tell* the surge how it will react to changes in topography, where it will erode and where it will deposit. I summarize some speculations based on these considerations below and illustrate them in Fig. 31:

- Topographic changes least affect a surge where the characteristic topographic wavelength λ is greater than the velocity relaxation wavelength λ_v ($\lambda_v / \lambda < 1$) and where the Mach number ($M = u/c^*$) is greatest.
- The drag forces that the substrate exerts upon the surge are greatest at transonic speeds and where $\lambda_v / \lambda > 1$.

- Topographic obstacles may induce localized flow instabilities in the surge's boundary layer (discussed below) where finite relaxation times contribute to unstable bulk density stratification.
- A possible result of this compressible, two-phase flow behavior is that topographic variability influences particle deposition for subsonic surges (*e.g.*, roughness elements cause dunes to be deposited), but for supersonic surges, particle relaxation is too slow to adjust to topographic variability, and particles do not stick to the substrate but rather tend to erode it into a form more compatible with λ_v (Fig. 31).

Erosional features in surge deposits are well documented. Moore (1967) pointed out the existence of longitudinal furrows in surge deposits on the slopes of Volcán Bárcena. He attributed these furrows to surge erosion where surges moved downslope from the crater. The furrows were terminated at the break in slope at the base of the volcano, beyond which dune beds were deposited. Fisher (1977) described these erosional features in surge deposits as *U-shaped channels*. Wohletz (in Gutmann and Sheridan, 1978) mapped and described these features as longitudinal dunes, formed by current vortices (spinning perpendicular to the flow) in the surge as it moved over and around a topographic barrier such as a crater rim (Wohletz, 1976). Where these current vortices constructively meet deposition of longitudinal dunes occurs, but where the vortices part, erosion of channels occurs. Kieffer and Sturtevant (1986) investigated erosional furrows in the Mount St. Helens blast-surge deposit and attributed them to flow instabilities in the boundary layer.

Silent but deadly. Sound is generated in a surge by particle impacts and by pressure disturbances propagated through the surge by its interaction with the substrate. If no disturbance perturbs the surge's motion, with time particles would tend to relax to the same speed as the gas phase and sound caused by particle impacts would decrease. However, the substrate over which a surge travels always has some degree of topographic irregularity, and where the surge impinges these points of irregularity, pressure disturbances are generated. These disturbances generally have frequencies in the audible range, and as they propagate, they perturb the surge's motion leading to particle impacts. But the propagation of these sound waves is controlled by the local bulk sound speed of the surge. Because of the finite time particles need to adjust to accelerations imparted by pressure signals, sound waves may be dispersed and attenuated depending upon their frequency and that of particle relaxation.

For example, consider a weak pressure disturbance of period t_{dist} caused by the surge impinging a topographic element. This is a very complicated problem that Marble (1970) analyzed for the case where $t_{dist} \sim t_t >> t_v$. He showed that the perturbation caused by the disturbance has a *wavy-wall* solution for the perturbation of the form $\exp[iKx/a_0 - \omega t]$ where a_0 is gas sound speed, x is distance, and K is the characteristic value of a plane wave of frequency $\omega/2\pi$. K in Marble's solution has a real and an imaginary part that express dispersion and attenuation, respectively: $K = K_1 + iK_2$:

$$K_1 = 1 + \frac{1}{1+(\omega t_v)^2}\left(\frac{K}{2}\right) + \frac{1}{1+(\omega t_t)^2}\left(\frac{\beta-1}{2}K\right) + \ldots \quad , \tag{14}$$

$$K_2 = \frac{\omega\tau_v}{1+\left(\omega\, t_v\right)^2}\left(\frac{K}{2}\right) + \frac{\omega\tau_t}{1+\left(\omega\, t_t\right)^2}\left(\frac{\beta-1}{2}K\right)+\ldots. \qquad (15)$$

Marble (1970) showed that solutions to this problem tend toward zero (disturbance decays) where bulk sound speeds are slowest; hence, sound attenuation is expected where $\omega\, t_v$ and $\omega\, t_t$ = 1, which occur at approximate solid fractions of $M^*/4$ and $(\beta - 1)M^*/4$, respectively.

Fig. 32 illustrates Marble's solution by showing attenuation as a function of topographic wavelength ratio. This example illustrates that where the velocity relaxation wavelength ($\lambda_v = u\, t_v$) is shorter than the characteristic wavelength of the topographic fabric λ and where Mach numbers are highest, attenuation is greatest. The meaning of this relationship suggests that sound can be effectively damped within a moving surge, such that the surge's movement produces little or no audible sound. Furthermore, where surges produce little or no sound, they may have their highest destructive potential, a potential with the greatest likelihood of modifying the substrate by erosion as well as exerting high dynamic pressures upon any obstacle in their path. In support of this theoretical argument, Takarada (1997 pers. com.) has described silent and destructive ash-cloud surges at Unzen volcano, and many sources describe the recent destructive pyroclastic flows from the Soufriere Hills volcano, Monserrat as silent.

Stratified flow of surges. A general observation is that the particle concentration decreases upward in the moving surge, making it density stratified. Valentine (1987) discusses how pyroclastic surges can be analyzed by stratified flow theory (*e.g.*, Yih, 1980), as summarized below.

Assuming that some degree of turbulence exists in a surge (this does not necessarily mean high *Re* flow), in which particles move with average and fluctuating velocity components, particle concentration profiles are governed by the Rouse number *Pn*, which is a measure of particle average settling velocity to the turbulence scale (Middleton and Southard, 1978). It is sensitive to particle volume concentration, particle settling speeds, and shear velocities, expressed as an average (Valentine, 1987):

$$Pn = \frac{1}{\theta_{pa}}\sum_i \theta_{pi}\frac{w_i}{ku^*} \quad , \qquad (16)$$

where θ_{pa} is the average particle concentration and θ_{pi} denotes the average volume concentration of particle average settling velocities w_i, k is the von Kármán constant (mixing length/height), and u^* is the average shear velocity. By defining a dimensionless height $\eta = h/d$ with d as the total surge thickness (Ghosh et al., 1986), the equilibrium (no net erosion or deposition) concentration profile relative to the particle concentration θ_{p0} at a reference level in the flow is (Fig 33):

$$\frac{\theta_p}{\theta_{p0}} = \left(\frac{\eta}{1-\eta_0} \frac{1-\eta}{\eta} \right)^{Pn} \quad . \tag{17}$$

As gravity pulls the surge downslope, its effect is the formation of gravity waves. The surge's lateral motion is then related to the frequency of the gravity waves called the Brunt-Väisälä frequency (Lin and Pao, 1979; Fig 33):

$$N(\eta) = \frac{1}{2\pi} \left(\frac{g}{d} \frac{Pn}{\eta(1-\eta)} \right)^{1/2} \quad . \tag{18}$$

The average velocity *u* of the surge is related to *N* by the Froude number $Fr = u / Ny_h$, where the term Ny_h is the speed of the velocity waves at height *h*

Because particle collisions and drag forces tend to give rise to turbulence, the Richardson number, representing the ratio of buoyancy forces to those of turbulence is important:

$$Ri = \frac{-gd}{\rho} \frac{\partial\rho/\partial\eta}{\left(\partial u/\partial\eta\right)^2} \quad . \tag{19}$$

Since the relative buoyancy of small particles can damp turbulence, laminar flow dominates where $Ri > 0.25$. Valentine (1987) shows how density stratification in a surge interacts with topographic obstacles (*blocking*) to form massive beds and layer 1- and 2-type deposits during waxing and waning flow (Fig. 34).

With *u* a function of *N*, one can calculate an average velocity profile that shows the character of the boundary layer at the base of the stratified pyroclastic surge (Fig. 35) where large shear stresses arise from a sharp velocity gradient in a fashion similar to that described by Hanes and Bowen (1985). Sohn (1997) discusses some controls on the form of the velocity gradient, depending upon the relative dominance of frictional and collisional forces in the boundary layer. The form of the velocity gradient controls the shear stresses in the boundary layer, and in turn, these shear stresses can influence particle motion. Fig. 36 illustrates an example of the possible influence of the boundary layer velocity profile upon particles of different sizes for hypothetical laminar and turbulent boundary layers (Valentine and Fisher, 1986). This example involves the following considerations.

- Shear stress in the boundary layer is given by $\tau_s = \mu (du_x/dh) - \rho u_x u_y$, where μ is the bulk Newtonian viscosity, *h* is height above the substrate, and u_x and u_y are the average velocity components parallel and perpendicular to the substrate.
- A laminar boundary layer velocity profile is given by a generalized form: $u_x = U [2(h/\delta) - (h/\delta)^2]$ where *U* = maximum velocity and δ is the boundary layer thickness, a complex function of pressure gradient, surface roughness, heat transfer, and free stream disturbances. The velocity gradient is given by $du_x/dh = U [(2/\delta - 2h/\delta^2]$.

- A turbulent boundary layer for a surge moving downslope under the influence of gravity, g, may show a velocity gradient expressed as $du_x/dh = g/k^2u$.
- Since shear forces acting on particles are proportional to particle surface area, and particle surface area is a function of particle diameter, one can find the height to which particles of different sizes will move to achieve force balance. In this idealized conceptualization, larger particles will reach a force balance at a higher level in the boundary layer than smaller ones, as shown in Fig. 36.

The above illustration of boundary layer effects upon particle size grading is just one possible explanation for the origin of inverse grading in surge planar bedforms. It demonstrates that a turbulent boundary layer might develop an inverse grading in which particle size increases mostly at the bottom of beds, in contrast to that produced by a laminar boundary layer for which only the top of individual beds shows a rapid increase in particle size. Such an explanation implies that deposition from a surge is aggradational (Braney and Kokelaar, 1992), involving much of the boundary layer.

3.2. Interpretation of bedforms

A common thread in many papers about the bedforms and textures of base surge is the application of analogies to fluvial/submarine sediments (*e.g.*, Crowe and Fisher, 1973; Fig. 37). Allen (1984) questioned these analogies because of the cohesive nature of surge particles and how it affects particle interaction with the substrate. Still, these analogies allowed various workers to interpret the origin of surge bedforms by flow regime, which in this context expresses whether the flow Froude number (Fr) is less than (low) or greater than (high) unity. Now Fr is a ratio of inertial to gravitational forces and can be expressed as a flow's velocity to its critical velocity, $u/(gh)^{1/2}$. Kieffer (1989) points out the Froude number is analogous to the Mach number ($M = u/c$) for compressible flows. The basic argument against using the common sedimentological flow regime analogy for pyroclastic surges is that surges do show compressibility effects, as discussed above, and most studied surges are deposited subaerially where there is a much greater difference between the densities of the *fluid* phase and the particulate phase. Accordingly, there is not a strong experimental nor observational basis for applying aqueous sedimentological classification and interpretation schemes.

With these considerations, I present an alternative point of view for analyzing the origin of various bedform textures displayed by pyroclastic surges. The approach I espouse is based mostly on observations and experiments with wind-blown sediments as Bagnold (1941; 1954) so elegantly described, and Allen (1984) believed were a good analogy. More recent wind-tunnel experiments (*e.g.*, Greeley et al., 1983) have further substantiated Bagnold's observations and have provided in-depth understanding of how dunes are formed by flow of particle and gas mixtures. This approach involves consideration of the modes by which particles move and interact with the gas phase, the substrate, and each other. These modes are, in simplistic character, described as: (1) ballistic; (2) traction; (3) saltation; and (4) suspension. Because motion is influenced by drag forces exerted upon particles by the medium through which they travel, and these drag forces are proportional to the particle's surface area, the particle's mass to surface area ratio is important. With increasing size

(volume) and density, particle inertia increases faster than its surface area; hence, large particles (say > 1 cm) will be only slightly effected by drag forces while small ones (< 1 mm) will have their motion dominated by drag forces while moving in a surge. Transport modes are briefly described here and illustrated in Fig. 38.

- **Ballistic** transport is perhaps the simplest particle motion where a particle moves from one point to another in a gravitational field. The effect of gravity is that a particle follows a parabolic path from where it is launched until it comes to rest on the substrate (Schultz and Gault, 1979).

- **Traction** transport includes particle rolling/sliding along substrate during which particle motion is determined by tractive forces exerted upon it by other particles and the gas (Sohn, 1997).

- **Saltation** transport involves periodic particle bouncing or hopping over the substrate, where particles follow repeated short ballistic trajectories that begin with each collision with and rebound off the substrate. Saltation trajectories (*e.g.*, Sagan and Bagnold, 1975) are influenced by drag forces exerted upon them by the gas phase and infrequent particle-particle collisions (Anderson and Hallet, 1986).

- **Suspension** transport occurs where the terminal fall velocity of particles is offset by turbulent fluctuations of the gas phase such that particles float within the gaseous medium (Kranck and Milligan, 1985).

As mentioned above, the grain size (or ratio of grain inertia to drag forces as it moves through the gas) is important in determining whether a particle will follow a simple ballistic trajectory or be strongly influenced by drag forces. Large particles upon being launched from the vent during movement of a pyroclastic surge may follow a generally parabolic path to the point where they impact the substrate and are deposited. With increasing drag forces, shear within the boundary layer of a surge may be great enough to cause some large particles to roll and slide along the substrate for some distance. Smaller particles may bounce after hitting the substrate and follow repeated parabolic trajectories, while the smallest particles may become suspended in turbulent eddies to be carried for some distance before turbulence decays sufficiently for them to come to rest on the substrate. In this fashion, grain size is a very important factor in determining transport and deposition within a surge.

Still, there is another important factor that determines the transport mode for grains and that is particle concentration. With increasing particle concentration, the likelihood of particle-to-particle collisions is increased. Such collisions transfer kinetic energy among grains, and by analogy to kinetic theory for gases, it produces what Bagnold (1954) termed a *dispersive pressure*, which is analogous to a viscosity for gases and fluids. Considering glassy particles in a surge, collisions can be modeled as nearly ideal elastic phenomena [*e.g.*, kinetic theory of ideal granular flow described by Savage (1979)], such that collision kinetic energy is conserved. However, due to the non-ideal character of shards and pumices because of their shape and internal heterogeneities, a small but finite amount of kinetic energy will be lost with each collision, energy that is converted to heat and deformation. Thus kinetic energy will

gradually be lost in a surge by collisions in addition to that lost by viscous dissipation and frcitional contact with the substrate. Ishikawa et al. (1991) have numerically modeled collisional granular flow for pyroclastic flows, but for highly concentrated granular flow, momentum transfer by frictional contact (Drake, 1990) so greatly dominates that kinetic theory does not apply.

With these considerations, one may characterize particle transport and deposition within a pyroclastic surge by these four main transport regimes, which are dependent upon typical particle size ranges (expressed in phi ϕ units) and concentration.

1. **Ballistic:** Large particles ($\phi < -4$), such as lapilli, blocks, and bombs, are generally launched at a high enough initial velocity such that air drag does not greatly affect their flight path, and they are not carried to any degree in the lateral flow field of a surge. The ballistic range of these large particles is determined by their mass, initial velocity, and initial launch angle, such that at any point where they land, they are fairly well sorted by size, leading to plane parallel, generally non-graded beds.
2. **Traction**: Relatively Large ($-4 < \phi < 1$) particles (including in certain cases very large blocks) have sufficient terminal velocities to accumulate in concentrated ($0.5 > \theta_p > 0.1$) regions generally within the basal boundary layer where shear stress is high and frequent grain collisions occur. Bagnold (1955) experimentally showed that grain collisions become significant when particle volume concentrations θ_p exceed 0.09. The result of high particle concentration is a relatively high bulk density and high effective viscosity. The *Re* number for such conditions shown in Fig. 28 is within the laminar flow regime, and as a result plane parallel beds will be deposited, generally showing an inverse grading as described for the boundary layer discussion illustrated in Fig. 38.
3. **Saltation:** Where relatively small ($1 < \phi < 4$) particles have sufficiently high velocity and large interparticle spacing, they bounce (hop) upon striking the substrate and can follow an undisturbed parabolic flight path (few collisions) before hopping again. Eventually particles stick to the substrate where a topographic irregularity prevents bouncing. The combination of high velocity and low θ_p (< 0.09) results in a relatively high *Re* number (Fig. 28) within the turbulent flow regime. As more and more particles stick to the substrate where topographic irregularities exist, the irregularities grow into dune forms. As the dunes grow, they tend to develop a wavelength similar to a characteristic hop length of saltating grains. Various types of dunes (Fig. 11) can develop depending upon the balance among surge velocity, particle concentration and size, and substrate texture, all of which influence where flow transitions exist and migrate with time.
4. **Suspension:** Very fine grained dust ($\phi > 4$) has a small terminal velocity such that turbulent eddies that form in a surge tend to keep this dust from falling out so that it remains aloft during transport. The combination of low particle concentration and low effective viscosity promotes high *Re* even though the surge velocity may be small. With high concentrations of this dust, turbulence can be damped, leading to deposition.

Origins of surge bedforms: are bedforms diagnostic of transport/depositional regime?
Fisher (1990) in his study of pyroclastic surges generated by the 18 May 1980 eruption of Mount St. Helens found strong evidence that thin surge deposits originated from parts of the

surge moving in different directions than those indicated by blast effects in topographically higher areas. He interpreted these observations to support the idea that deposition from surges occurs from their base (boundary layer) where flow properties are quite different than those of the surge cloud above. This line of reasoning suggests that the depositional regime is different from the transport regime. Still, it is also likely that most mass is transported in the lower parts of a surge from which deposition is occurring; hence, the deposits reflect the local environment in which most of the surge's mass is transported.

The main problem with interpretation of surge processes is that distal observations of the event only record the movement of the lean-phase dust cloud surrounding the surge. Until recent measurements of surges at Unzen volcano in Japan, there has been no real knowledge of the surge transport environment. Only observations of wind-tunnel (*e.g.*, Greeley et al., 1984) and shock-tube (*e.g.*, Hwang, 1986) experiments have provided tangible insight along with that afforded by theory.

Despite uncertainties about the conditions of transport in surges and whether or not surge deposits lend insight about the transport regime, one is left with the fact that pyroclastic surges show a multiplicity of bedforms, and the textures of the bedforms indicate a depositional environment that fluctuates between laminar and turbulent. With the arguments for transport and deposition given above and the interpretation that planar beds show features of laminar flow and dune beds suggest turbulent flow, the fact that massive beds often show internal gradations to both dune and planar (pebble stringers) bedforms leads to an interesting though difficult to prove hypothesis: massive beds show aspects of both flow regimes. This hypothesis suggests that massive beds result from deposition in a critical flow regime between laminar and turbulent. This critical flow regime is buffered—that is the surge tends towards lower *Re* values and laminar flow during its gradual deceleration with runout. But during runout, the surge deposits particles and becomes less concentrated with a lower bulk viscosity, leading to an increase in *Re* towards more turbulence. Such a buffered flow regime is most likely where particle sorting is poorest and there is a competition among tractive, saltating, and suspended transport. This hypothesis is useful in consideration of the differences between pyroclastic flows and surges discussed below.

Pyroclastic surge or pyroclastic flow? Especially for the novice, the question of how to distinguish a pyroclastic surge deposit from that of a pyroclastic flow is a nagging problem. Fisher (1990) suggests use of the term *pyroclastic density current*, because it gets around the problem of distinguishing the two. In this discussion, I suggest that, while both surge and flow deposits are products of pyroclastic density currents, there are significant differences in their deposits, differences that indicate origins from density currents of fundamentally different character. As originally envisioned, Sparks and Walker (1973) distinguished the ground surge deposits as a separate pyroclastic rock type from fall and flow deposits, classified according to their mode of transport from the vent to place of rest. Since the transportation mode cannot be easily observed, it must be deduced from the characteristics of the deposits. In this light, Sparks and Walker (1973) listed these surge deposit characteristics that are different from those of flow deposits (ignimbrites):

1. Extreme heterogeneity, well bedded and often laminated, showing great variations in grain size and sorting;
2. Relative thinness, commonly < 1 m thick (ignimbrites are commonly > 10 m thick);
3. Pinch and swell structures seemingly unrelated to the substrate topography;
4. Occurrence on slopes > 10° (slopes on which ignimbrites are missing);
5. General decrease in both average thickness and grain size with increasing distance from the vent;
6. Poorly confined by drainage areas or valleys (as are ignimbrites) and tend to mantle topography.

Furthermore, Sparks and Walker (1973) characterized surges as having a much lower density and more turbulence than flows. This characterization lead these authors to assert that surges are analogous to turbulent torrents or floods while pyroclastic flows are analogous to laminar mudflows. From these arguments, a general characterization has prevailed in the years since that surges are lean, turbulent currents while flows are dense, laminar currents. But confusion has arisen in discrimination of the deposits, since there seems to be a gradation in field relationships between the two deposit types. An example of this gradation is the nuée ardente, which shows features of both dense pyroclastic flows and relatively low density ground surges.

From a genetic point of view, Wohletz and Sheridan (1979) conceptually point out that the difference between pyroclastic surges and flows is that surges form from highly unsteady (rapidly changing velocity) pulses of tephra that typically loose their kinetic energy rapidly while pyroclastic flows form from much more steady flow and constant flux. Accordingly, surge deposits reflect their unsteadiness and nonuniformity by thin beds and bedforms that change texture and grain size over small lateral and vertical distances, whereas flow deposits commonly are more massive and have fairly homogeneous textures over relatively large lateral and vertical distances. To be sure, some pyroclastic flow deposits do show well developed bedding in their basal portion and do show dune bedforms, in many cases displayed as pumice lenses. But the greatest similarity between surge and flow deposits are reflected in the massive bedforms of surge deposits, which have the overall texture displayed by the bodies of typical pyroclastic flow deposits. Surge massive beds are commonly best developed in areas of rapid slope change, such as paleodrainages and valley fills; where such massive beds are thick (> 1 m) they appear to have been channeled by the paleovalley (Wohletz and Sheridan, 1979).

If one assumes that the massive beds of pyroclastic surges form by a similar transport and depositional mechanism as massive portions of pyroclastic flows, then some speculations can be drawn regarding the difference between pyroclastic flows and surges. These speculations are based on the following observations:

- surge deposits show bedforms that can be interpreted to have formed from laminar (planar beds) to highly turbulent flow (dune beds) as discussed above,;
- massive beds are intermediate in grain size character between planar and dune beds;
- massive beds show textural gradation to both planar and dune beds;
- massive beds are often stratigraphically enclosed by planar and dune beds.

From these observations one can speculate that massive beds represent the product of a flow regime between laminar and turbulent, and by analogy, the same is true for pyroclastic flows that produce massive deposits. From the above discussion of such an intermediate flow regime, one that is buffered so that it never becomes fully turbulent nor laminar, pyroclastic flows can be thought of as having a rather limited range of bulk density (or void fraction) while surges, being highly unsteady, rapidly fluctuate in bulk density between fully laminar and fully turbulent flow over rather short intervals of time and distance. Accordingly, it is not entirely correct to assume that surges are lean and turbulent and flows are dense and laminar. Arguments surrounding this discussion will likely be based in semantics, as discussed below.

A terminology problem. The Reynolds number *Re* is an often cited parameter in study of conventional sediments (those deposited in water and in air). Recalling that *Re* is the ratio of inertial to viscous forces, where surges (gas-particulate mixtures) are dense, they will have a high grain collision viscosity, and their flow is *viscous*, dominated by this collisional viscosity, resulting in low values of *Re* and laminar flow. On the other hand, where surges are lean (low θ_p), grain collisions are relatively infrequent, collisional viscosity is low; and flow is dominated by particle inertia, which can be termed *inertial* flow. For small particles moving in such a lean mixture the effect of drag forces leads to turbulence and high *Re* values. This preceding terminology is common fluid dynamics usage, but it may be confused with similar terms used in classical sedimentology, for which the bulk behavior of the interparticle phase is ignored. It has been common in sedimentology to use the term *inertial* for laminar flow (where momentum is transferred by grain collisions). For saltating flow, sedimentologists consider the viscosity of the transport medium important and have called this regime *viscous* flow, even though particle motions are dominantly turbulent.

A further terminology problem arises from the fact that sedimentological theory ignores compressibility effects, so bulk density, pressure, and velocity gradients/discontinuities are not usually considered. Kieffer (1989) in analysis of compressible and incompressible motion equations offers a simple solution based on the analogy between Froude number and Mach number mentioned above. This analogy suggests that the sedimentology-based flow regime classification of *low* and *high* is analogous to *subsonic* and *supersonic* flow, respectively, and that hydraulic jumps are analogous standing shock waves. The utility of this analogy depends on the extent one can correlate thermodynamic pressure with hydrostatic pressure and sound speed with the speed of gravitational waves.

3.3. Sequential fragmentation/transport analysis

Because of the difficulties in studying pyroclastic surge mechanisms by observation and measurements of moving surges in the field and the high degree of sophistication necessary to make scale-models in the laboratory, theoretical advances can be made by study of granulometric data. However, traditional granulometric analysis has been based largely on empirical classification schemes founded in log-normal statistics, which have no close ties to the physics of particle motion. No matter how complex the physics are, field studies do

support the hypothesis that surge transport mechanisms do strongly influence grain-size variations. The following section describes a method for studying grain-size variations of pyroclastic samples that helps constrain the physical nature of surge transport mechanism. The method is based on sequential fragmentation/transport theory (SFT) developed by Wohletz et al. (1989). Application of analytical techniques utilizing SFT have yet to be strongly developed, owing to its complex mathematical basis, but experimental evidence (Brown, 1989; Wohletz, 1995; Zimanowski, pers. com., 1997) shows real promise.

SFT is based upon the fact that particles such as those in surge deposits derive from a sequence of fragmentation events occurring at their source during eruption as well as during subsequent transport (abrasion). Transport of fragments also tends to sequentially sort particles by size, a sequence that is controlled by multiphase flow relaxation, discussed above, during which particles of similar size move to regions where forces tend toward equilibrium. The particle size distribution in any sample results from an integration of the effects of all the physical sequences of fragmentation and transport that the sample has experienced. SFT expresses this integral and embodies some fundamental solutions that allow prediction of the final grain-size distribution. I review the mathematical basis for SFT analysis from Wohletz et al. (1989) in Appendix A, and below I illustrate how it can be applied to pyroclastic surge samples.

Applying SFT. SFT sample analysis involves a data inversion technique in which sieve data are best-fit to optimized SFT parameters. Typical surge samples show several or more overlapping subpopulations, reflecting both fragmentation and transport sorting of particles. Because subpopulation parameters reflect both fragmentation and transport effects, careful analysis of field data is required to separate these effects. One method involves creation of a weighted synthetic composite distribution from all samples from a deposit or selected samples from similar bedforms. This composite sample provides a reference or bulk distribution that, in the case of fragmentation, is a representation of the parental (source) distribution, or for transport mechanism, an idealized distribution for a given transport mechanism. For example, a given sample might be the combination of particle subpopulations transported to the sample location ballistically, by traction carpet, saltation, and/or suspension. Noting the ranges in modal size and SFT dispersion parameter γ, one can then assign with some confidence each subpopulation to a given transport mode (*e.g.*, the phi range given earlier, and ballistic $\gamma \approx$ -0.8, suspension $\gamma \approx$ -0.3, saltation $\gamma \approx$ -0.5, and traction $\gamma \approx$ -0.6; Wohletz et al., 1989). SFT can be applied to understanding source materials and their size modification by surge (Figs. 39 and 40). It is practically impossible to get SFT parameters from sieve data without specialized software (available from the author). The software allows the user to identify and decompose subpopulations (subpopulation decomposition is discussed in Wohletz et al., 1989) from a polymodal sample and to specify their SFT parameters by an optimization method as illustrated in Figs. 39 and 40. Fig. 41 from Wohletz et al. (1995) shows the variation of model transport processes with distance from the vent, variations that predict a facies distribution that can be tested by field observation.

Surge deposits represent only the portion of ejecta deposited near the vent. Nonetheless, whole-deposit grain size characteristics do reflect the total population of ejecta erupted. A test of this hypothesis by SFT is reported by Wohletz and Raymond (1993) for the

MISERS GOLD dust-lofting experiment, mentioned earlier in this manuscript. In this test, samples of the surge deposit (including ejecta and material swept-up from the substrate by the surge) were compared with samples representing the parental material ejected from the high-explosive cratering event. SFT analysis of these materials demonstrates that the surge deposits (as a whole) inherit the subpopulation character of the source (Fig. 42). This result indicates that the fragmentation mechanisms during an eruption control to a large part the grain-size subpopulations fed to a pyroclastic surge. If one assumes that these grain-size characteristics are important in determining depositional mechanisms (as discussed above), then one might conclude that eruptions involving different fragmentation mechanisms can produce pyroclastic surge deposits of different bedforms. Such an argument is especially attractive for interpretation of pyroclastic surge deposits consisting of a large portion of lithic constituents, derived from the host rocks excavated during eruption and crater formation. Furthermore, using SFT, one can make estimates of the total volume of pyroclastic ejecta from an eruption for which only a portion is deposited in pyroclastic surges. The estimate is based upon comparison of surge sample subpopulation fractions with samples of unsorted ejecta found near the crater, assumed to represent the bulk parental ejecta size distribution. Fig. 43 illustrates this comparison for the MISERS GOLD experiment for which the surge ejecta are depleted in finer subpopulations. This fraction of depleted material in the surge deposit represents the fraction of ejecta lofted into atmospheric suspension, giving an estimate of the total ejecta volume, an estimation found to be extremely accurate by aircraft sampling (Wohletz and Raymond, 1993). This method is similar to that proposed by Walker (1980) and has a great significance for commercial aviation in that it can predict the size distribution of atmospheric dust encountered by aircraft by analysis of that emplaced in surge deposits.

3.4. Wet and dry surges

Wohletz and Sheridan (1983) described wet and dry hydrovolcanic eruptions that produced pyroclastic surge deposits that are generally known as *wet* and *dry* surges, respectively (*e.g.*, Frazzetta et al., 1983; Dellino et al., 1990). Table 6 lists the characteristics of wet and dry surges; the main distinguishing characteristics are that dry surges generally show numerous well developed thin beds that are often poorly consolidated while wet surges typically have well indurated, poorly developed bedding and bedding that is dominated by massive bedforms (Fig. 44).

The origin of wet and dry surges stems from the thermodynamic state of steam incorporated in the surge as is moves from the vent. This state is typically referred to as hot and dry (superheated steam) or cool and wet (condensing saturated steam). In hydrovolcanic eruptions, steam generated by interaction of magma with water attains an initial thermodynamic state as a function of the amount of heat the water absorbs from the magma during eruption, largely determined by the water/magma mass ratio. For dry eruptions (water/magma ratio < 0.5), steam is superheated and expands during surge runout nearly isothermally, because of the large mass of hot solid particles relative to the mass of steam produced. Superheated steam is optically transparent, so that the surge has a dark color of the tephra it carries. On the other hand, for wet eruptions (water/magma ratio > 0.5), steam is nearly saturated after eruption and expands more adiabatically, cooling and condensing

during surge runout. The condensation process forms tiny water droplets that give surges a white color. While some of the steam may condense on particles deposited near the vent, much is carried along in the surge such that the surge becomes more humid with runout distance. Added to adiabatic cooling is cooling caused by entrainment of the relatively cool atmosphere, which enhances condensation as well as adding ambient moisture. Sparks et al. (1997) have extensively described condensation of moisture in volcanic plumes, which can lead to localized heavy precipitation. For surge eruptions, such precipitation can make cool surge deposits very wet.

Based upon observations of surge deposits at Vulcano (Frazzetta et al., 1983) in which dry surge deposits are more common near the vent and gradually change to wet surges with distance, there is the possibility that wet and dry facies distribution might constrain water/magma interaction ratios in hydrovolcanic eruptions. In the next section, I illustrate a hypothetical situation in which the rate of steam condensation might be calculated for pyroclastic surges (Fig. 45).

Condensation of steam in surges. If the amount of water exsolved during magmatic eruption or the water/magma ratio of a hydrovolcanic eruption is known, the thermodynamic state of that water just after eruption can be easily constrained (*e.g.*, Wohletz, 1986). Assume that during runout of a surge, steam pressure and temperature decrease through expansion and mixing with ambient (cool) air, leading to condensation of the steam. To get a semi-quantitative measure of the amount of steam condensation, one can attempt solution of the continuity equation:

$$\frac{\partial \rho_g}{\partial t} + \frac{\partial \left(\rho_g v_0 \right)}{\partial r} = J_d \quad , \tag{20}$$

where ρ_g = steam density, t = time, v_0 = initial surge velocity, and r = radial distance, and J_d represents the atmospheric gas source. One method for analytical solution, based on field evidence, involves expanding the temporal derivative (Wohletz and Heiken, 1992):

$$\frac{\partial \rho_g}{\partial t} = \frac{\partial \rho_g}{\partial \theta_p} \frac{\partial \theta_p}{\partial r} \frac{\partial r}{\partial N} \frac{\partial N}{\partial t} \quad , \tag{21}$$

where the right-hand-side terms show the multiplicative effects of the derivatives expressing (1) initial surge inflation by steam, (2) deflation with runout, (3) surge radius as a function of its volume, and (4) surge volume increase with expansion during runout, respectively. These derivatives are discussed in Appendix B.

The derivatives (Appendix B) shown on the right-hand-side of Eq. (21) can be numerically integrated with time to obtain solutions converging to equal the atmospheric gas sources, if any, minus the spatial derivative of the continuity equation [second term on left-hand-side of Eq. (20)]. An illustrative but very hypothetical example set of possible solutions are shown in Table 7. This example considers surges generated by hydrovolcanic eruptions of

several different water/magma ratios. These ratios determine the initial thermodynamic conditions of an erupted mixture of steam and hydroclasts as discussed by Wohletz and Heiken (1992). Because the initial surge velocities are not necessarily known for these eruptions, they can be approximated by two simple models of surge generation: (1) column collapse where collapse height h_c is constrained by the water/magma-ratio-limited explosive energy (Wohletz et al., 1995), and the initial surge velocity is equal to that determined by its gravitational potential energy from $v_0 = (2gh_c)^{1/2}$, and (2) blast conditions for which $v_0 = c_1$*, the bulk gas-dynamic sound speed from Eqs. (12) and (13). Additionally, two endmember thermodynamic conditions are assumed for the surges generated by these hydrovolcanic eruptions: adiabatic and isothermal expansion, which determine the volume fraction of liquid water erupted as described by Wohletz (1986). Results are illustrated in Figs. 46 - 49, for which divisions between dry surge, wet surge, and lahars are based on the deposit water fraction. These hypothetical results predict that blast-type eruptions can produce wetter deposits than do column collapse eruptions, because of their greater modeled initial velocities and runout distances.

3.5. Blast waves and pyroclastic surges

Volcanoes produce pyroclastic surges by column collapse, (directed) blast, and catastrophic slope failure (avalanche). As describe above the initial velocity of a surge is a function of collapse height and/or bulk sound speed. For runout of surges produced by column collapse and avalanche, the surge speed is essentially controlled by accelerations/decelerations along an energy line (Fig. 50; Malin and Sheridan, 1982). Blasts typically occur where the erupted tephra column is overpressured and forms a jet, as is typical for hydrovolcanic explosions and sudden release of near-surface, gas-charged magma. For blast eruptions (Fig. 51), the surge speed is controlled by gas expansion within a jet-like structure, in which shock waves form where the jet interacts with the environment (Kieffer, 1984).

In blast eruptions accompanied by pyroclastic surges, a leading bow-shock can rapidly propagate ahead and away from the emerging surge cloud, and multiple shock waves my migrate or stand within the flow. An important damage factor for such surge eruptions is the magnitude of these shock waves, which can impart sufficient dynamic pressure changes to the local environment to cause damage to structures. In general the strength of shock waves decrease with distance from their source (*e.g.*, Taylor, 1950). Using the analysis for shock propagation described by Chisnell (1957), Fig. 52 shows a model of shock-wave dissipation as a function of shock strength ($Y = p_{shock}/p_{atm}$). An interesting aspect of shock waves is that even very weak shocks ($Y \approx 0.1$) produce sound pressures well above the human threshold of pain (~120 dB). While blast eruptions of similar size as that of the 1980 Mount St. Helens blast produce shocks that decay to very low levels within 10 km of the vent, surges associated with very large caldera eruptions with overpressures approaching 10 MPa may propagate shock waves that can cause serious damage for many tens of km from the vent.

Shock waves are accompanied by discontinuous changes in flow speed, density and temperature. For mixtures of gas and particulates, finite relaxation times produce shock waves

of finite thickness, causing departure from ideal behavior. However, that departure is not thought to be too significant to approximate shock-wave effects from conservation equations known as the *Rankine-Hugoniot* equations (*e.g.*, Zel'dovich and Razier, 1966; Shapiro, 1953). These equations are:

$$\rho_0 U = \rho_1 (U - u) \qquad \text{(Mass - 22)}$$

$$mu = \left(p_1 - p_0 \right) \qquad \text{(Momentum - 23)}$$

$$\rho_0 U + mE_0 + \tfrac{1}{2} mU^2 = \rho_1 (U - u) + mE_1 + \tfrac{1}{2} m(U - u)^2 \qquad \text{(Energy - 24)}$$

where ρ = density, u = velocity, U = shock velocity, m = mass, E = internal energy, and subscripts 0 and 1 denote unshocked and shocked states.

Solution of the Rankine-Hugoniot equations, using the Riemann invariant for free expansion, following Wohletz and Valentine (1990), yields algebraic expressions for the 1-D flow field in which the shock strength is given by shock strength Y = p_1 / p_0 and ψ is the limit of isentropic expansion given by (β - 1) / (β + 1):

$$\mathbf{M} = \frac{U}{c_0} = \left(\frac{\mathrm{Y} + \psi}{1 + \psi} \right)^{1/2} \quad , \qquad \text{(Mach Number - 25)}$$

$$u = c_0 \frac{\left(1 - \psi\right)\left(\mathrm{Y} - 1\right)}{\left[\left(1 + \psi\right)\left(\mathrm{Y} + \psi\right)\right]^{1/2}} \quad , \qquad \text{(Flow Speed - 26)}$$

$$\rho = \rho_0 \left(\frac{\psi + \mathrm{Y}}{1 + \psi \mathrm{Y}} \right) \quad , \qquad \text{(Flow Density - 27)}$$

$$T = T_0 \left(\frac{\mathrm{Y}\left(1 + \psi \mathrm{Y}\right)}{\psi + \mathrm{Y}} \right) \quad . \qquad \text{(Shock Temperature - 28)}$$

Values for these shock-wave effects are plotted in Fig. 53 as a function of shock overpressure, from which one can see that modest shock overpressures of 0.4 to 0.6 MPa are sufficient to raise temperature to that of cellulose ignition; however, I do not know if charred materials have ever been attributed to volcanic shock waves. A simplified approach to calculating the dissipation of these blast wave properties as a function of explosive yield in kilotons (1 kt = 4.2×10^{12} J = thermal energy contained in ~ 3.5×10^{9} kg magma) is given in

Glasstone and Dolan (1977). Using the 18 May 1980 eruption of Mount St. Helens as an example, Fig. 54 shows the dissipation of blast wave effects with range from the vent for this blast, which Kieffer (1981) estimated at ~7 Mt. Blast overpressures (0.04 MPa at 10 km and 0.002 MPa at 50 km) empirically predicted by this method are several times higher than those Kieffer (1981) theoretically predicted, which likely reflects the difference of an idealized explosive source from that of a volcano. In summary, Fig. 55 illustrates a schematic representation of one possible volcanological situation for blast-drive surges.

4. Conclusions: surges are hazardous but economically significant

The concept of pyroclastic surge developed from analogies to the base surge in underground/underwater, man-made explosions. Especially in nuclear explosions, the base surge was recognized as one of the most devastating components of large near-surface explosions, not only because of its ability to spread radioactive debris, but also its blast-wave qualities that impart high dynamic pressures and accelerations upon obstacles such as buildings and other manmade structures. Similarly pyroclastic surges are very devastating. But due to their evanescence and the relatively sparse deposits they leave, there is little in the geologic record that helped geologists recognize the severity of pyroclastic surges during explosive eruptions.

Pyroclastic surges originate by directed blast, column collapse, debris avalanche, jetting and surging flow at the fronts of pyroclastic flow, turbulent eleutriation and transport of ash from the tops of pyroclastic flows, and likely other volcanic events where highly unsteady flow dominates. Surges display a multitude of bedforms and depositional textures, indicative of transport and/or deposition from a density current with properties spanning laminar to turbulent regimes. Temporal and spatial variations in surge deposits lead to great complexity in efforts to characterize them. Because of this complexity, facies designations are a convenient way to characterize and interpret the evolution of surge deposits.

Important to understanding the mechanism of surges is the fact that they involve the high-speed flow of a compressible mixture of gas and solid particles in a situation where shock waves develop and propagate. This transport and depositional regime leads to deposits analogous to submarine and fluvial sediments; however surge deposits result from transport and depositional mechanisms very different from those of conventional sediments. Fluid dynamic theory and laboratory experiments for pyroclastic surges have not been extensively developed, but nonetheless hold promise for better understanding the origin of the deposits, under what circumstances surges form, how they evolve during runout, and when and where they might strike. From the standpoint of field analysis of surge deposits, this author recommends studies aimed at compiling quantitative data, data that may eventually be used and interpreted despite the ever-changing theoretical frameworks that are in popular usage. One example of such data is granulometry for which sequential fragmentation/transport analysis promises results based upon a firm physical basis and affording many different interpretive schemes.

Pyroclastic surges may be difficult to distinguish from aqueous sediments, but their

discrimination is of utmost importance to recognizing volcanic hazards (*e.g.*, McPhie et al., 1990). Eruptive phases that involve pyroclastic surge generation may be relatively infrequent at volcanoes that otherwise display less hazardous activity such as lava-flow emplacement. Such infrequency combined with the fact that volumetrically, surge deposits are rather small compared with other volcanic products, is the scenario in which their devastating effects might be easily overlooked during hazard analysis. Examples of such historic situations include Volcano Island eruptions at Taal in the Philippines and Mount St. Helens where prior to its 1980 eruptions, surges were not documented (Crandell et al., 1975).

Despite the hazardous nature of pyroclastic surges, they provide beneficial aspects of economic significance. Some examples of economical significance include:

- Pyroclastic surge eruptions can be associated with hydrothermal events that produce ore carrying fluids, and this association lends insight into ore mineralization processes (*e.g.*, Branch 1976).
- Pyroclastic surges act as hosts for ore mineralization (*e.g*, Nelson and Giles 1985; Christiansen et al., 1986).
- Surge eruptions excavate craters and fracture host rocks, resulting in development of the necessary fracture permeability for hydrothermal systems and ore deposition (*e.g.*, Wohletz and Heiken 1992).
- Distribution of lithic materials in surge deposits allow reconstruction of the sub-crater host rock stratigraphy and alteration regime (*e.g.*, Funiciello et al. 1976), information that can potentially save exploratory drilling costs.
- The existence of profitable geothermal systems is more probable where wet pyroclastic surges are erupted (Wohletz and Heiken 1992).

Appendix A: Origin of the SFT Equations

Solution of the fragmentation equation. The most important assumption in SFT is that the physical mechanisms of fragmentation are mass sensitive—that is the physical equations that express fragmentation are dependent upon mass as a fundamental variable. This assumption is implicit in formulation of the Navier-Stokes equations for which mass is a primary variable. For fragmentation processes, this mass sensitivity can be expressed as a transfer function $f(m' \rightarrow m)$, which models the production of an ensemble of daughter particles by the breakup of a parental mass [note that the symbol $m' \rightarrow m$ in this transfer function denotes the formation of a daughter particle of mass m from a parental particle of mass m']. Brown (1989) gives background and analysis to show that this transfer function has a power-law form, which proves to be adequate for describing most fragmentation mechanisms:

$$f(m' \rightarrow m) = \left(\frac{m}{m_1} \right)^{\gamma} \quad , \tag{A-1}$$

where m_1 is a normalizing mass and the exponent ($\gamma > -1$) is the measure of mass sensitivity of the fragmentation process. *Sudden* fragmentation processes (explosive blasts) have few sequential steps and $\gamma \approx -1$, but repeated comminution such as occurs during surge transport have higher values of γ With this transfer function, SFT conserves mass over any number of sequential steps in a single or multiple fragmentation event.

The basic formulation of sequential fragmentation (Brown, 1989) portrays how a large parental mass is broken down to small daughter populations of fragments (Fig. A-1):

$$n(m) = c \int_{m}^{\infty} n(m') f(m' \rightarrow m) dm' \quad , \tag{A-2}$$

where $n(m)$ is the number of particles of mass m arising from a parental ensemble of particle $n(m')$. Exact solutions (Brown, 1989; Wohletz et al., 1989) show a power-law behavior for larger particles of the distribution and an exponential decay in number with increasing fineness (Fig. A-2):

$$n(m) = \frac{N_T}{m_1}\left(\frac{m}{m_1}\right)^{\gamma} \exp\left[\frac{\left(m/m_1\right)^{\gamma+1}}{\gamma+1}\right] \quad , \tag{A-3}$$

$$m^2 n(m) = N_T m_1 \left(\frac{m}{m_1}\right)^{\gamma+2} \exp\left[-\frac{\left(m/m_1\right)^{\gamma+1}}{\gamma+1}\right] \quad . \tag{A-4}$$

In these solutions N_T is the total number of fragments in a sample population and the value $m^2 n(m)$ is the mass of particles for logarithmically spaced bins of size m to $m + dm$.

Solution of the transport equation. As a particle population is transported, it is sorted by the mass sensitivity of the transporting agent in a sequential fashion from one incremental location to the next to its final rest position. The probability that a given particle of mass m is deposited at some position x is $p(\xi)dx = dx/\xi$, where, similar to fragmentation, the transporting function ξ is mass sensitive (*e.g.*, drag law functions) by a power-law (Wohletz et al., 1989):

$$\xi = \xi_0 \left(\frac{m}{m_1}\right)^{-\gamma} \quad . \tag{A-5}$$

Conserving mass and momentum, the sequential transport equation (Wohletz et al., 1989) combines both integration over mass m and distance x (Fig. A-3):

$$n(x,m) = c_2 \int_0^m \int_{x-\xi}^0 n(x',m)\, p(\xi) dx'\, dm' \quad . \tag{A-6}$$

Integration provides an inexact solution, but the solution is exact for the range of parameters in nature, where γ is analogous to sorting (dispersion):

$$m^2 n(x,m) \cong W\left(\frac{m}{m_1}\right)^2 \exp\left[-\left(\frac{x}{\xi_o}\right)\frac{\left(m/m_1\right)^{\gamma+1}}{\gamma+1}\right] \quad , \tag{A-7}$$

for which *W* is a normalizing constant. Converting logarithmic mass to size via the common phi transformation, one has a distribution useful for sieve data:

$$\frac{d\mathbf{M}}{d\phi} = W\ell^6 \exp\left[-\frac{x}{\xi_o}\frac{\ell^{3(\gamma+1)}}{\gamma+1}\right] \quad , \tag{A-8}$$

for which **M** is the total mass retained in a size bin (*e.g.*, sieve weight).

Noting that particles are of various shapes and densities, the conversion of mass to size is achieved by:

$$m = \frac{4}{3}\pi S\rho\left(\frac{\ell}{2}\right)^3 \quad , \tag{A-9}$$

where the particle diameter is ℓ and $S = P_a^2/(4\pi A)$ is the common shape factor. Taking the derivatives of shape and density in Eq. (A-9) shows that the mass distribution must be multiplied by three terms:

$$\frac{d\mathbf{M}}{d\phi} = -m^2 n(x,m)\left[3\ln(2) + \frac{dS}{S\,d\phi} + \frac{d\rho}{\rho\,d\phi}\right] \quad . \tag{A-10}$$

The resulting solution shows that typical pyroclastic samples will consist of several subpopulations, reflecting the effects of shape and density:

$$\frac{d\mathbf{M}}{d\phi} = W\ell^6 \exp\left[-\frac{\ell^{3(\gamma+1)}}{\gamma+1}\right] + W_S\ell^6 \exp\left[-\frac{\ell^{3(\gamma_S+1)}}{\gamma_S+1}\right] + W_\rho\ell^6 \exp\left[-\frac{\ell^{3(\gamma_\rho+1)}}{\gamma_\rho+1}\right] \tag{A-11}$$

In Eq. (A-11), the values *W*, W_S, and W_ρ describe the subpopulation fractions for a given fragmentation mechanism, shape effects, and density effects, respectively. In application to surge deposit samples, subpopulations also arise from the various transportation mechanisms, each acting on a particular shape/density subpopulation, such that a sample might show

several subpopulations, each with a particular W and γ value that reflect the cumulative effect of transport modes discussed above.

Appendix B: Analysis of Surge Steam Condensation

The four derivatives on the right-hand side of Eq. (21) can be expanded by considerations of bulk density and thermodynamic relationships as well as field constraints. These derivatives express (1) initial surge inflation by steam, (2) deflation with runout, (3) surge radius as a function of its volume, and (4) surge volume increase with expansion during runout, as described below.

(1) The initial surge inflation by steam upon eruption can be related to particle volume concentration θ_p, a measure of its degree of effective fluidization (Wohletz and Sheridan, 1979). Since θ_p determines the surge's bulk density by $\rho_b = \theta_p\rho_p + (1 - \theta_p)\,\rho_g$, the gas density ρ_g must vary with θ_p:

$$\frac{\partial \rho_g}{\partial \theta_p} = \frac{\rho_b - \rho_p}{\left(1-\theta_p\right)^2} \quad . \tag{B-1}$$

(2) Radial deflation [steam condensation and segregation from the surge (Woods and Bursik, 1994)] is assumed to proceed linearly with time until the particle concentration reaches that of a fixed bed (0.6) at the final runout time t_f such that $\partial\theta_p/\partial t = (0.6 - \theta_p)/t_f$. Assuming that surge deceleration a from an initial velocity v_0 is constant during runout over distance r, the derivative θ_p with respect to r is:

$$\frac{\partial \theta_p}{\partial r} = \frac{\left(0.6-\theta_p\right)a / v_0}{\left(v_0^2 - 2ar\right)^{1/2}} \quad . \tag{B-2}$$

(3) As commonly observed (*e.g.*, Wohletz and Sheridan, 1979) surge runout distance increases with surge volume. This relationship can be expressed by noting that the bulk volume V of a surge cloud is related to its bulk density ρ_b by $V = [\rho_b + (\rho_{max} - \rho_b)r/r_f\,]^{-1}$ where ρ_{max} is that of a fixed bed (taken at 1.5 Mg/m^3), which occurs at maximum runout r_f where the surge comes to a halt. Accordingly, one may express this relationship by the derivative:

$$\frac{\partial r}{\partial V} = \frac{-r_f\left[\rho_b + \left(1.5-\rho_b\right)r / r_f\right]^2}{1.5-\rho_b} \quad . \tag{B-3}$$

(4) Since the surge volume is directly proportional to the steam volume, one can assume ideal gas behavior by $V = (\kappa/p)^{1/\beta}$ where V is volume, κ = constant; p is pressure, and β is the isentropic exponent, a function of θ_p (Eq. 11). The derivative of this state equation with time is complicated by the fact that p and θ_p are a functions of runout time. For

simplicity, the steam pressure is assumed to decrease linearly with time during deceleration of the surge:

$$\frac{\partial V}{\partial t} = \left[\ln\left(\frac{\kappa}{p}\right)\right]\left(\frac{\kappa}{p}\right)^{1/\beta}\left[\frac{1-1/\beta}{2\theta_p\left(\ln\theta_p\right)^2}\right]\left[\frac{\left(0.6-\theta_p\right)a/v_0}{\left(v_o^2-2ar\right)^{1/2}}\right]\left[v_0+at\right] + \left(1/\beta\right)\left(\kappa/p\right)^{(1-\beta)/\beta}\left\{\frac{\kappa\left(p_{atm}-p\right)a/v_0}{\left[p-\left(p-p_{atm}\right)at/v_0\right]^2}\right\} \quad \text{(B-4)}$$

Acknowledgments

Shinji Takarada and Alexis Lavine provided thoughtful and helpful reviews of initial versions of this manuscript. Marcus Bursik and Tak Koyaguchi greatly improved the presentation of the theoretical discussions. This work was done under the auspices of the U.S. Department of Energy.

References

Allen, J.R., 1984. Sedimentary structures, their character and physical basis. Elsevier, Amsterdam, 663 pp.

Anderson, R.S. and Hallet, B., 1986. Sediment transport by wind: toward a general model. Geol. Soc. Amer. Bull. 97: 523-535.

Bagnold, R.A., 1941. The physics of blown sand and desert dunes. Methuen, London, 265 p.

Bagnold, R.A., 1954. Experiments on a gravity-free dispersion of large solid spheres in a Newtonian fluid under shear. Proc. Roy. Soc., A255: 49-63.

Bagnold, R.A., 1955. Some flume experiments on large grains but little denser than the transporting fluid, and their implications. Inst. Civil Eng. Proc., Part 3 Paper No. 6041: 174-205.

Bouma, A.H., 1962. Sedimentology of some flysch deposits: a graphic approach to facies interpretation. Elsevier, Amsterdam.

Branch C.D. (1976) Development of porphyry copper and stratiform volcanogenic ore bodies during the life cycle of andesitic stratovolcanoes. In: R.W. Johnson (Editor), Volcanism in australasia, Elsevier Sci Pub, Amsterdam, 337-342.

Braney, M.J. and Kokelaar, P., 1992. A reappraisal of ignimbrite emplacement: progressive aggradation and changes from particulate to non-particulate flow during emplacement of high-grade ignimbrite. Bull. Volcanol., 54: 504-502.

Brinkley Jr., S.R., Kirkwood, J.G., Lampson, C.W., Revelle, R., and Smith, S.B., 1950. Shock from underwater and underground blasts. In: The effects of atomic weapons, Los Alamos Scientific Laboratory, Los Alamos New Mexico.

Brown, W. K., 1989. A theory of sequential fragmentation and its astronomical applications, J. Astrophys. Astron., 10: 89-112.

Brown, W.K. and Wohletz, K.H., 1995. A derivation of the Weibull distribution based on physical principles and its connection to the Rosin-Rammler and the lognormal distributions. J. Appl. Phys., 78(4): 2758-2763.

Campbell, C.S. and Brennen, C.E., 1985. Computer simulation of granular shear flow. J. Fluid Mech., 151: 167-188.

Carlson, R.H. and Roberts, W.A., 1963. Project Sedan mass distribution and throwout. The Boeing Company, Seattle, Washington, PNE-217F, 144 pp.

Carey, S.N., 1991. Transport and deposition of tephra by pyroclastic flows and surges. In: R.V. Fisher and G.A. Smith (Editors), Sedimentation in volcanic settings, Soc. Sedimen. Geol. (SEPM) Spec. Pub., 45: 39-57.

Carey, S.N., Sigurdsson, H., and Sparks, R.S.J., 1988. Experimental studies of particle-laden plumes. J. Geophys. Res., 93: 15314-15328.

Cas, R.A.F. and Wright, J.V., 1987. Volcanic Successions: Modern and Ancient. Allen and Unwin, London, 528 pp.

Chisnell, R.F., 1957. The motion of a shock wave in a channel, with applications to cylindrical and spherical shock waves. J. Fluid Mech., 2: 286-298.

Christiansen, E.H., Sheridan, M.F., and Burt, D.M., 1986. The geology and geochemistry of Cenozoic topaz rhyolites from the western United States. Geol. Soc. Amer. Spec. Pap., 205: 82 pp.

Crandell, D.W., Mullineaux, D.R., and Rubin, M., 1975. Mount St. Helens volcano: recent and future behavior. Sci., 187: 438-441.

Crisci, G.M., De Rosa, R., Lanzafame, G., Mazzuoli R., Sheridan, M.F., and Zuffa, G.G., 1981. Monte Guardia sequence: a late-Pleistocene eruptive cycle on Lipari (Italy). Bull. Volcanol., 44-3: 241-255.

Crowe, B.M. and Fisher, R.V., 1973. Sedimentary structures in base-surge deposits with special reference to cross-bedding, Ubehebe Craters, Death Valley, California. Geol. Soc. Amer. Bull., 84: 663-682.

Dellino, P., Frazzetta, G., and La Volpe, L., 1990. Wet surge deposits at La Fossa di Vulcano: depositional and eruptive mechanisms. J. Volcanol. Geotherm. Res., 43: 215-233.

Drake, T.G., 1990. Structural features in granular flows. J. Geophys. Res., 95(B1): 8681-8696.

Fisher, R.V., 1968. Puu Hou littoral cones, Hawaii. Geol. Rundsch., 57: 837-864.

Fisher, R.V., 1977. Erosion by volcanic base-surge density currents: U-shaped channels. Geol. Soc. Amer. Bull., 88: 1287-1297.

Fisher, R.V., 1979. Models for pyroclastic surges and pyroclastic flows. J. Volcanol. Geotherm. Res., 6: 305-318.

Fisher, R.V., 1983. Flow transformations in sediment gravity flows. Geol., 11: 273-274.

Fisher, R.V. 1990. Transport and deposition of a pyroclastic surge across an area of high relief: the 18 May 1980 eruption of Mount St. Helens, Washington. Geol. Soc. Amer. Bull., 102: 1038-1054.

Fisher, R.V. and Heiken, G., 1982. Mt. Pelée, Martinique: May 8 and 20, 1902 pyroclastic flows and surges. J. Volcanol. Geotherm. Res., 13: 339-371.

Fisher, R.V. and Schmincke, H-U., 1984. Pyroclastic Rocks. Springer-Verlag, Berlin, 472 pp.

Fisher, R.V. Schmincke, H-U., and Bogaard, P., 1983. Origin and emplacement of a pyroclastic flow and surge unit at Laacher See, Germany. J. Volcanol. Geotherm. Res., 17: 375-392

Fisher, R.V., Smith, A.L., and Roobol, M.J., 1980. Destruction of St. Pierre, Martinique by ash cloud surges, May 8 and 20, 1902. Geol., 8: 472-476.

Fisher, R.V. and Waters, A.C., 1969. Bedforms in base-surge bed deposits: Lunar implications. Sci., 165: 1349-1352.

Fisher, R.V. and Waters, A.C., 1970. Base-surge bed forms in maar volcanoes. Amer. J. Sci., 268: 157-180.

Frazzetta, G., La Volpe, L., and Sheridan, M.F., 1983. Evolution of the Fossa cone, Vulcano. J. Volcanol. Geotherm. Res., 17: 329-360.

Funiciello, R., Locardi, E., Lombardi, G., and Parotto, M., 1976. The sedimentary ejecta from phreatomagmatic activity and their use for location of potential geothermal areas. Intern. Congr. Therm. Waters, Geotherm Energy and Volcanology of the Mediterranean area, Athens.

Ghosh, J.K., Mazumder, B.S., Saha, M.R., and Sengupta, S., 1986. Depostion of sand by suspension currents: Experimental and theoretical studies. J. Sed. Pet., 56: 57-66.

Glasstone, S. and Dolan, P.J., 1977. The effects of nuclear weapons, U.S. Dept. of Defense and U.S. Energy Res. Develop. Admin., U.S. Gov. Printing Office, Washington, D.C, third edition, 653 pp.

Greeley, R., Marshall, J.R., and Leach, R.N., 1984. Microdunes and other aeolian bedforms on Venus: wind tunnel simulations. Icarus, 60: 152-60.

Gutmann, J.T. and Sheridan, M.F., 1978. Geology of the Pinacate volcanic field. In: D.M. Burt, and T.L. Péwé (Editors), Guidebook to the Geology of Central Arizona, Ariz. Bur. Geol. Min. Tech. Spec. Pap., 2: 47-59.

Hack, J.I., 1942. Sedimentation and volcanism in the Hopi Buttes, Arizona. Geol. Soc. Amer. Bull., 53: 335-372.

Haff, P.K., 1986. A physical picture of kinetic granular fluids. J. Rheol., 30(5): 931-948.

Harlow, F.H. and Amsden, A.A., 1975. Numerical calculation of multiphase fluid flow. J. Comput. Phys., 17: 19-52.

Hoblitt, R.P., Miller, C.D., and Vallance, J.W., 1981. Origin and stratigraphy of the deposit produced by the May 18 directed blast. In: P.W. Lipman and D.R. Mullineaux (Editors), The 1980 eruptions of Mount St. Helens, Washington, U.S. Geol. Survey Prof. Paper, 1250: 401-420.

Hui, K. and Haff, P.K., 1986. Kinetic grain flow in a vertical channel. Int. J. Multiphase Flow, 12: 289-298.

Hwang, C.C., 1986. Initial stages of the interaction of a shock wave with a dust deposit. Int. J. Multiphase Flow, 12: 655-666.

Ishikawa, Y., Hatno, H., and Shirai, T., 1991. Mechanism of pyroclastic flow, its numerical simulation method, and measures. Tech. Memo. PWRI 3005 :73 pp. (in Japanese with English abstract).

Johnson, S M., 1971. Explosive excavation technology. Lawrence Radiation Laboratory report AD-727 651: 229 pp.

Kieffer, S.W., 1981. Fluid dynamics of the May 18 blast at Mount St. Helens. U.S. Geol. Surv. Prof. Pap., 1250: 379-400.

Kieffer, S.W., 1982. Dynamics and thermodynamics of volcanic eruptions: Implications for the plumes on Io. In: D. Morrison (Editor), Satellites of Jupiter, University of Arizona Press, 647-723.

Kieffer, S.W., 1984. Factors governing the structure of volcanic jets. In: F.R. Boyd (Editor), Explosive volcanism: inception, evolution, and hazards, Studies in Geophysics, National Academy Press, Washington, 143-157.

Kieffer, S. W., 1989. Geologic Nozzles. Rev. Geophys., 27(1): 3-38.

Kieffer, S.W. and Sturtevant, B., 1986. Erosional furrows formed during the lateral blast at Mount St. Helens, May 18, 1980: indicators of longitudinal vortices in the boundary layer. Abstr. Intl. Volcanol. Cong., New Zealand, 53.

Kneller, B., 1995. Beyond the turbidite paradigm: physical models for deposition of turbidites and their implications for reservoir prediction. In: A.J. Hartley and D.J. Prosser (Editors), Characterization of deep marine clastic systems, Geol. Soc. Spec. Pub. 94, 31-49.

Kranck, K. and Milligan, T.G. 1985. Origin of grain size spectra of suspension deposited sediment. Geo-Marine Let., 5: 61-66.

Krinsley, D., Greeley, R., and Pollack, J.B., 1979. Abrasion of windblown particles on Mars—erosion of quartz and basaltic sand under simulated Martian conditions. Icarus, 39: 364-384.

Kuntz, M.A., Rowley, P.D., MacLeod, N.S., Reynolds, R.L., McBroome, L.A., Kaplan, A.M., and Lidke, D.J., 1981. Petrography and particle-size distribution of pyroclastic flow, ash-cloud, and surge deposits. In: P.W. Lipman and D.R. Mullineaux (Editors), The 1980 eruptions of Mount St. Helens, Washington, U.S. Geol. Survey Prof. Paper, 1250: 525-540.

Lin, J.-T. and Pao, Y.-H., 1979. Wakes in stratified fluids. Ann. Rev. Fluid Mech., 11: 317-338.

Lowe, D.R. 1982. Sediment gravity flows: II. Depositional models with special reference to the deposits of high-density turbidity currents. J. Sedimen. Petrol., 52: 279-297.

Malin, M.C. and Sheridan, M.F., 1982. Computer-assisted mapping of pyroclastic surges. Sci., 217: 637-640.

Marble, F.E., 1970. Dynamics of dusty gas. Ann. Rev. Fluid. Mech., 2: 397-446.

Mattson, P.H. and Alavarez, W., 1973. Base surge deposits in Pleistocene volcanic ash near Rome. Bull. Volcanol., 37: 553-571.

McPhie, J., Walker, G.P.L., and Christiansen, R.L., 1990. Phreatomagmatic and phreatic fall and surge deposits from explosions at Kilauea volcano, Hawaii, 1790 A.D.: Keanakakoi ash member. Bull. Volocanol., 52: 334-354.

Middleton, G.V. and Southard, J.B., 1978. Mechanics of sediment movement. Soc. Econ. Paleontol. Mineral. Short Course 3, Eastern Section, 6.37-6.41.

Moore, J.G., 1967. Base surge in recent volcanic eruptions. Bull. Volcanol., 30: 337-363.

Moore, J.G. and Sisson, T. W., 1981. Deposits and effects of the May 18 pyroclastic surge. U.S. Geol. Surv. Prof. Pap., 1250: 421-438.

Morimoto, R., 1959. Submarine eruption of the Myôjin reef. Bull. Volcanol., 23: 151-160.

Nelson, C.E. and Giles, D.L., 1985. Hydrothermal eruption mechanisms and hot spring gold deposits. Econ. Geol. 80: 1663-1639.

Nordyke, M.D., 1961. On cratering: a brief history, analysis, and theory of cratering. Univ. Calif. Lawrence Rad. Lab., Livermore, California, UCRL-6578, 72 pp.

Richards, A.F., 1959. Geology of the Islas Revillagigedo, Mexico, 1. Birth and development of Volcán Bárcena, Isla San Benedicto (1). Bull. Volcanol., 2(22): 73-123.

Robin, C., Komorowski, J.-C., Boudal, C., and Mossand, P., 1990. Mixed-magma pyroclastic surge deposits associated with debris avalanche deposits at Colima volcanoes, Mexico. Bull. Volcanol., 52: 391-403.

Sagan, C. and Bagnold, R.A., 1975. Fluid transport on Earth and aeolian transport on Mars. Icarus, 26: 209-218.

Savage, S.B., 1979. Gravity flow of cohesionless granular materials in chutes and channels. J. Fluid. Mech., 92: 53-96.

Schmincke, H.-U., Fisher, R.V., and Waters, A.C., 1973. Antidune and chute and pool structures in the base surge deposits of the Laacher See area, Germany. Sediment., 20: 553-574.

Self, S. and Sparks, R.S.J., 1978. Characteristics of widespread pyroclastic deposits formed by the interaction of silicic magma and water. Bull. Volcanol., 41(3): 196-212.

Self, S., Kienle, J., and Huot, J.P., 1980. Ukinrek maars, Alaska, II. Deposits and formation of the 1977 craters. J. Volcanol. Geotherm. Res., 7: 39-65.

Shapiro, A.H., 1953. The dynamics and thermodynamics of compressible fluid flow, Vol. I. Wiley, New York, 647 pp.

Shoemaker, E.M., 1957, Primary structures of maar rims and their bearing on the origin of Kilbourne Hole and Zuni Salt Lake, New Mexico (Abstract). Geol. Soc. Amer. Bull., 68: 1848.

Shultz, P.H. and Gault, D.E., 1979. Atmospheric effects on Martian ejecta emplacement. J. Geophys. Res., 84: 7669-7687.

Sheridan, M.F., 1979. Emplacement of pyroclastic flows: a review. Geol. Soc. Amer. Spec. Pap. 180: 125-136.

Sheridan, M.F. and Updike, R.G., 1975. Sugarloaf Mountain tephra–a Pleistocene rhyolitic deposit of base-surge origin in northern Arizona. Geol. Soc. Amer. Bull., 86: 571-581.

Sheridan, M.F. and Wohletz, K.H., 1983. Hydrovolcanism: basic considerations and review. J. Volcanol. Geotherm. Res., 17: 1-29.

Sohn, Y.K., 1997. On traction-carpet sedimentation. J. Sedimen. Res., 67: 502-509.

Sohn, Y.K. and Chough, S.K., 1989. Depositional processes of the Suwolbong tuff ring, Cheju island (Korea). Sediment., 36: 837-855.

Sohn, Y.K. and Chough, S.K. 1992. The Illchulbong tuff cone, Cheju Island, South Korea: depositional processes and evolution of an emergent, Surtseyan-type tuff cone. Sediment., 39: 523-544.

Sparks, R.S.J., 1976. Grain size variations in ignimbrites and implications for the transport of pyroclastic flows. Sedimen., 23: 147-188.

Sparks, R.S.J. and Walker, G.P.L. 1973. The ground surge deposit: a third type of pyroclastic rock. Nature, 241: 62-64.

Sparks, R.S.J., Bursik, M.I., Carey, S.N., Gilbert, J.S., Glaze, L.S., Sigurdsson, H., and Woods, A.W., 1997. Volcanic plumes. John Wiley & Sons, New York, 574 pp.

Taylor, Sir G., 1950. The formation of a blast wave by a very intense explosion I. Theoretical discussion. Proc. Roy. Soc., A201: 159-174.

Travis, J.R., Harlow, F.H., and Amsden, A.A., 1975. Numerical calculation of two-phase flows. Los Alamos National Laboratory manuscript LA-5942-MS, Los Alamos, NM, 20 pp.

Valentine, G.A., 1987. Stratified flow in pyroclastic surges. Bull. Volcanol., 49: 616-630.

Valentine, G.A., 1988. Field and theoretical aspects of explosive volcanic transport processes. Los Alamos National Laboratory Thesis LA-11441-T, Los Alamos, New Mexico, 216 pp.

Valentine, G.A., Buesch, D., and Fisher, R.V., 1989, Basal layered deposits of the Peach Springs Tuff, northwestern Arizona, USA. Bull. Volcanol., 51: 395-414.

Valentine, G.A. and Fisher, R.V., 1986. Origin of layer 1 deposits in ignimbrites. Geol., 14: 146-148.

Valentine, G.A., and Wohletz, K.H., 1989, Numerical models of Plinian eruption columns and pyroclastic flows: Journal of Geophysical Research, v. 94, p. 1867-1887.

Walker, G.P.L., 1980. The Taupo Pumice: product of the most powerful known (ultraplinian) eruption? J. Volcanol. Geotherm. Res., 8: 69-94.

Walker, G.P.L., 1984. Characteristics of dune-bedded pyroclastic surge bedsets. J. Volcanol. Geotherm. Res., 20: 281-296.

Walton, O.R., and Braun, R.L., 1986. Viscosity, granular-temperature, and stress calculations for shearing assemblies of inelastic, frictional disks. J. Rheol., 30(5): 949-980.

Waters, A.C. and Fisher, R.V., 1971. Base surges and their deposits: Capelinhos and Taal Volcanoes. J. Geophys. Res., 76: 5596-5614.

Wilkes, D., 1946. Bikini breath of death. Sci. New Let., 50: 84.

Wohletz, K.H., 1977. A model of pyroclastic surge. M.Sc. Thesis, Arizona State Univ., Tempe, AZ, 174 pp.

Wohletz, K.H., 1983. Mechanisms of hydrovolcanic pyroclast formation: grain-size, scanning electron microscopy, and experimental results. J. Volcanol. Geotherm. Res., 17: 31-63.

Wohletz, K.H., 1986. Explosive magma-water interactions: thermodynamics, explosion mechanisms, and field studies. Bull. Volcanol., 48: 245-264.

Wohletz, K. H., 1987. Chemical and textural surface features of pyroclasts from hydrovolcanic eruption sequences. In: J.R. Marshall (Editor), Clastic Particles, Van Nostrand Reinhold Company Inc., New York, 79-97.

Wohletz, K.H. and Heiken, G., 1992. Volcanology and Geothermal Energy. University of California Press, Berkeley, California, 432 pp.

Wohletz K and Krinsley, D, 1982, Scanning electron microscopy of basaltic hydromagmatic ash. Los Alamos National Laboratory Report, LA-UR 82-1433, 43 pp.

Wohletz, K.H., McGetchin, T.R., Sandford II, M.T., and Jones, E.M., 1984. Hydrodynamic aspects of caldera-forming eruptions: numerical models. J. Geophys. Res., 89: 8269-8285.

Wohletz KH, McQueen RG, and Morrissey M, 1995, Analysis of fuel-coolant interaction experimental analogs of hydrovolcanism, In: *Intense Multiphase Interactions* (T G Theofanous and M Akiyama, Eds.) Proceedings of US (NSF) Japan (JSPS) Joint Seminar, Santa Barbara, CA, June 8-13, 1995, 287-317.

Wohletz, K.H., Orsi, G., and de Vita, S. 1995. Eruptive mechanisms of the Neapolitan Yellow Tuff interpreted from stratigraphy, chemistry, and granulometry. J. Volcanol. Geotherm. Res., 67: 263-290.

Wohletz, K.H. and Raymond Jr., R., 1993. Atmospheric dust dispersal analyzed by granulometry of the MISERS GOLD event. J. Geophys. Res., 98: 557-566.

Wohletz, K.H. and Sheridan, M.F. 1979. A model of pyroclastic surge. Geol. Soc. Amer. Spec. Pap., 180: 177-193.

Wohletz, K.H. and Sheridan, M.F., 1983. Hydrovolcanic explosions II. Evolution of basaltic tuff rings and tuff cones. Amer. J. Sci., 283: 385-413.

Wohletz, K.H., Sheridan, M.F., and Brown, W.K., 1989. Particle size distributions and the sequential fragmentation/transport theory applied to volcanic ash. J. Geophys. Res., 94: 15,703-15,721.

Woods, A.W. and Bursik, M.I., 1994. A laboratory study of pyroclastic flows. J. Geophys. Res., 99: 4375-4394.

Yamamoto, T., Takarada, S., and Suto, S., 1993. Pyroclastic flows from the 1991 eruption of Unzen volcano, Japan. Bull. Volcanol., 55: 166-175.

Yih, C.-S., 1980. Stratified flows. Academic, New York, 103-141.

Young, G.A., 1965. The physics of the base surge. U.S. Naval Ordnance Lab NOLTR 64-103, AD-618733, White Oak Maryland, 294 pp.

Zel’dovich, Ya.B. and Razier, Yu.P., 1966. Physics of shock waves and high-temperature hydrodynamic phenomena. Volumes I and II, Academic, New York, 916 pp.

Table 1. Tripartite Classification of Pyroclastic Materials

Class	*Emplacement Mechanism*	*Aerial Dispersal*	*Deposit Textures*	*Grain-Size Characteristics*	*Eruption Mechanism*
Fall	Ballistic, aerodynamic drag modified, suspension	Symmetrical along wind vectors, relatively wide spread	Mantles topography, normally and inversely graded (Plinian)	Well sorted by terminal fall velocities, coarser near vent fining with distance	All
Flow	Steady, lateral movement over substrate by grain flow, saltation, and suspension	Directed, radial from vent, following drainages up to tens of km	Massive, confined to topographic lows, fine base with inverse pumice grading, some bedded intervals	Poorly sorted, fine to coarse ash matrix supports lapilli, blocks, and bombs, common near vent breccia	Plinian, Vulcanian, Peléean, Merapian
Surge	Unsteady, lateral blast over substrate by pulsating suspension, saltation, and grain flow, locally accelerated by shocks	Directed, partially confined by drainage (some mantling), up to several vent radii from source	Thinly bedded, showing a variety of bedforms, dune planar, and massive, wet sediment deformations	Moderate to good sorting, fine to coarse-ash matrix with zones of fine ash depletion, supports lapilli, blocks, and bombs	Vulcanian, Surtseyan, Plinian, phreatic, hydrothermal

Table 2. Common Surge Vent Types

Character	*Tuff Ring/Maar*	*Tuff Cone*	*Scoria Cone*
Height/Width Ratio	1:10 - 1:30	1:9 - 1:11	1:5 - 1:6
Lithology	Mostly sideromelane tuff and lapilli tuff, with substantial amounts of palagonitic tuff breccia, containing blocks of lava and sediments; some accretionary lapilli	Palagonitic and sideromelane tuff and tuff breccia, possibly scoria and lava within the vent, abundant accretionary lapilli	Tachylitic cinders and scoria, traces of sideromelane ash, lava flows
Bedding	Well-defined, relatively thin beds, massive bedding where base was below local water level	Poorly defined, relatively thick beds, some thin beds at the base and top	Massive bedding, poorly defined
Sedimentary Structures	Well-developed graded bedding with dune, massive, and plane-parallel structures, impact sags around ballistic fragments, soft sediment deformations	Graded bedding at base and top, bulk of cone is nongraded massive beds, soft-sediment deformations	Crude inverse grading in avalanche structures
Mechanism for Ejecta Dispersal	Pyroclastic surge, fallout, and slumping	Pyroclastic surge and flow, fallout, and lahars	Ballistic fallout and avalanching

Table 3. Common Surge Bedforms

Fallout	*Sandwave*	*Massive*	*Planar*
-Normal grading -Angular fragments -Moderately well sorted -Internal structure generally well defined	-Laminar structures -Layers commonly mm thick -Fine grain size (~2 ϕ) -Cross laminations -Festooned bedding -Ripple laminations -Shoot-and-pool structures -Antidunes -Bedding in sets	-Weak to non-extant internal structures -Poor sorting -Scour features at base -Beds generally >20 cm thick -Deflation structures -Medium grain sizes (0-2 ϕ) -Pebble stringers	-Strong plane-parallel stratification -Coarse grain size (0-3 ϕ) -Beds average 2 cm in thickness -Inverse grading common -Long wavelength (>5 m) undulations

Table 4. Common Surge Facies

Facies	*Characteristics*
Vent	Explosion breccia, consisting of large blocks and bombs that are both framework and matrix supported; matrix of coarse ash, intercalations of fallout lapilli, and surge beds
Sandwave	Predominantly sandwave to massive bedding transitions; low primary dips; little alteration; fine grain sizes
Massive	Sandwave, massive, and planar bedding structures all present—massive beds predominating and showing some alteration, up to 25^{o} dips neat vent
Planar	Planar beds predominate, some massive beds; coarse grain sizes; may have high primary dips near vent
Wet Surge	Strong evidence of wet emplacement, including abundant accretionary lapilli; high primary dips with soft-sediment deformations; poorly developed stratification; palagonitization; induration; tuff-breccia appearance; intergranular vesiculation; bedding consists mostly of massive, planar, and laharic textures
Dry Surge	Fresh deposits poorly indurated with little palagonitization; thinly bedded, sandwave facies change to massive then to planar with increasing distance from vent; low primary dips
Tuff Cone	Explosion breccia near vent at base; overlain by small amounts of dry surge and abundant wet surge deposits and lahars
Tuff Ring	Mostly dry surge deposits overlying explosion breccia and fallout beds near vent
Composite Cone	Alternating dry and wet facies; dry surges show progression from planar to massive to sandwave facies with increasing distance from vent; wet surges change to lahars with distance from vent
Caldera	Dry surges overlying Plinian fallout at base of ignimbrite, becoming wetter as eruption progresses and pyroclastic flows are deposited; pyroclastic flows can be surge-like in caldera eruptions that are hydrovolcanic

Table 5. Origins of Surge Grain Morphology

Eruptive Mechanism (Grain Morphology)	*Transport (Edge Modification)*	*Alteration (Secondary Minerals)*
blocky, curviplanar surfaces	grain rounding	vesicle fillings
vesicular	grooves and scratches	skin cracks
drop-like or fused skin	steplike fractures	microcystalline encrustations
deformation planes	dish-shaped fractures	solution/precipitation
adhering particles	chipped edges	glass hydration
platy	cracks	palagonite
mosslike	upturned plates	clays
	v-shaped depressions	

Table 6 Characteristics of Wet and Dry surges

Dry	*Wet*
Abundant sandwave structures	Abundant massive, tuff-breccia beds
Well-developed thin bedding (1 to 5 cm thickness)	Poorly developed bedding; strata found in thicknesses of 10 cm to several meters; wet sediment deformations
Low ($<12^o$) initial dips	High initial dips (up to 25^o) are common
Young deposits poorly indurated	Highly indurated young deposits
Little palagonitization	High degree of palagonitization
Scarce accretionary lapilli	Abundant accretionary lapilli
Low thickness-to-aerial-extent ratio	High thickness-to-aerial-extent ratio

Table 7. Modeled Dry-to-Wet Transitions in Surges

R_m[a]	*Water Volume Fraction*[b]			*Initial Velocity*[c]		*Scaled Distance*	
	Total	Isothermal	Adiabatic	Blast	Column Collapse	Dry-Wet	Wet-Lahar
0.10	0.17	--	0.03	223	346	--	--
0.35	0.41	--	0.18	371	545	0.86[d]	--
0.70	0.58	0.13	0.37	435	322	0.08	0.84[d]
1.00	0.67	0.45	0.50	414	203	0.05	0.32[d]
2.00	0.80	0.73	0.73	389	79	0.03	0.04

[a] R_m is the water/magma mass ratio for hydrovolcanic explosions.
[b] Wohletz (1986) describes how R_m can be used to calculate the isothermal and adiabatic steam fraction from an idealized water/magma interaction, which constrains the amount of liquid water existing after interaction.
[c] Initial velocities for a blast eruption are described in the text
[d] Denotes hypothetical facies transition (dry-wet or wet-lahar) only if all water condenses (water added from atmosphere).

Figures

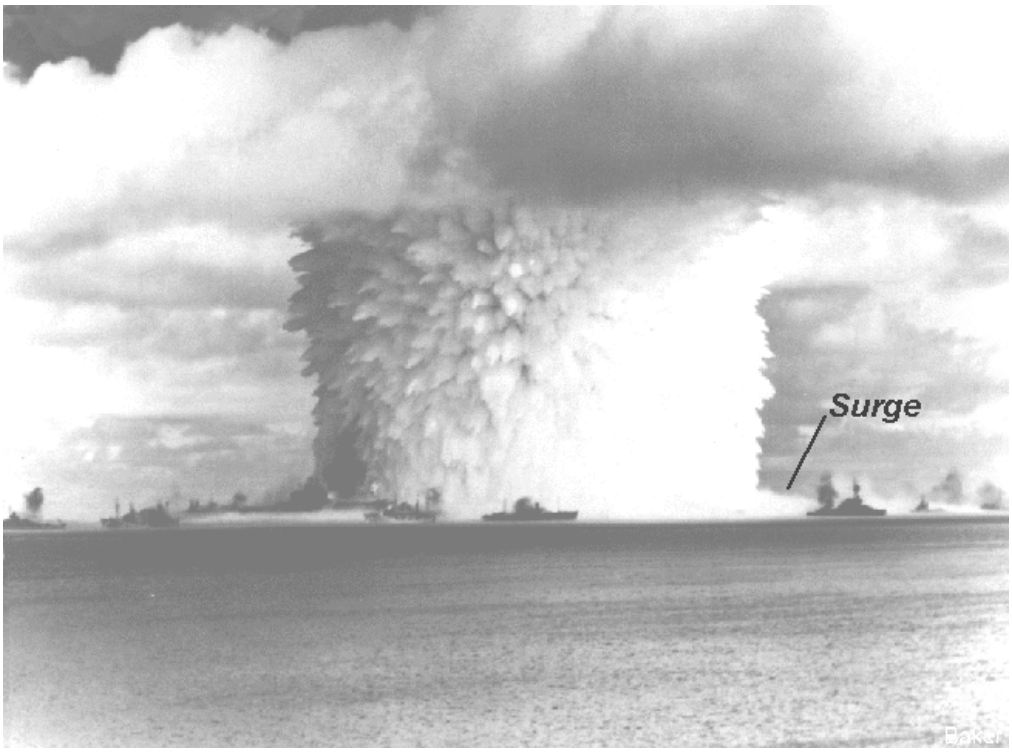

Fig. 1. Photograph of Test Baker (20 kt) in 1946, showing the base surge moving away from the explosion stem (column). The surge front is approaching Naval vessels in the foreground as jets of ejecta (water droplets) are propelled outward and downward from the stem feeding the surge through stem fallback. Photograph from Los Alamos National Laboratory archives.

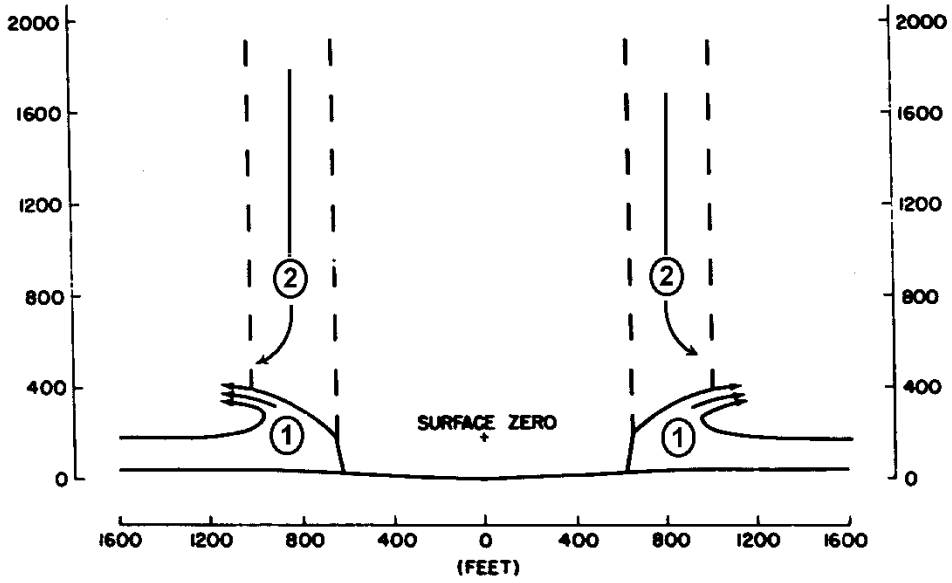

Fig. 2. Figure adapted from Young (1965) showing the origin of the (1) primary surge by ballistic ejection and shock wave and the (2) secondary surge by column subsidence (collapse). Note that the scale is in feet, retained from the original work.

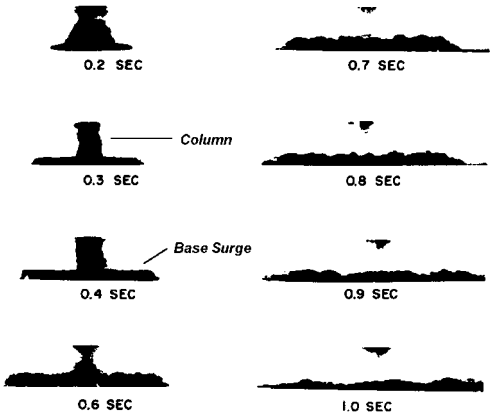

Fig. 3. Figure from Young's (1965) laboratory simulations of the base surge formed by release of a dense liquid in a water tank allowed development of some scaling laws he used to analyze the base surge from Test Baker.

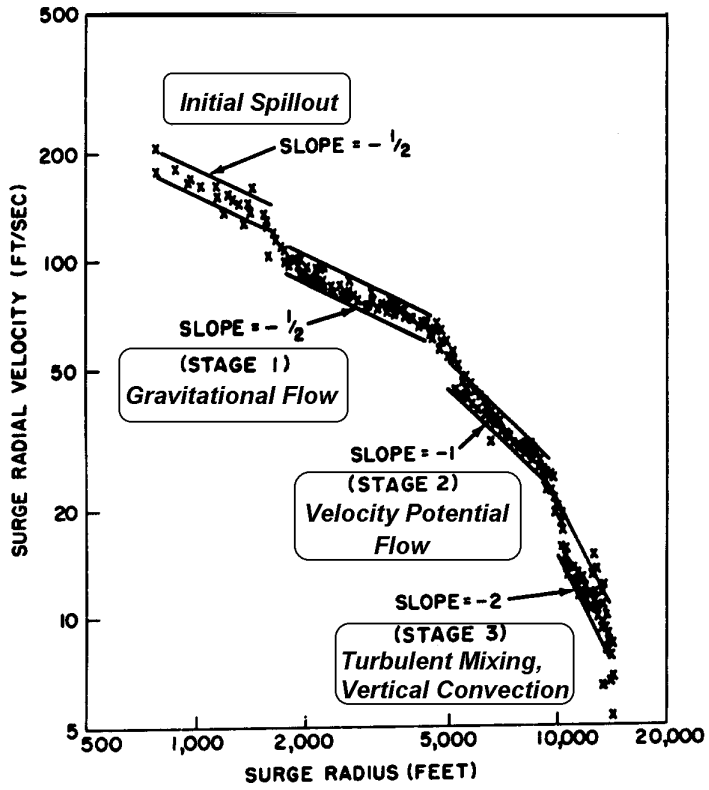

Fig. 4. Figure adapted from Young's (1965) surge model, based on radial velocity as a function of surge radius, shows three distinct stages of surge movement in which its horizontal velocity is determined by the sequence of gravitational flow, potential flow, and flow dominated by turbulent mixing. Note that the scale is in feet, retained from the original work.

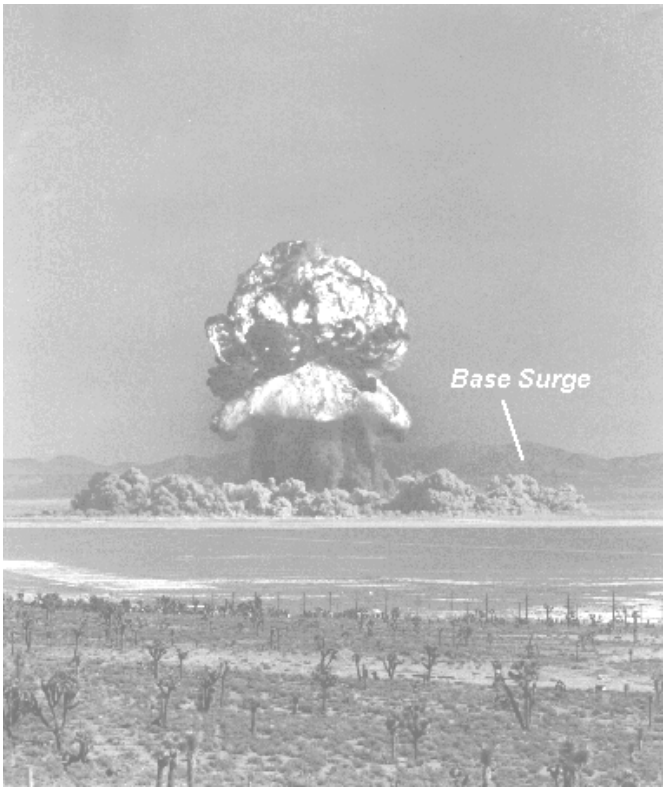

Fig. 5. Base surge developed during nuclear test Fizeau (11 kt) conducted in Nevada in 1957. Photograph from Los Alamos National Laboratory archives.

Fig. 6. Shock wave from MISERS GOLD incinerating pine trees (approximately 15 m tall). Photograph is courtesy of the U. S. Army.

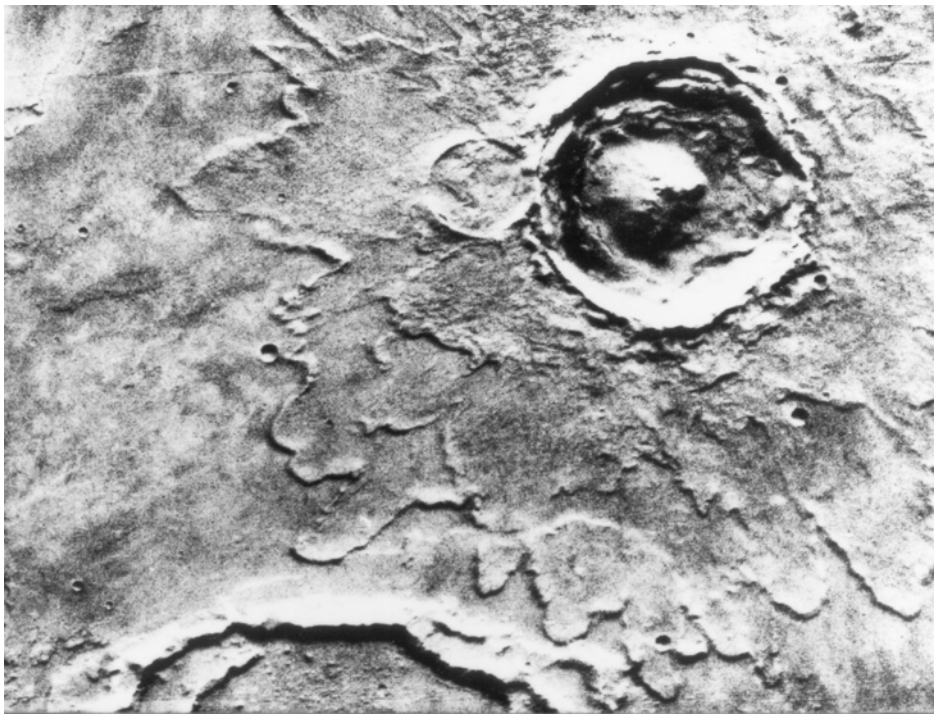

Fig. 7. Yuty crater on Mars (Viking image 003107), showing multiple lobes of rampart ejecta sheets that apparently interacted with topographic obstacles, which is most easily explained by horizontal transport.

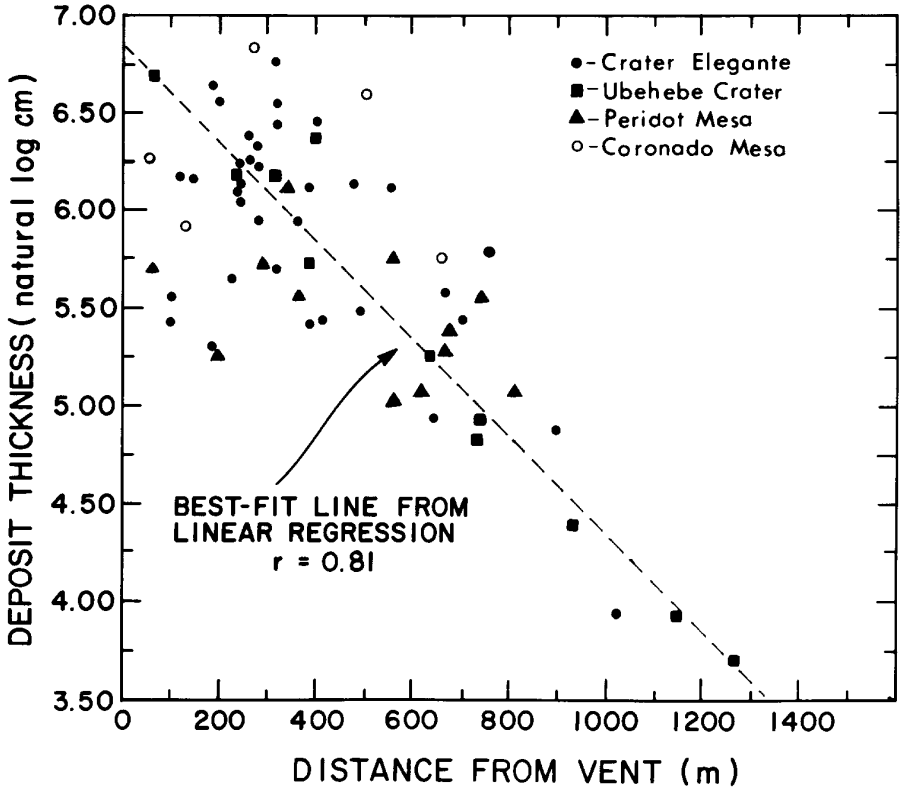

Fig. 8. Surge deposit thickness with distance from the vent (Wohletz and Sheridan, 1979).

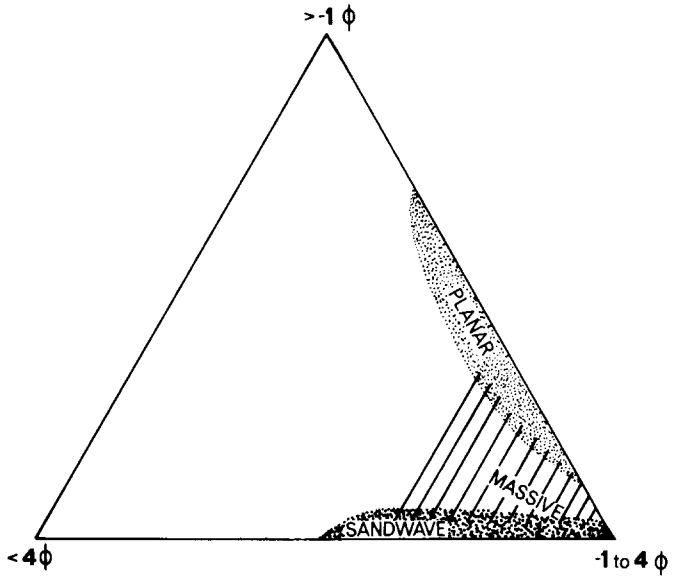

Fig. 9. General grain size for three surge bedforms from Wohletz and Sheridan (1979).

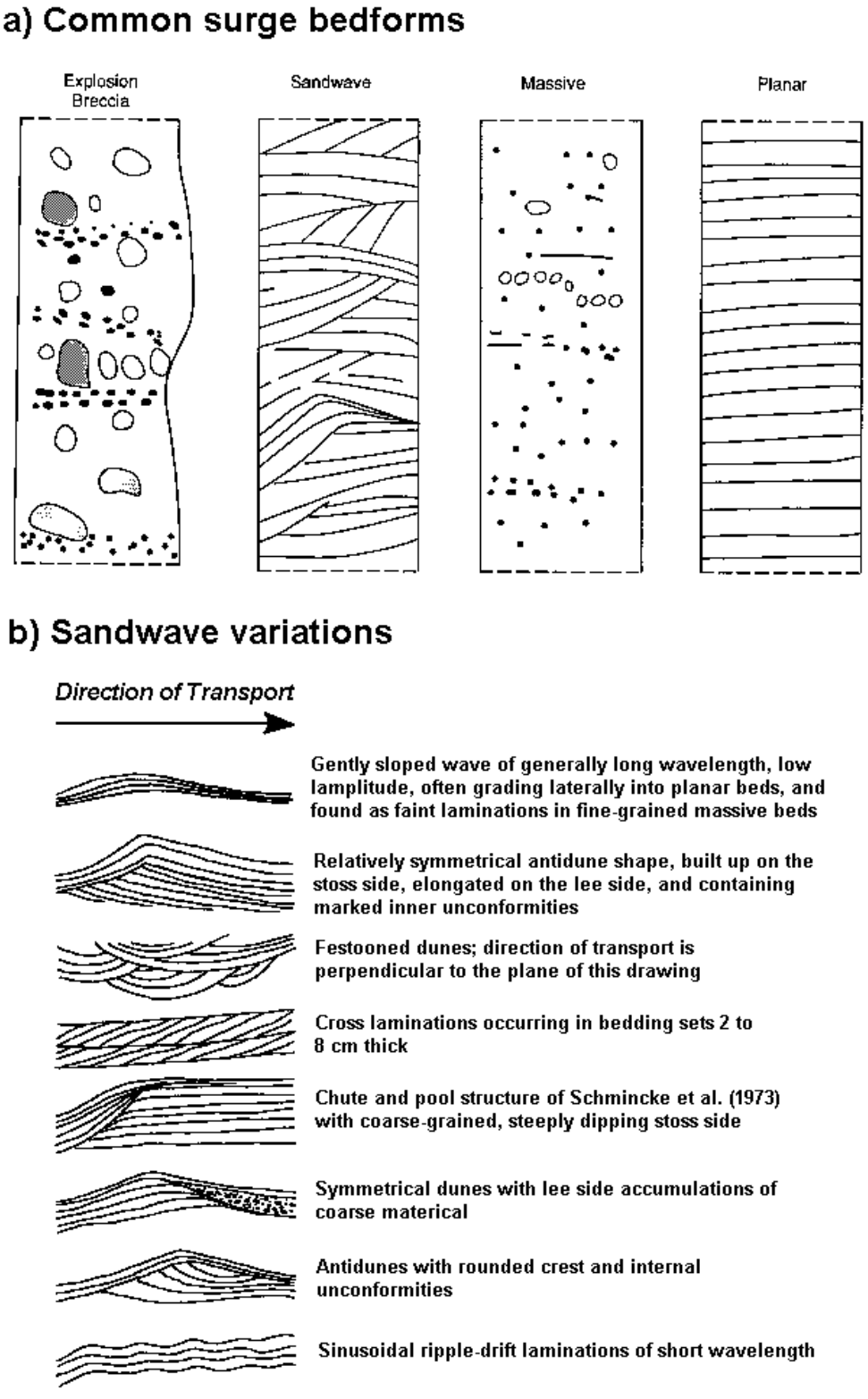

Fig. 10. (a) Common surge bedforms from Wohletz and Heiken (1992). (b) Variations of surge sandwave (dune) structures from Wohletz and Sheridan (1979).

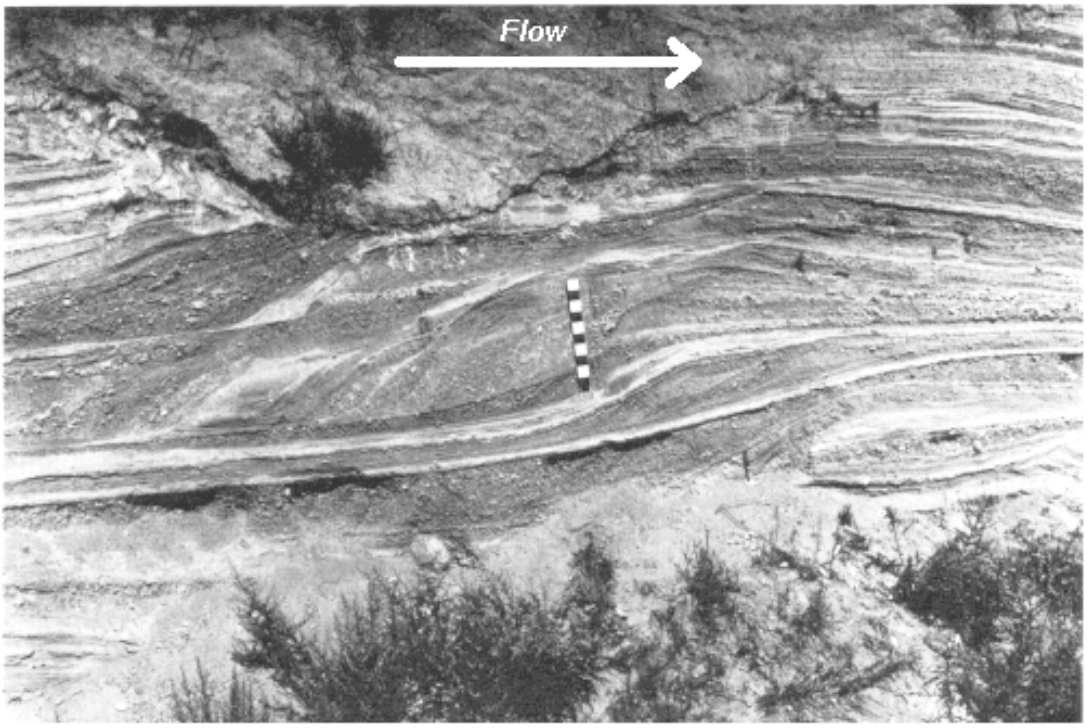

Fig. 11. Antidune showing chute and pool structure. The scale shows 10-cm intervals. Photograph adapted from Schmincke et al. (1973).

Fig. 12. Ground surge layer (~1 m thick) from the Peach Springs Tuff. Photograph from Valentine (1988).

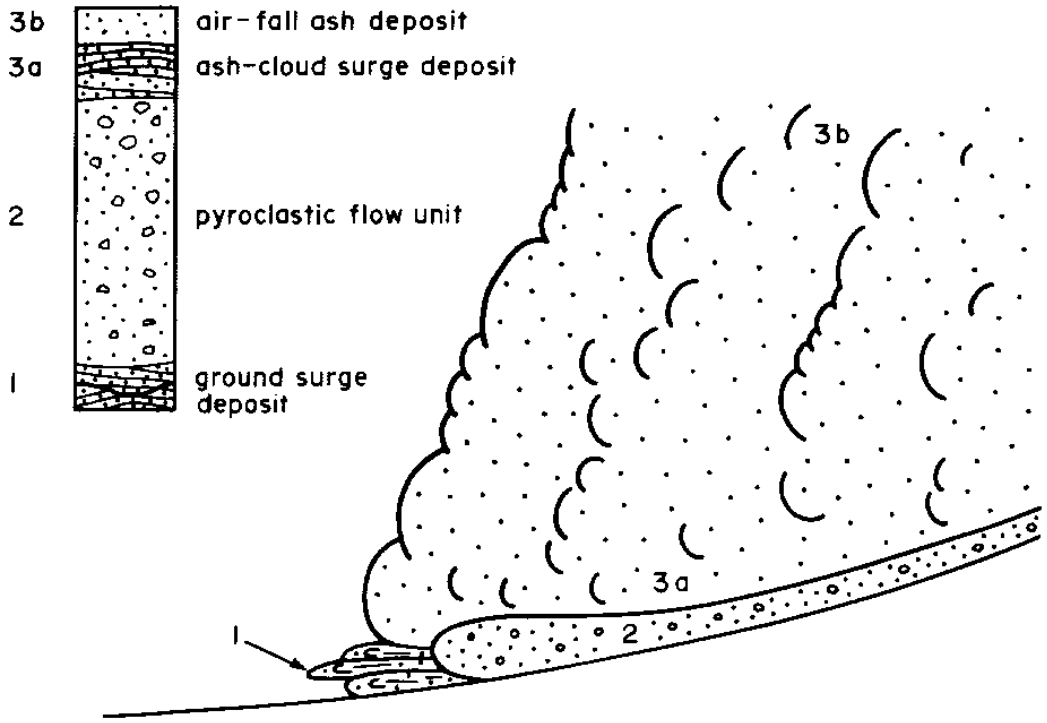

Fig. 13. Figure from Cas and Wright (1988) showing the origin of the ground surge and ash-cloud surge.

Markovian Stratigraphic Analysis of Surge Deposits

$$\begin{bmatrix} \text{S-S} & \text{S-M} & \text{S-P} \\ \text{M-S} & \text{M-M} & \text{M-P} \\ \text{P-S} & \text{P-M} & \text{P-P} \end{bmatrix}$$

SANDWAVE	MASSIVE	PLANAR
0.48 0.10 0.02	0.20 0.05 0.03	0.10 0.02 0.02
0.10 0.20 0.02	0.05 0.45 0.03	0.02 0.20 0.06
0.02 0.02 0.04	0.03 0.03 0.12	0.02 0.06 0.50

Fig. 14. Idealized (hence symmetric) Markovian matrices showing fraction of bedform transitions where S = sandwave, M = massive, and P = planar beds. Transitions are measured on set vertical intervals and are denoted by S-S (sandwave to sandwave), S-M (sandwave to massive), and so forth (Wohletz and Sheridan, 1979).

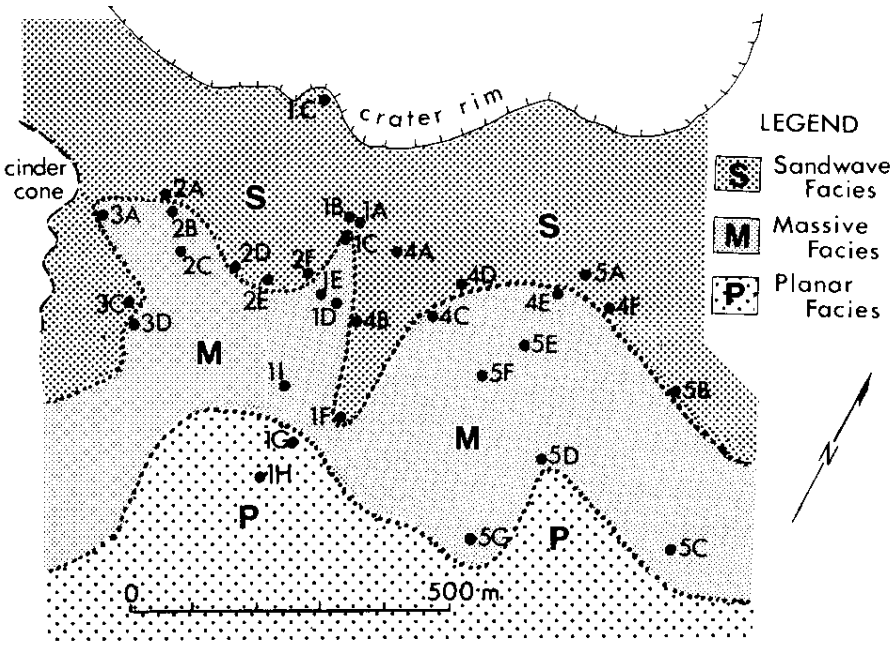

Fig. 15. Pyroclastic surge facies map of the south side of Crater Elegante maar, Mexico (Wohletz and Sheridan, 1979).

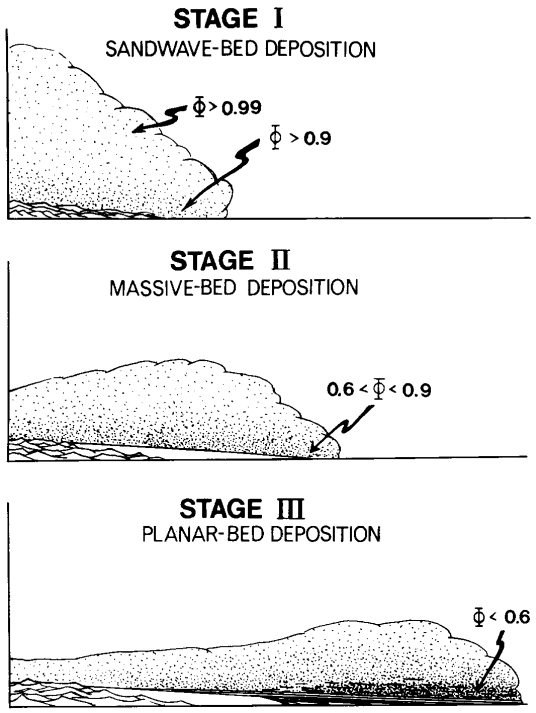

Fig. 16. Schematic illustration of a surge cloud at three stages of development as is moves from its source with increasing particle concentration and decreasing turbulence (Wohletz and Sheridan, 1979).

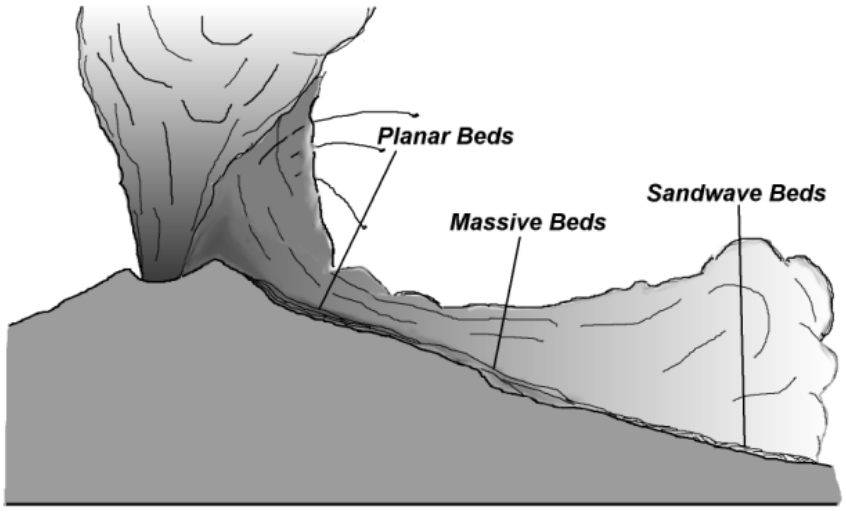

Fig. 17. Surge facies developing on the slopes of a cone show the effects of increasing inflation and velocity with distance, modeled after Vulcano, Italy.

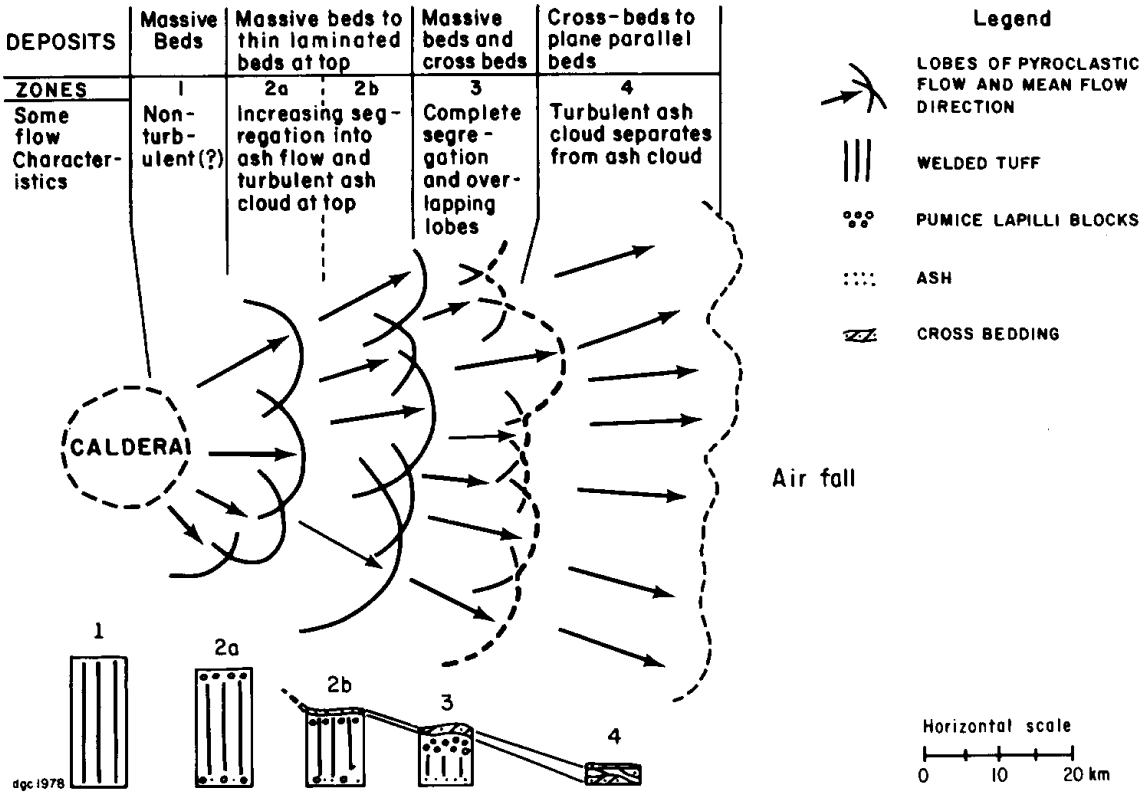

Fig. 18. Figure from Fisher (1979) showing facies development for ash-cloud surges in the Bandelier Tuff, New Mexico.

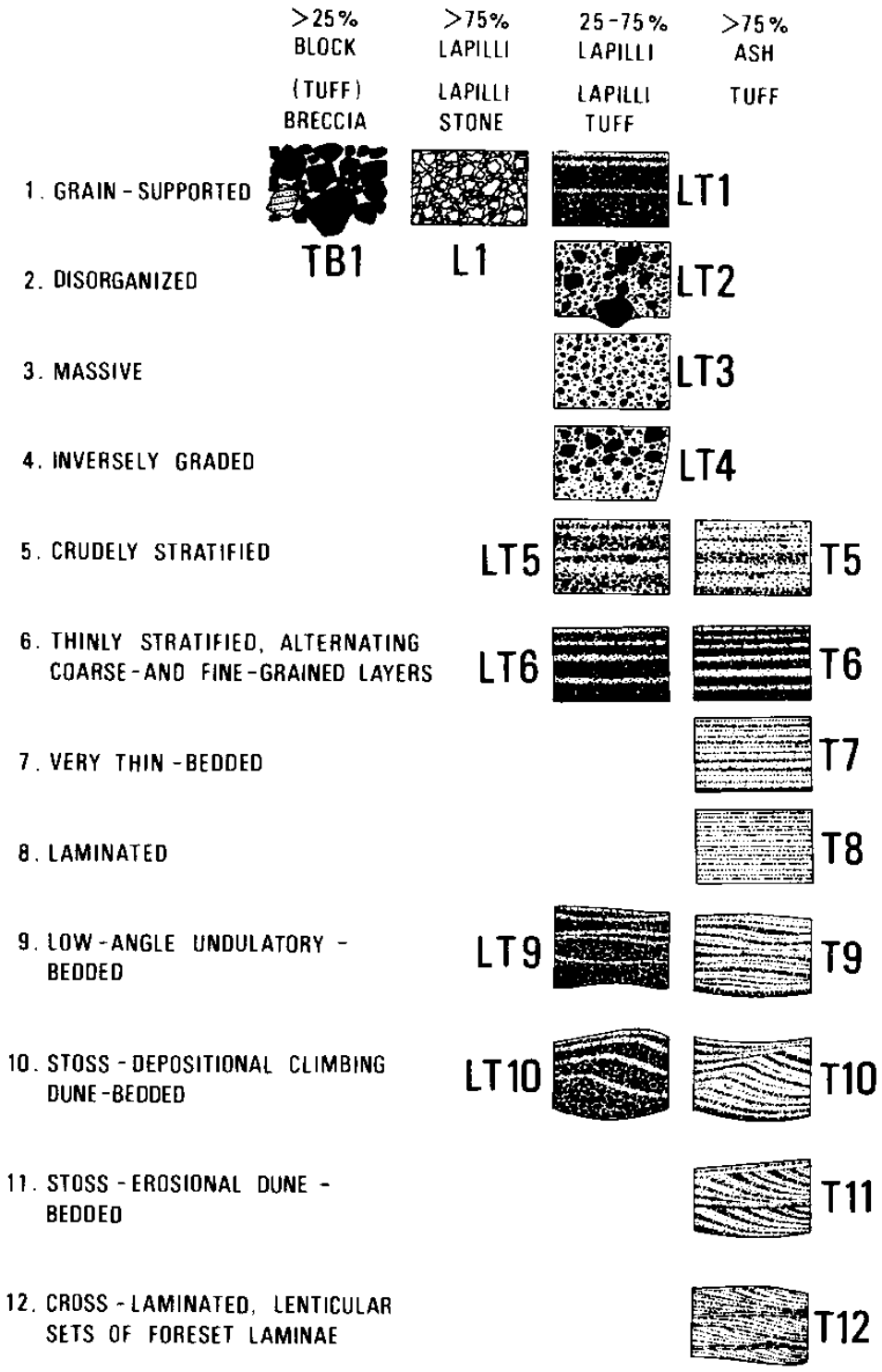

Fig. 19. Figure from Sohn and Chough (1989) showing their surge facies classification scheme for the Suwolbong pyroclastic sequence, Korea.

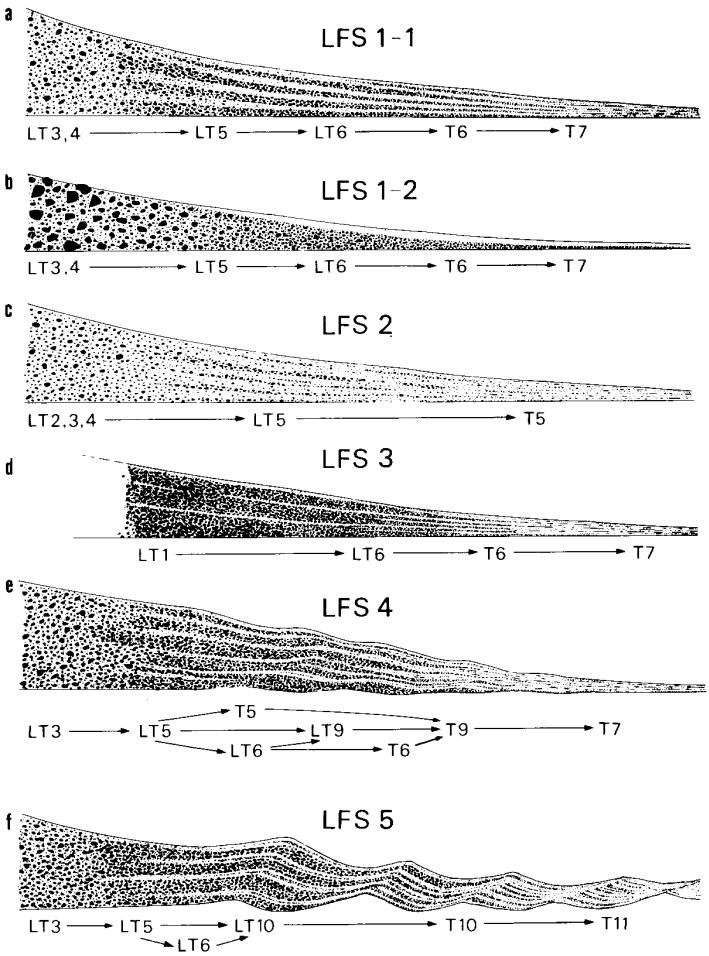

Fig. 20. Figure from Sohn and Chough (1989) showing six types of lateral facies sequences (LFS; a - f) constructed from field occurrence and facies transition analysis of surge deposits in the Suwolbong pyroclastic sequence, Korea. Facies are denoted by terms defined in Fig. 19.

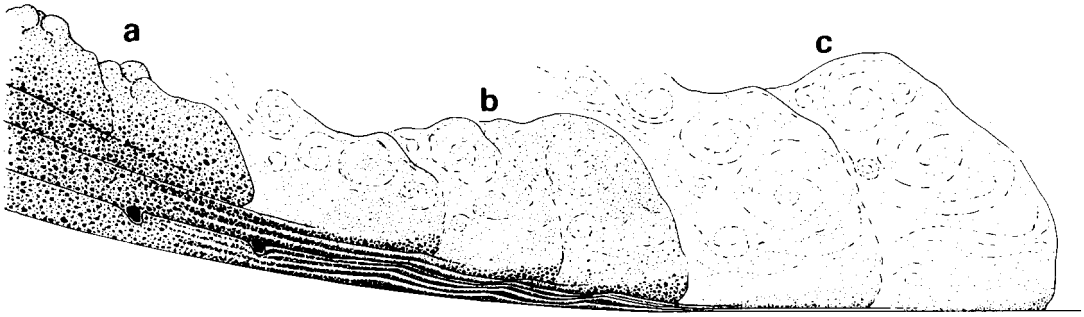

Fig. 21. Illustration from Sohn and Chough (1980) of a surge at three stages (a - c) of development, showing a progressive decrease in particle concentration with development of turbulence.

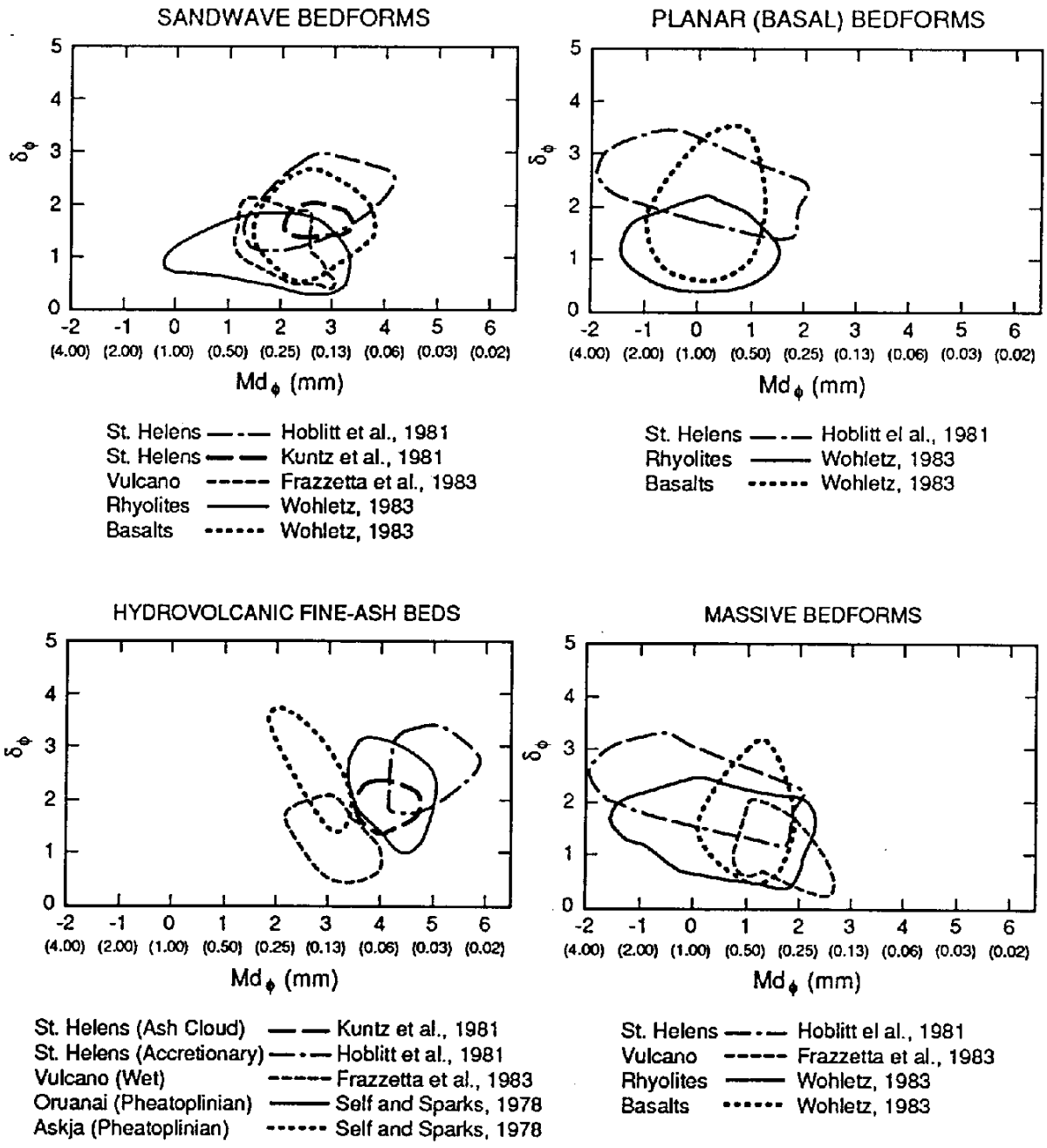

Fig. 22. Sorting (σ_ϕ) *vs* median diameter (Md_ϕ) plots for surge bedform types from Sheridan and Wohletz (1983).

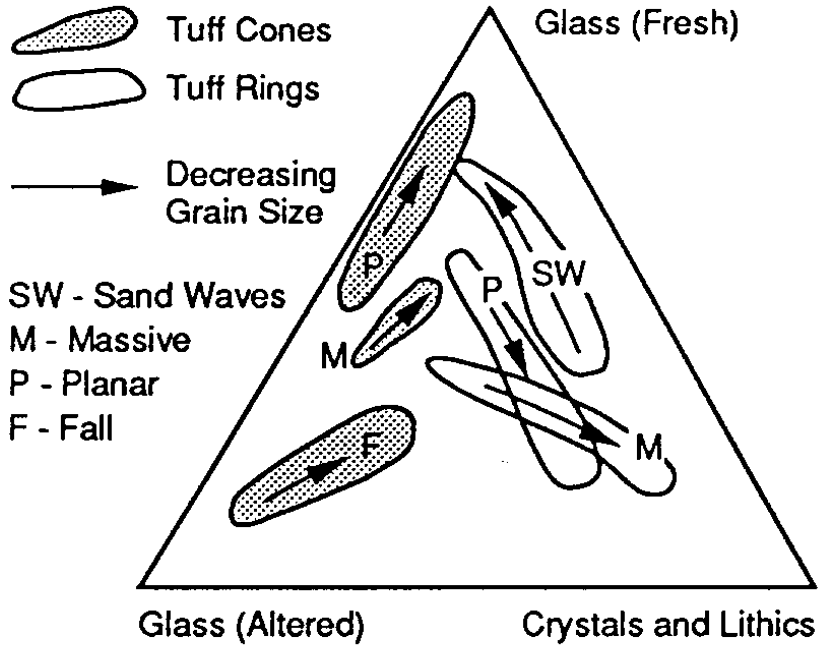

Fig. 23. General variations in surge constituents for tuff cones and rings (Wohletz and Heiken, 1992).

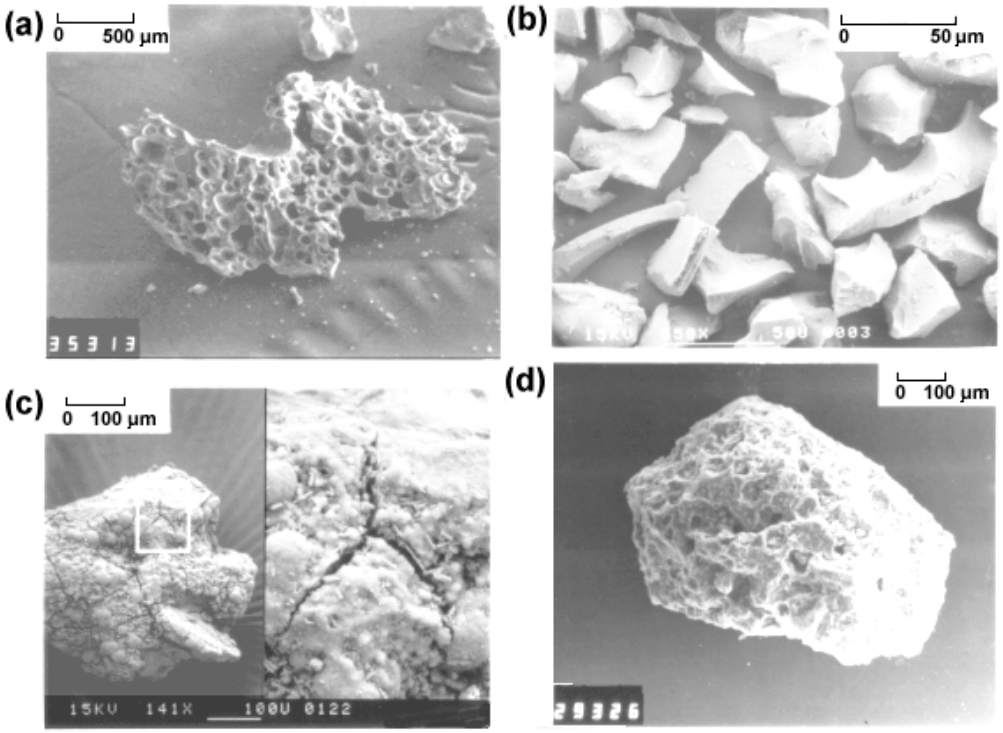

Fig. 24. Typical grain morphologies in surge deposits. Photos (a**)** and (b**)** show fresh surfaces, but (c) and (d) show typical surge alteration features.

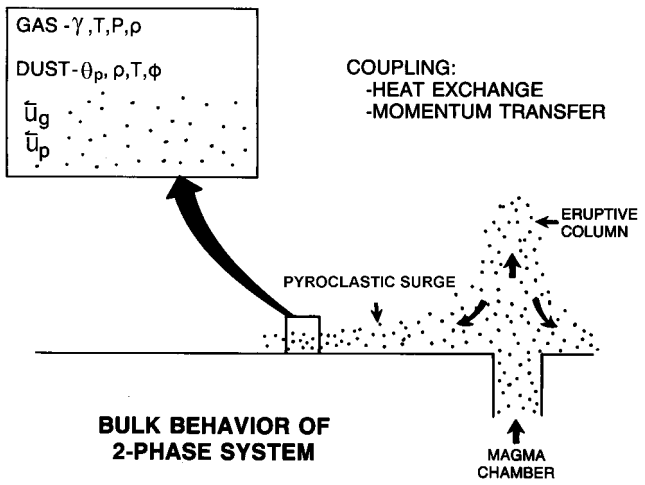

F**ig. 25.** Considering a pyroclastic surge as a two-phase (particles and gas) system, flow equations (Navier-Stokes) can be written separately for each phase. Because the phases interact and move as a single complex fluid, the behaviors of each phase are related by "coupling". In this simple model coupling is achieved by heat and momentum transfer between the phases where the important parameters are temperature (T), pressure (P), density (ρ), velocity (u), particle size (ϕ) and concentration (θ_p).

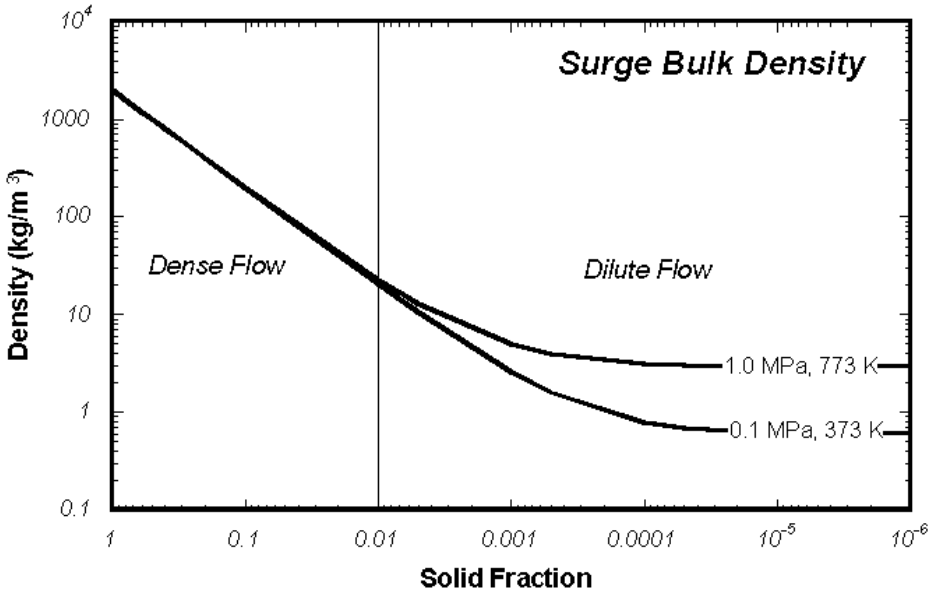

Fig. 26. Bulk densities of a cool, wet surge and hot, dry surge clouds, consisting of tephra particles and steam at 0.1 MPa (saturated) and 1.0 MPa (superheated), respectively. The bulk density is a function of solid particle fraction where values greater than ~0.6 represent a particles in continuous contact, dense flow from 0.6 to 0.01, and dilute flow at solid fractions less than 0.01.

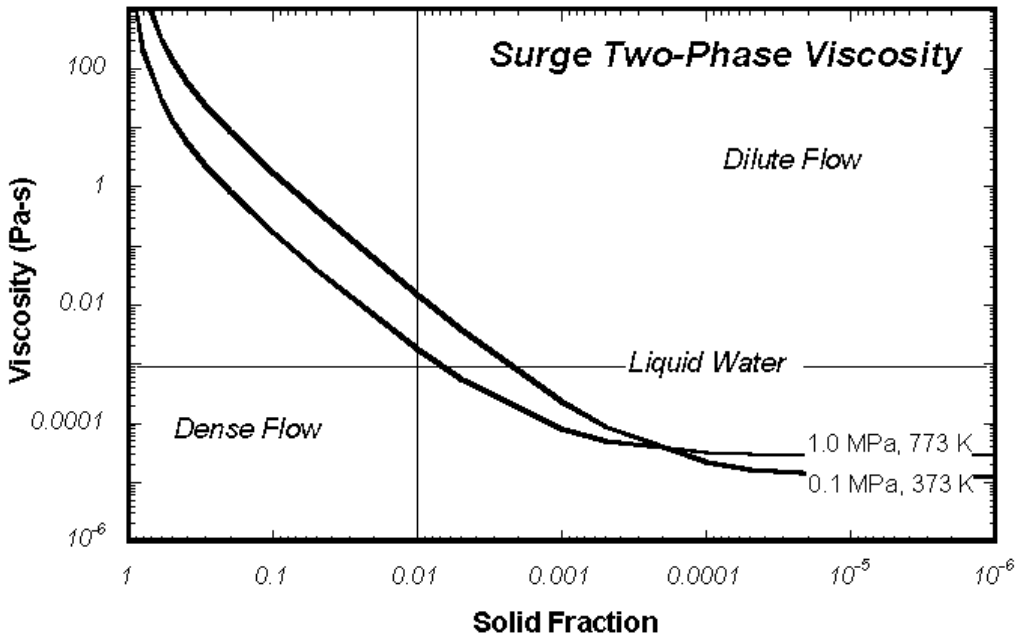

Fig. 27. Model-dependent two-phase (bulk) surge viscosities are shown as a function of solid fraction for a cool, wet surge and a hot, dry surge. Where the surge is very dilute (lean), the viscosity is nearly that of steam, but with greater concentration of particles rises to values greater than that of liquid water in the range of dense fluidization.

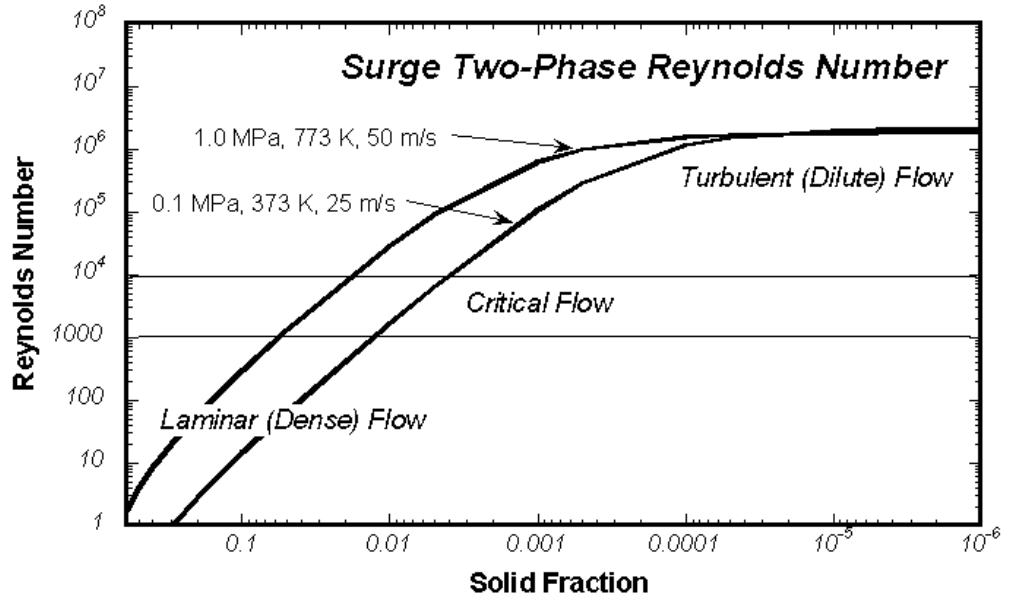

Fig. 28. Effective Reynolds number for a surge increases with solid fraction from values in the laminar flow regime for dense flows to those in the turbulent regime for dilute flows. Model curves are shown for a cool, wet surge moving at 25 m/s, and a hot, dry surge moving at 50 m/s. The characteristic length scale used in this example is the mean particle diameter.

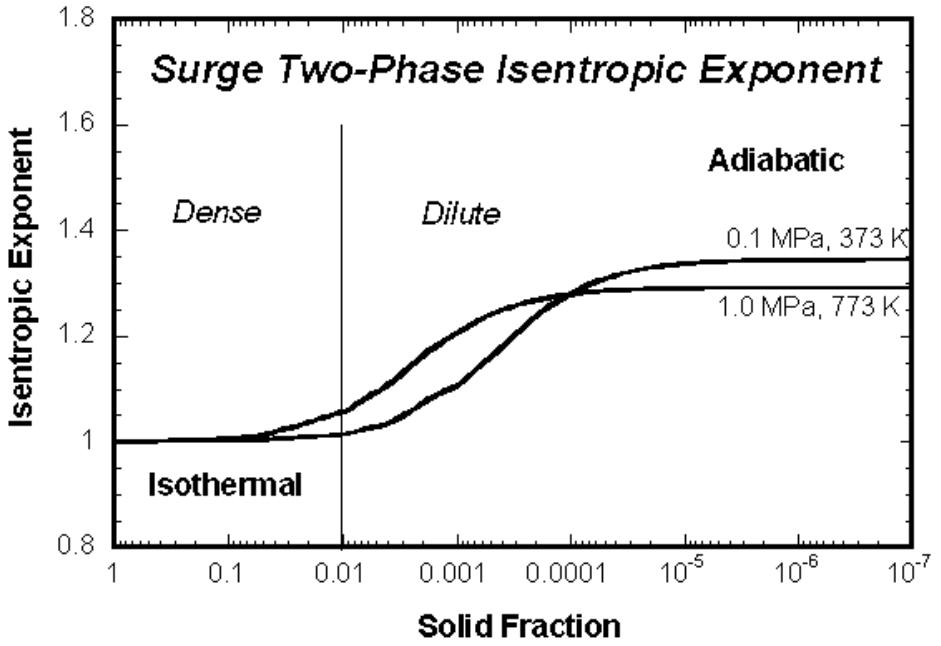

Fig. 29. The isentropic exponent increases from isothermal values to adiabatic values of nearly pure steam as the solid fraction in a surge increases. This exponent determines how much steam expands during its decompression from near-vent eruptive conditions to those where it reaches atmospheric pressure during runout.

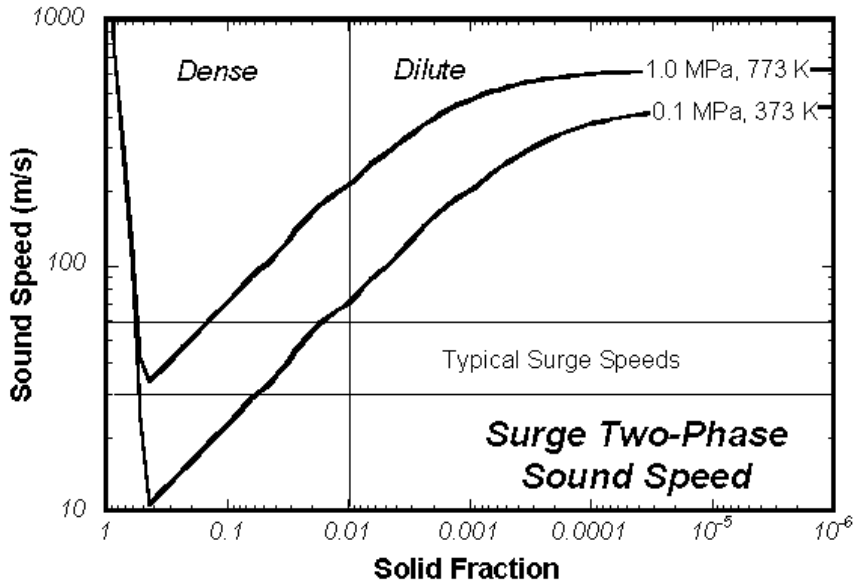

Fig. 30. While the internal sound speed of a fixed bed of particles or a nearly pure steam surge is on the order of hundreds of meters per second, it drops off to values less than those of typical surge runout speeds for dense fluidized surges.

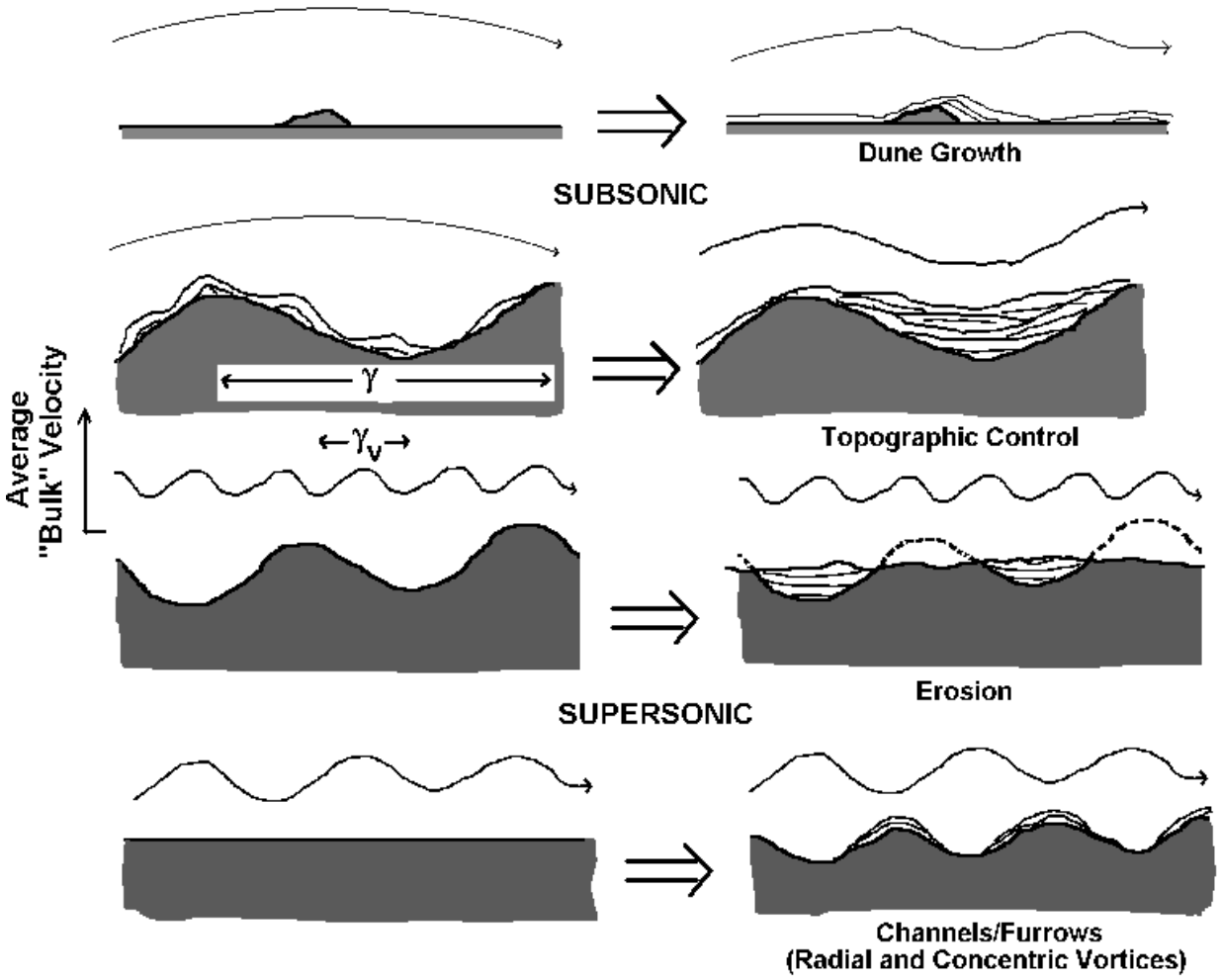

Fig. 31. Hypothetical deposition and erosion as a function of two-phase velocity fluctuation λ_v and topographic λ wavelengths for subsonic and supersonic flow.

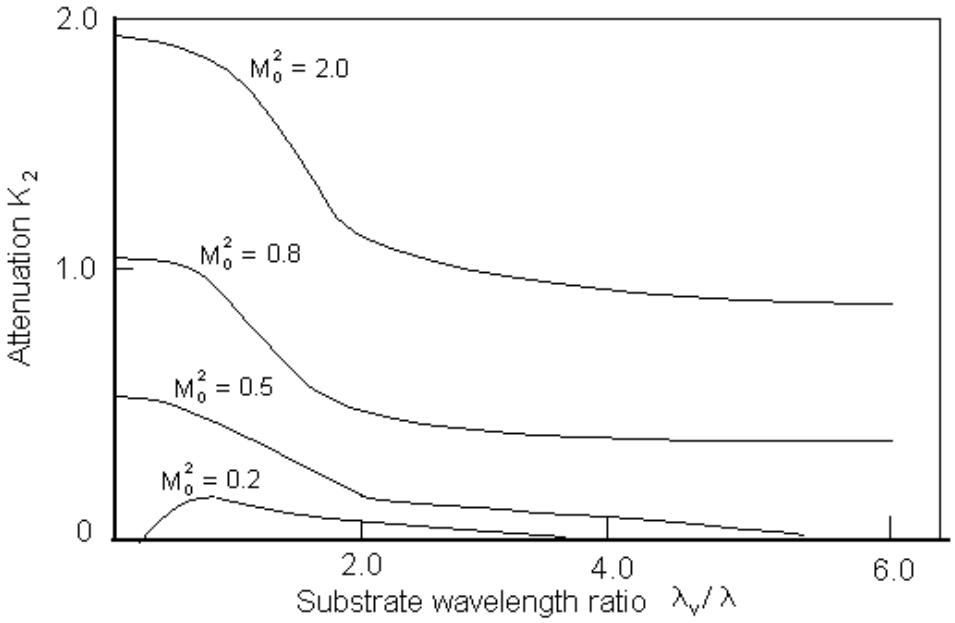

Fig. 32. A wavy-wall solution (Marble, 1970) for sound attenuation in a pyroclastic surge that interacts with topography with a characteristic fabric wavelength of λ. The characteristic wavelength of velocity equilibration between the gas and particles in the surge is $\lambda_v = t_v\, u$ where t_v is the relaxation time over which particles and gas attain a similar velocity u. Curves are shown for surges at different *frozen* Mach numbers M_0, the ratio of the surge velocity to the mixture's sound speed where particles and gas are moving at the same speed. The attenuation is greatest for surges moving at internally supersonic speeds, which may range down to several tens of meters per second for surges having solids concentrations greater than 0.01 (Fig. 30). For this solution, the velocity relaxation time is assumed to equal the thermal relaxation time, the solid concentration is low (<0.001; $m_p \sim m_g$), and the gas has an isentropic coefficient of 1.4 (air).

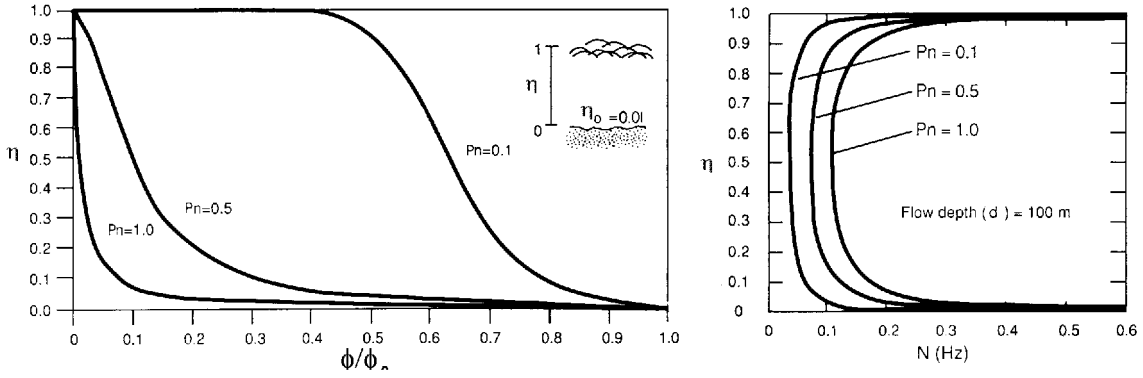

Fig. 33. Figures adapted from Valentine (1987) showing the relative particle concentration (ϕ/ϕ_0) and Brunt-Väisälä frequency (N) as a function of dimensionless height (η) for a surge at three values of Rouse number (Pn).

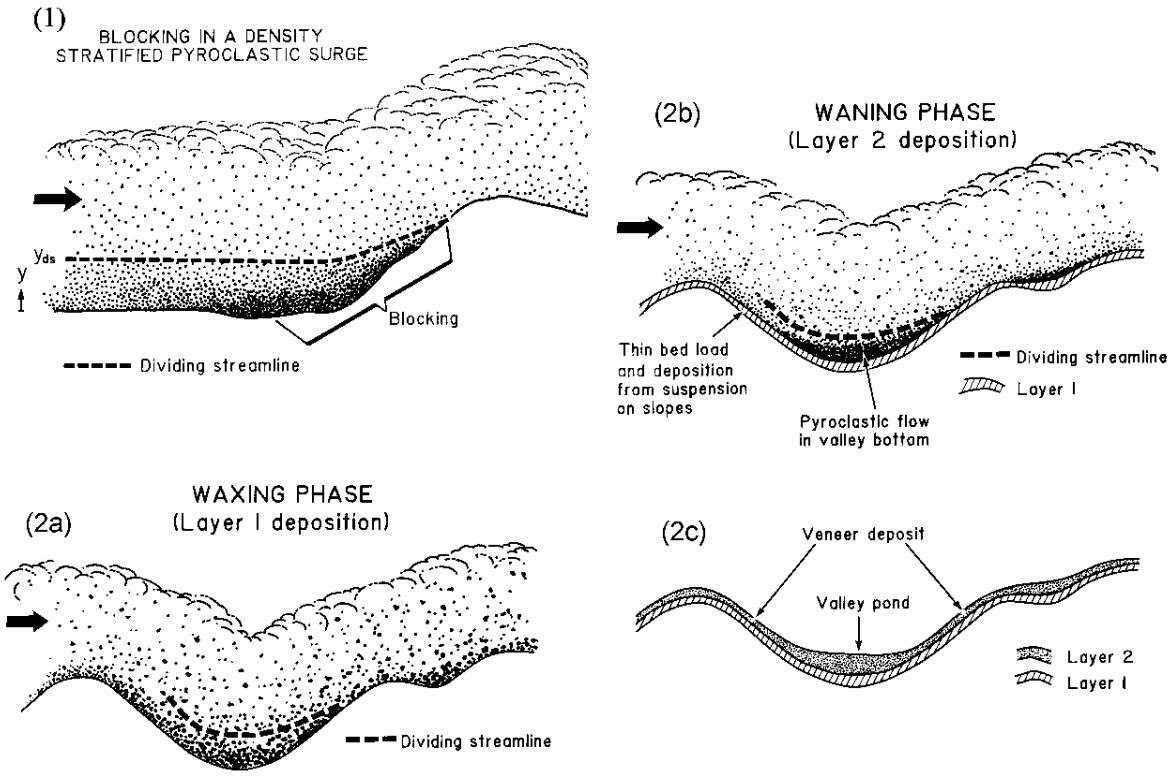

Fig. 34. Diagrams from Valentine (1987). Diagram 1 depicts the *blocking* of a stratified surge as it encounters a topographic obstacle where denser lower portions cannot flow over the obstacle but stop or flow around it, leading to massive bed emplacement. In the diagrams 2a - 2c, the waxing (2a) and waning (2b) of a pyroclastic flow (or surge) leads to deposition of first coarser-grained (massive) and then finer-grained (bedded) deposits, producing valley pond and veneer deposits commonly formed by surges.

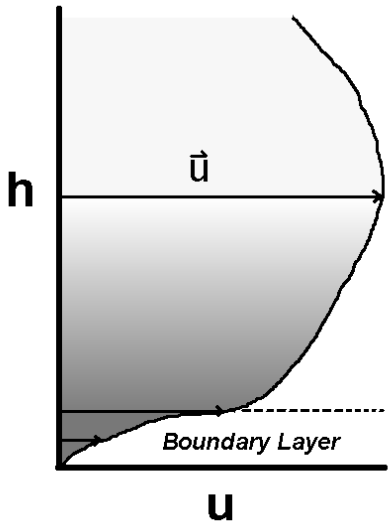

Fig. 35. Idealized velocity (*u*) profile for a surge showing the boundary layer.

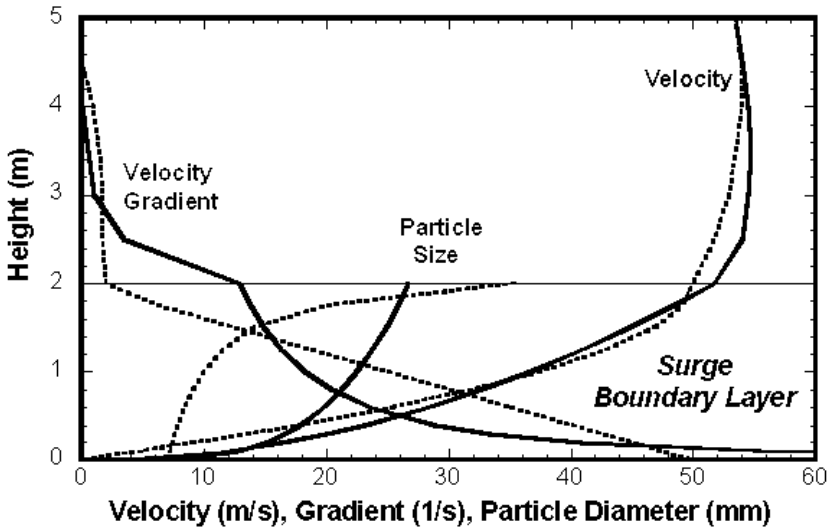

Fig. 36. Calculated development of inverse grading in the boundary layer of a pyroclastic surge. Velocity increases with height according to hypothetical turbulent (solid) and generalized laminar (dotted) and a models, producing a high velocity gradient near the bottom of the profile decreasing with height; larger particles will be at equilibrium at higher positions in the boundary layer.

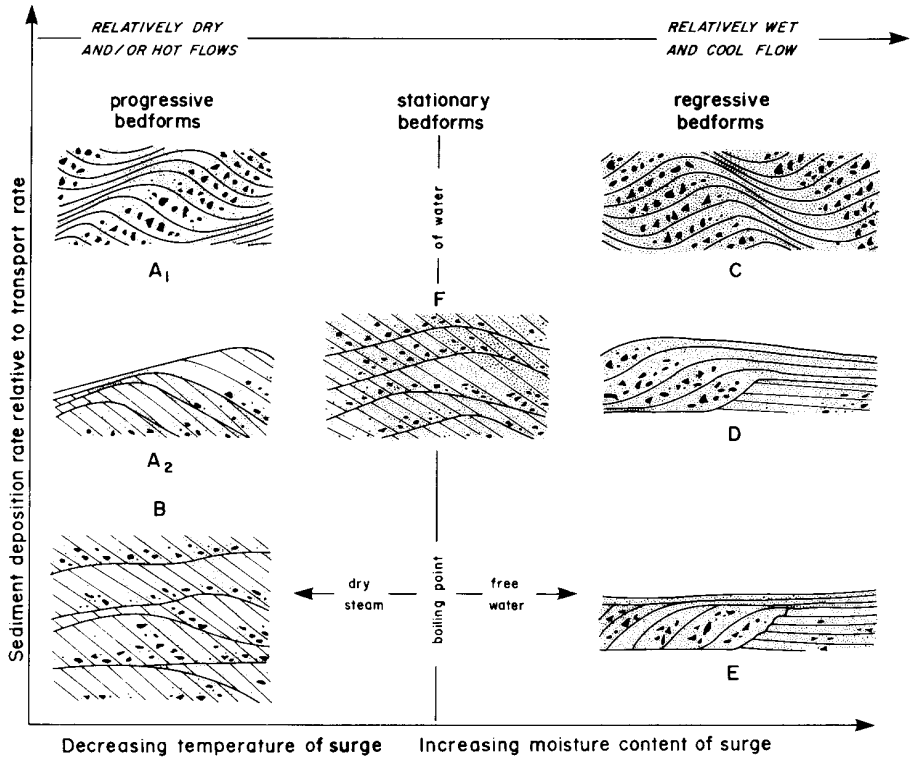

Fig. 37. Figure from Allen (1984) showing an example interpretation scheme for pyroclastic surges, relating sandwave bedforms to depositional rate, temperature, and moisture.

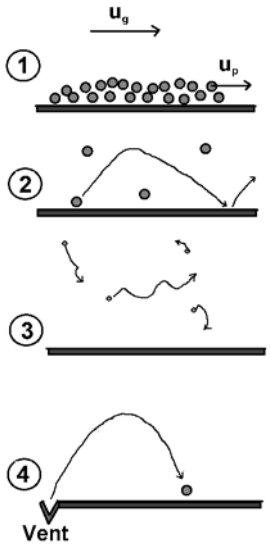

Fig. 38. Illustrates four primary modes of particle transport in a pyroclastic surge: (1) traction; (2) saltation; (3) suspension; and (4) ballistic.

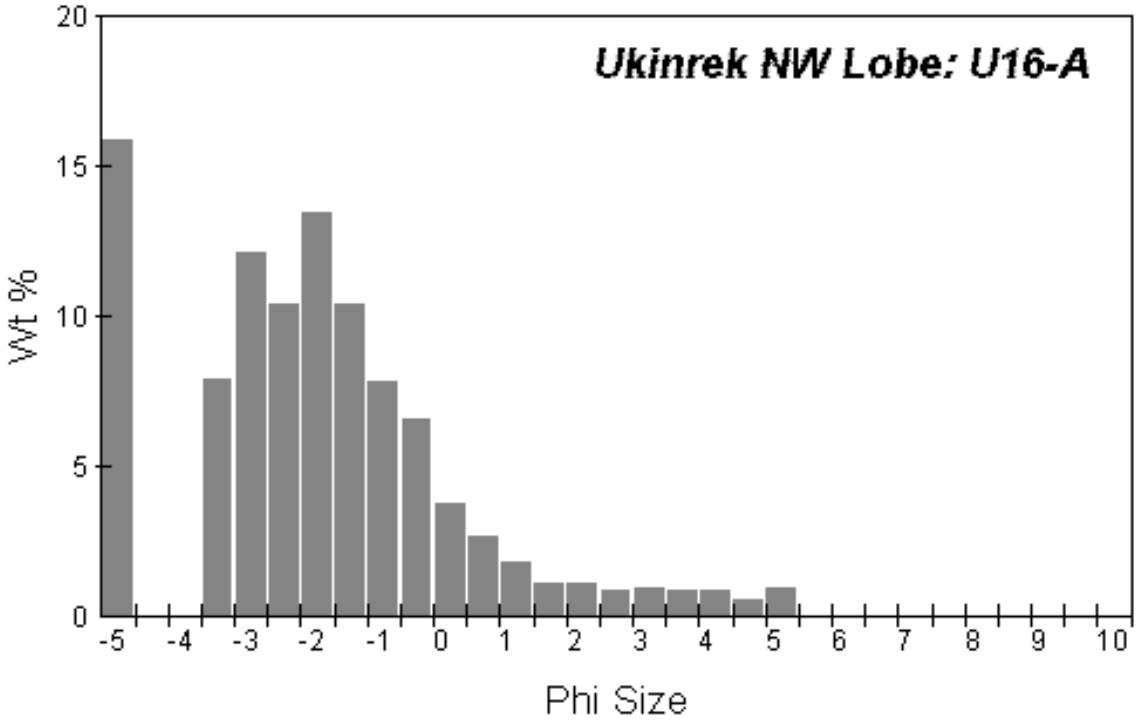

Fig. 39. Histogram plot of surge sample from the Ukinrek maar volcano, showing several peaks, the most prominent being coarse (phi = -5), caused by ballistic materials.

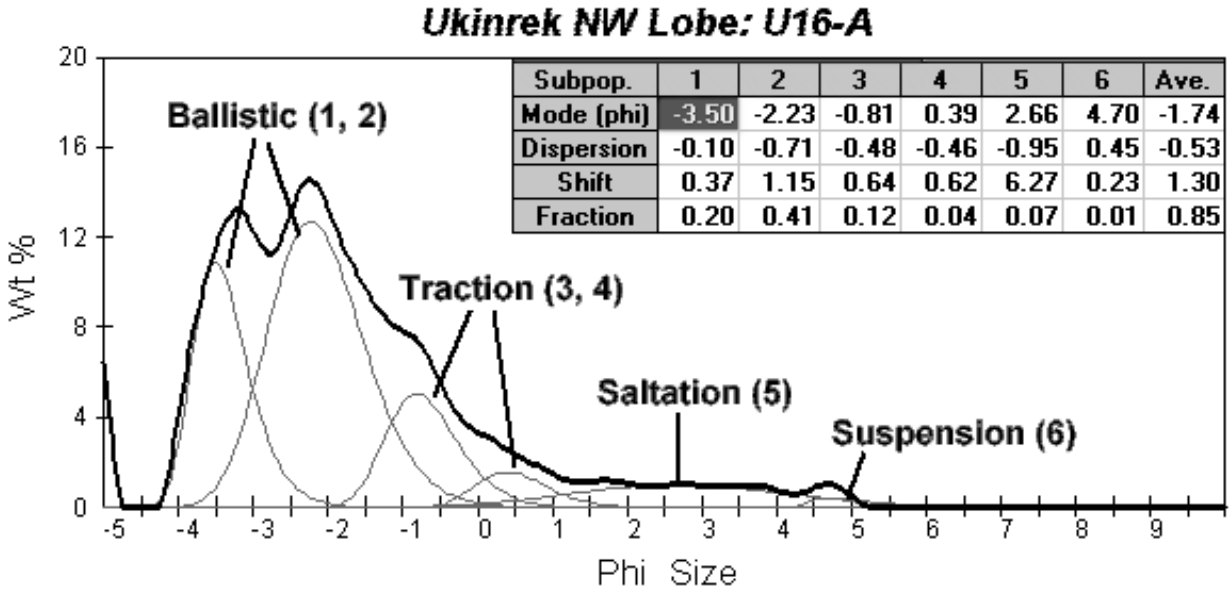

Fig. 40. Using the SFT software (available on the Internet at http://geont1.lanl.govWohletz/ SFT.htm) six subpopulations can be distinguished in the Ukinrek surge sample. The transport mode for each subpopulation is identified by its mode and dispersion range.

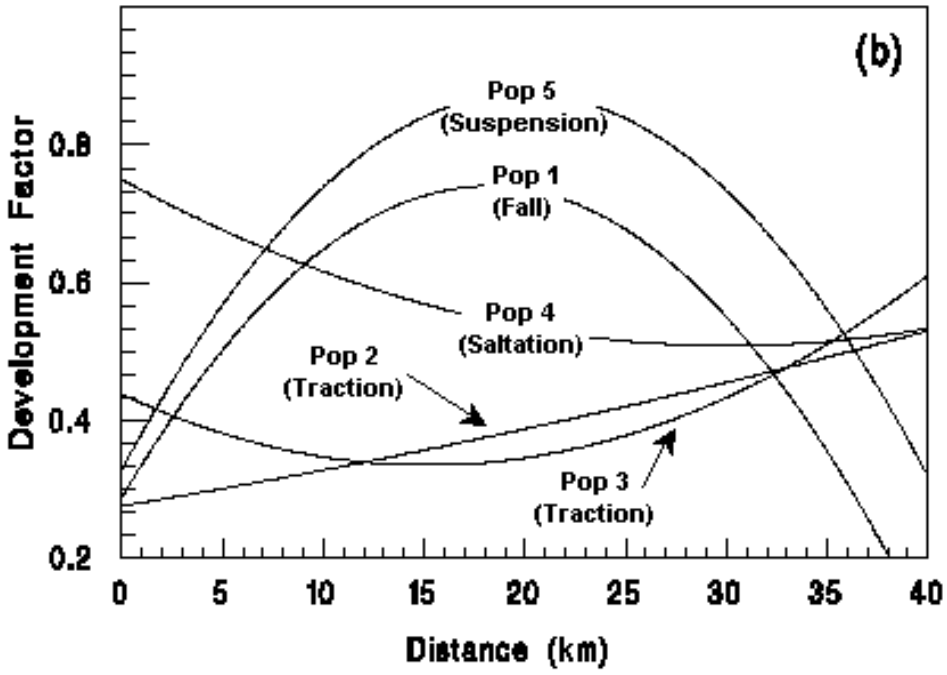

Fig. 41. By combining the mode fraction and dispersion (γ) values for each population, a development factor can be defined to show the relative importance of transport modes as a function of distance. This plot shows of NYT lower member surges and falls and shows saltation dominating near the vent, a mixture of saltation, traction, and suspension at medial distances, and traction at distal locations (Wohletz et al. 1995).

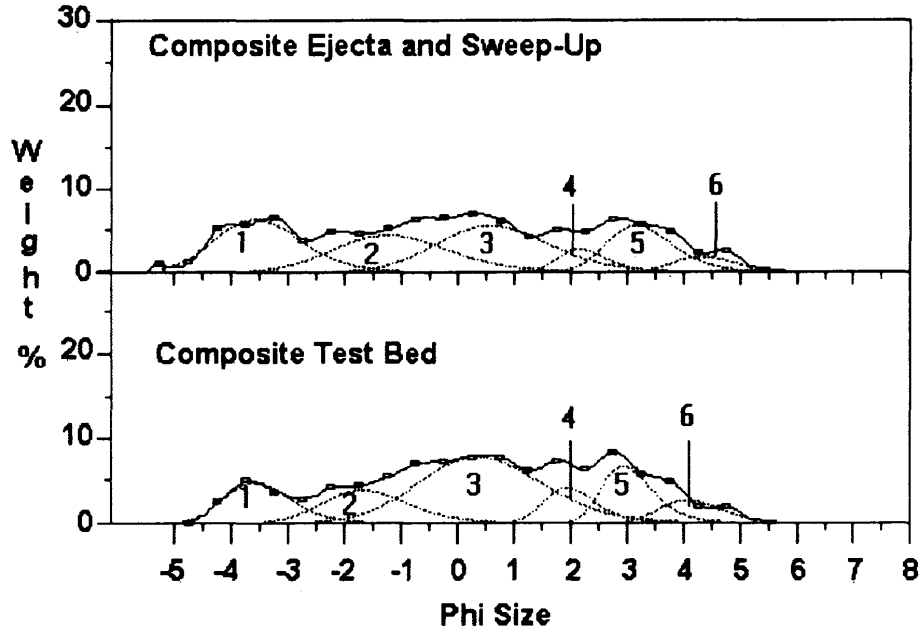

Fig. 42. In this illustration from Wohletz and Raymond (1993), SFT analysis shows that the surge deposits (ejecta and sweep-up) inherit the subpopulations from the source materials (test bed) for the MISERS GOLD cratering experiment (Figs 6.11 - 6.13).

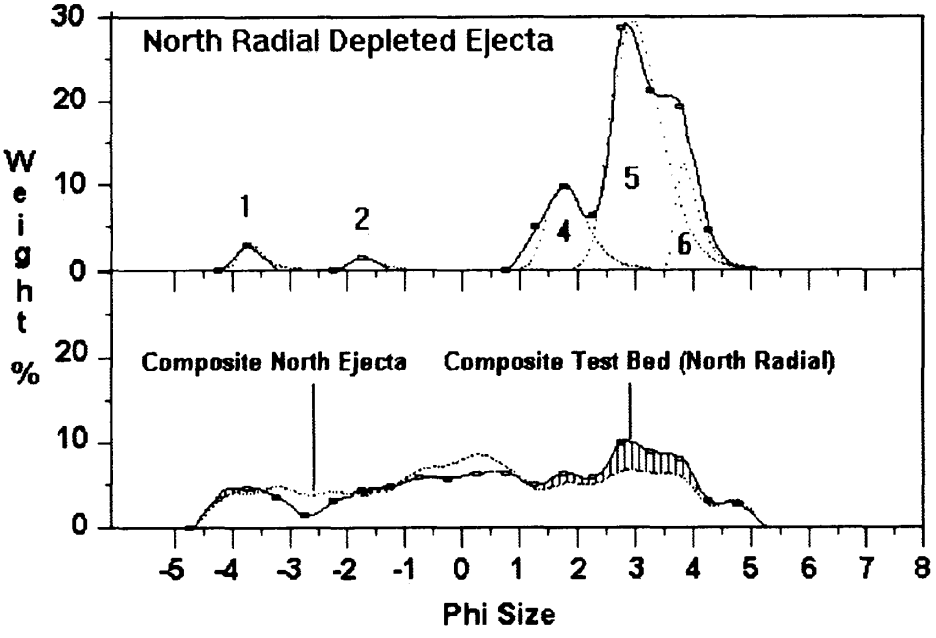

Fig. 43. For the MISERS GOLD experiment comparison of the surge ejecta with the source distribution predicts fines depletion in the surge (depleted ejecta--shaded area). Knowing the volume of the surge ejecta allowed estimation of the volume of fines lofted into the atmosphere, which was verified by atmospheric sampling (Wohletz and Raymond 1993).

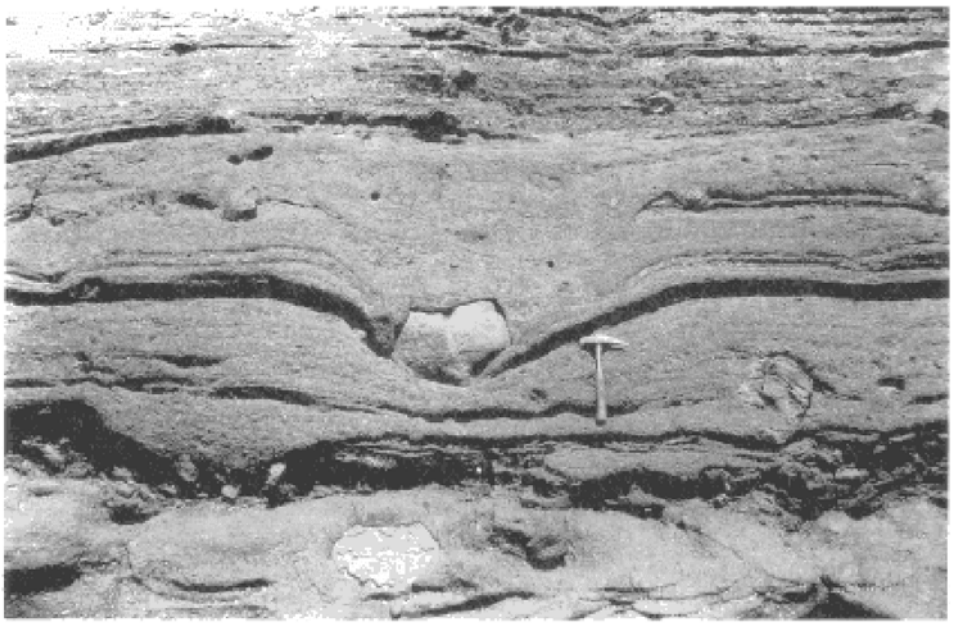

Fig. 44. A typical wet-surge outcrop exposure described by Sohn and Chough (1992) showing irregular and scour-fill deposits and massive bedded deposits. Photograph from Sohn and Chough (1992).

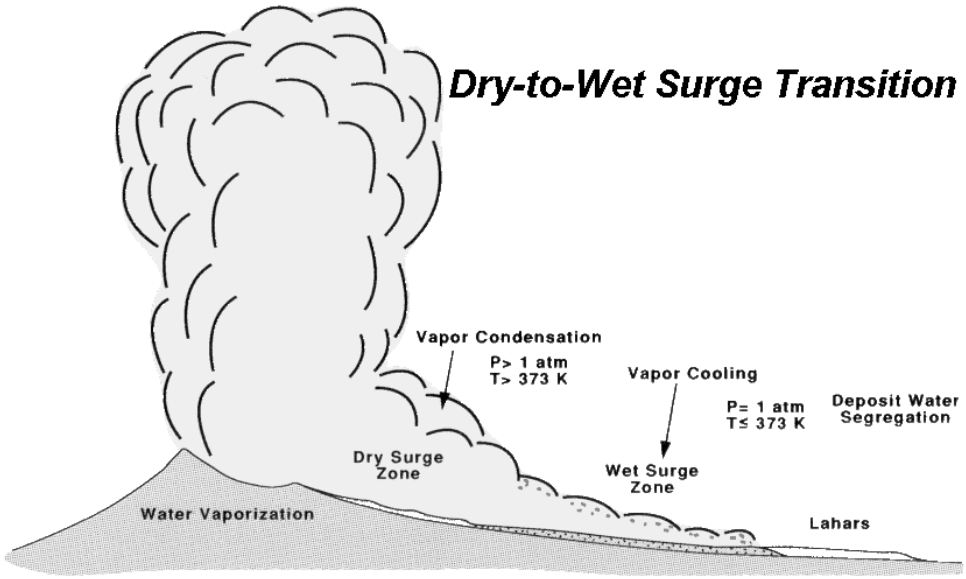

Fig. 45. The vaporization of water during hydrovolcanism leads to generation of superheated steam that upon expanding drives a dry surge. With runout of the lean-phase surge, cooling by adiabatic expansion and mixing with the atmosphere causes condensation of the steam on pyroclasts, forming wet surge deposits. Segregation of the water in wet surges mobilizes the tephra as hyperconcentrated debris flows, forming lahars.

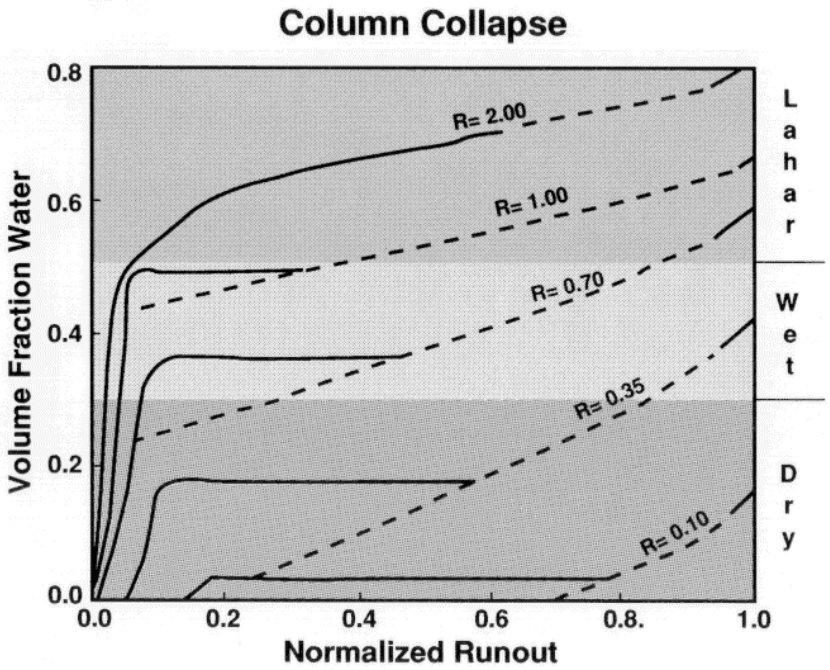

Fig. 46. For a surge generated by column collapse, the volume fraction of water condensed from steam is a function of the initial water/magma mass ratio (shown as R for this plot) and runout distance. Solid lines show the amount of water accumulating in the deposits for simple adiabatic cooling. Dashed lines show maximum deposit water volume fraction where all steam condenses.

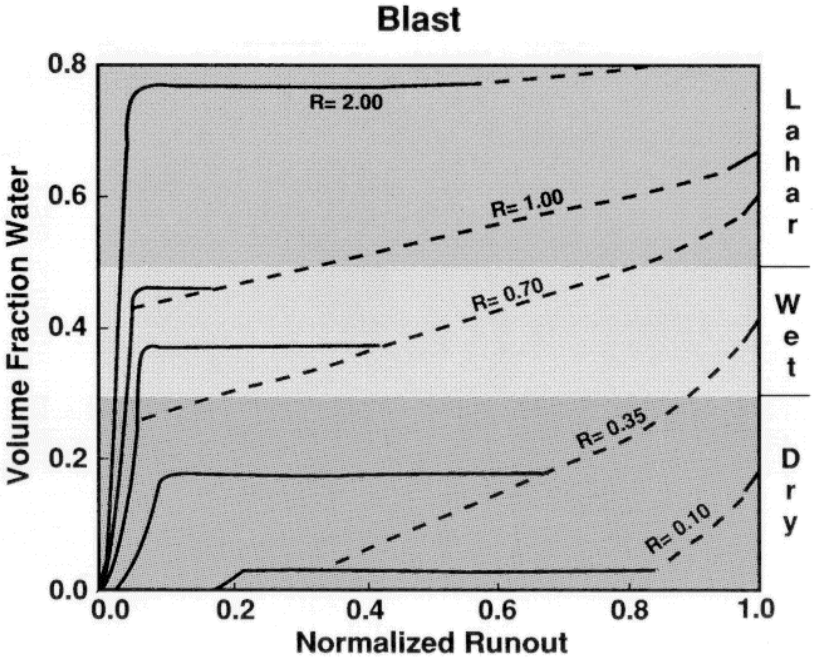

Fig. 47. For blast eruption conditions, runout speeds are lower at low R values (initial water/magma mass ratio) and higher at high R values than those for the column collapse

model, producing slightly different dry and wet facies distributions.

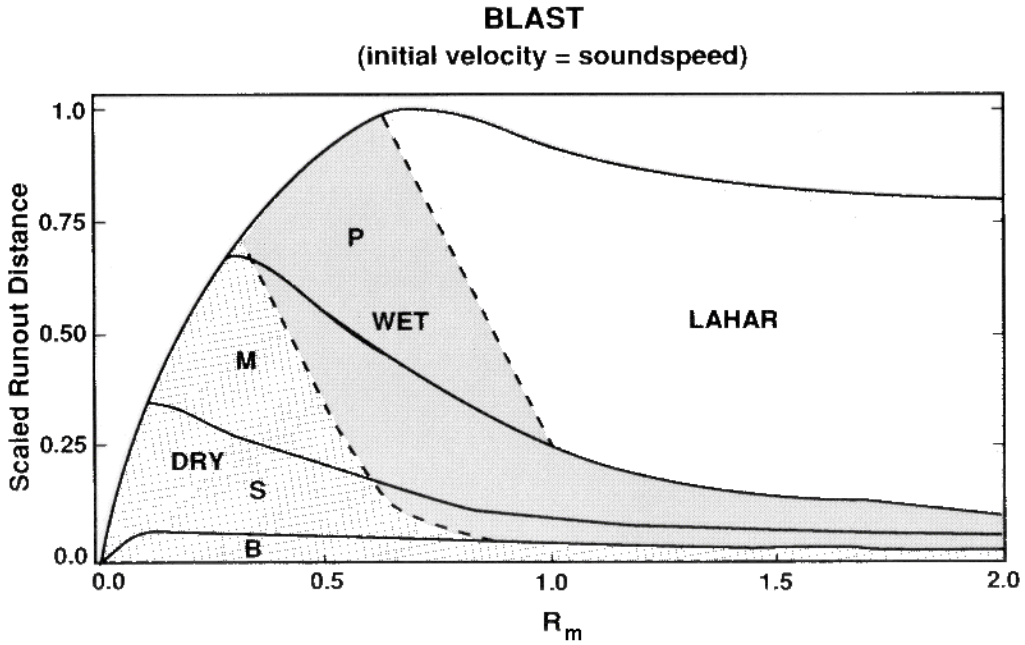

Fig. 48. Based upon the relationship of particle concentrations (a function of R_m) to bedform type (Br = breccia, S = sandwave, M = massive, P = planar), this plot shows surge facies distribution as a function of the eruption water/magma mass ratio R_m for a column collapse eruption.

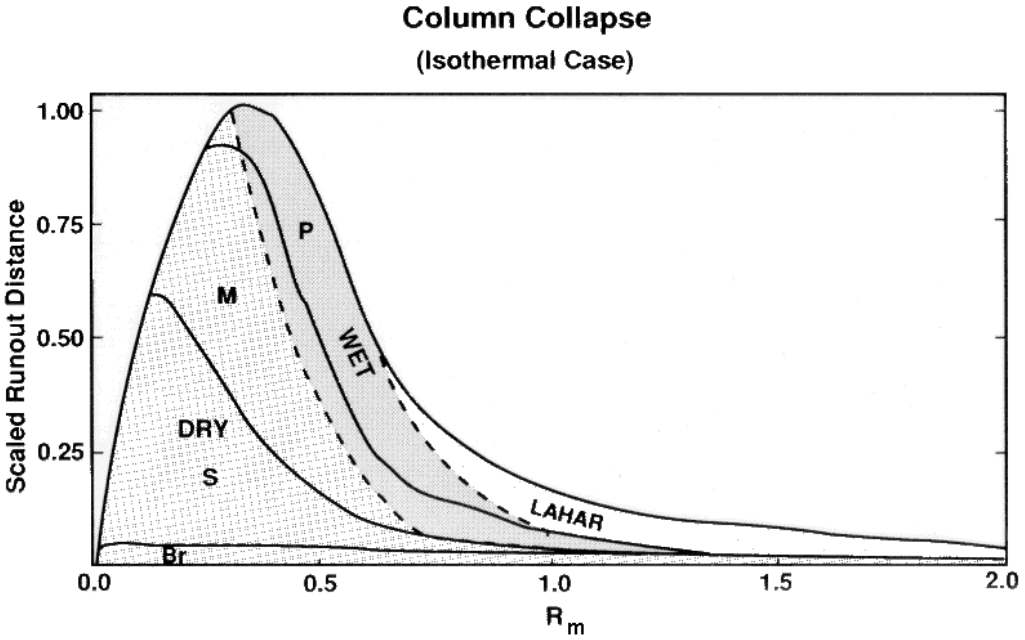

Fig. 49. The blast model produces a much more extensive laharic facies because higher runout speeds at $R_m > 1$ than those of the column collapse model produce deposits of greater runout distance.

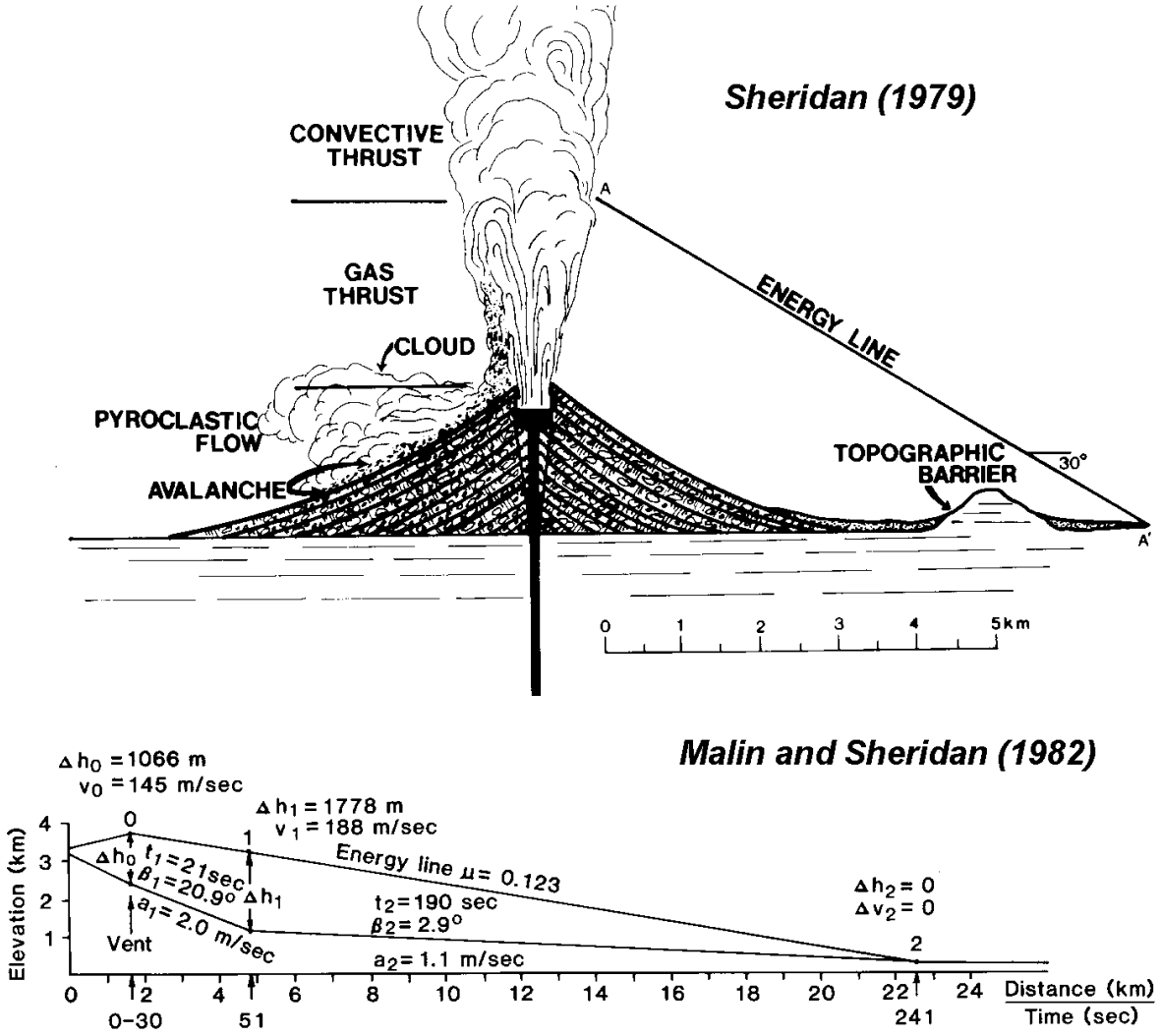

Fig. 50. The energy line concept of Sheridan (1979) is very useful in predicting the path and runout of pyroclastic surges. Malin and Sheridan (1982) demonstrated the energy line for the 1980 Mount St. Helens eruption, where the surge initial velocity (v_0) is determined by the column's collapse height (Δh_0), and its runout velocity (v_1 and v_2) is proportional to the height of the energy line above the topography (Δh_1 and Δh_2), and slope of the energy line expressed as the Heim coefficient (μ), respectively. The acceleration of the surge (a_1 and a_2) changes with time (t_1 and t_2) and is primarily determined by the slope (β_1 and β_2) over which it moves, respectively.

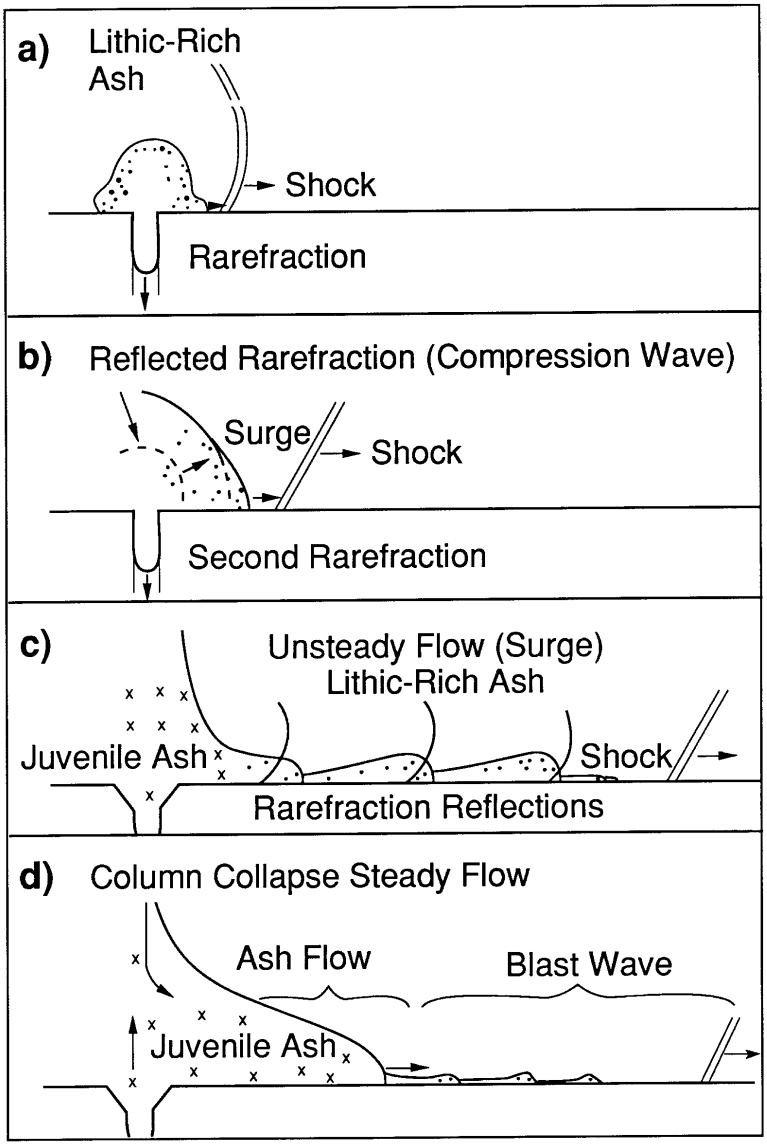

Fig. 51. Development of a laterally moving blast wave from the initial moments of a magmatic eruption where multiple shock waves are propagated by reflection of rarefaction waves within the vent (Wohletz et al., 1984).

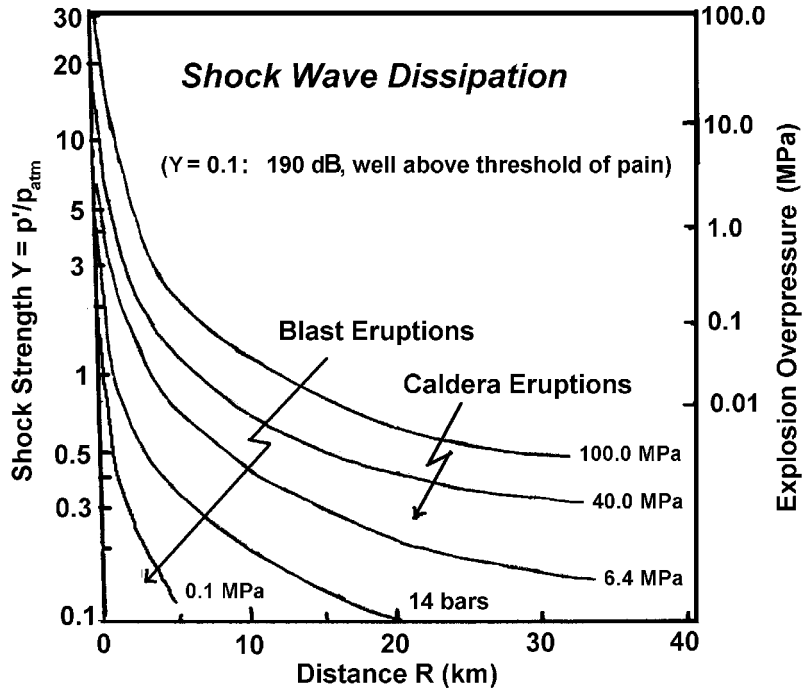

Fig. 52. Shock waves exponentially dissipate with distance from the vent, and for typical blast eruptions giving rise to surges, the shock overpressure decays to less than 0.1 MPa within several km. Still, these modest shock strengths are well above the human threshold of pain, and as they increase to those occurring in large caldera eruptions, they cause heating of the gas to temperatures that can ignite wood.

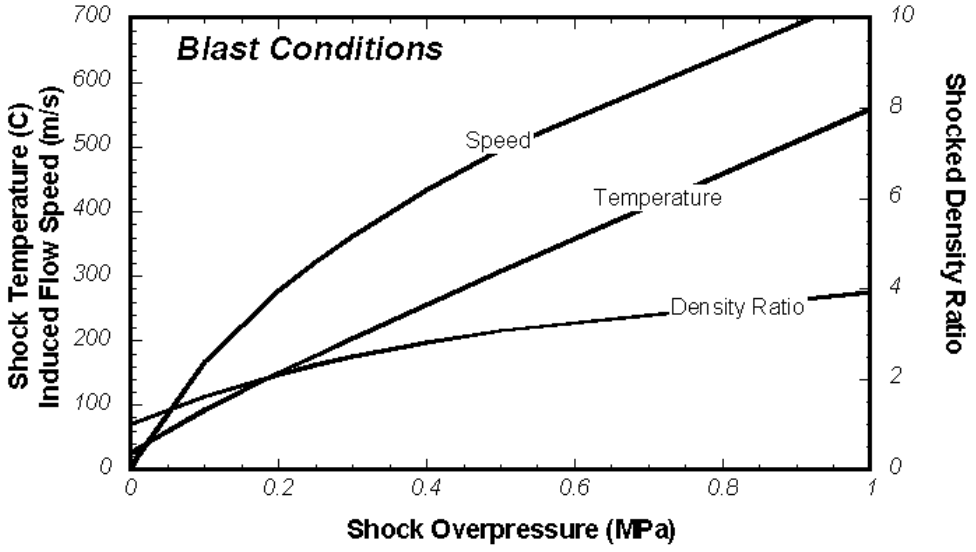

Fig. 53. A blast-generated shock wave (calculated by solutions given for the Rankine-Hugoniot equations) compresses ambient air to higher temperatures and densities as well as inducing transient currents.

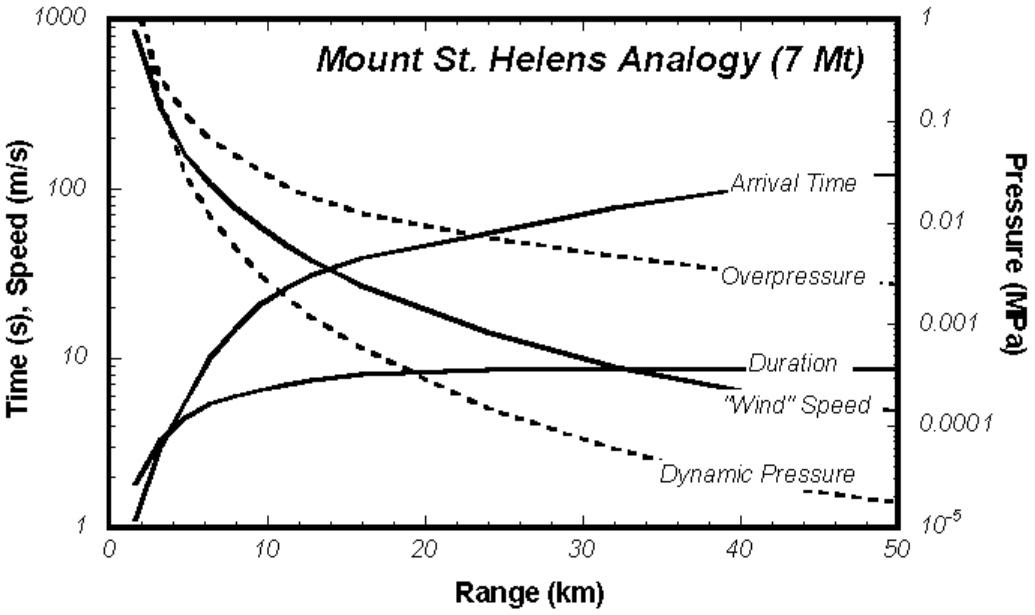

Fig. 54. Radial variation in blast-driven shock-wave properties calculated for a blast with the yield equivalent to 7 Mt, the value calculated by Kieffer (1981) for the 18 May 1980 blast at Mount St. Helens. This model, developed from empirical relationships for a base surge driven by a surface nuclear explosion (Glasstone and Dolan, 1977), shows the decay of blast overpressure, dynamic pressure, and "wind" speed (air currents accelerated by the shock) with distance. The arrival time of the blast and its duration increase with range.

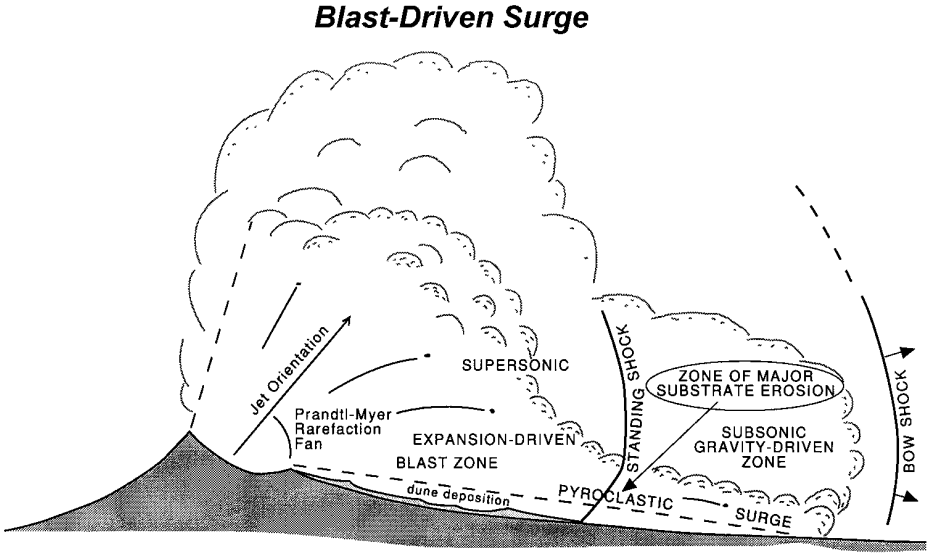

Fig. 55. Illustration of the hypothetical interplay of surge runout and blast wave propagation.

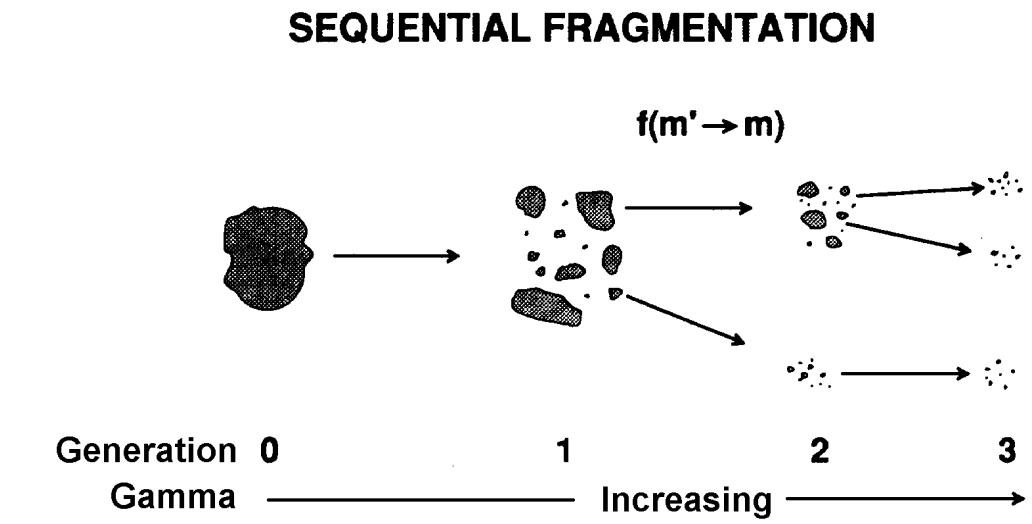

Fig. A-1. Schematic illustration depicting sequential fragmentation where generation 0 denotes the parental mass that fragments by sequential steps into daughter ensembles of smaller particles. With each new step, the daughter ensemble becomes the parental mass for the next step and gamma increases.

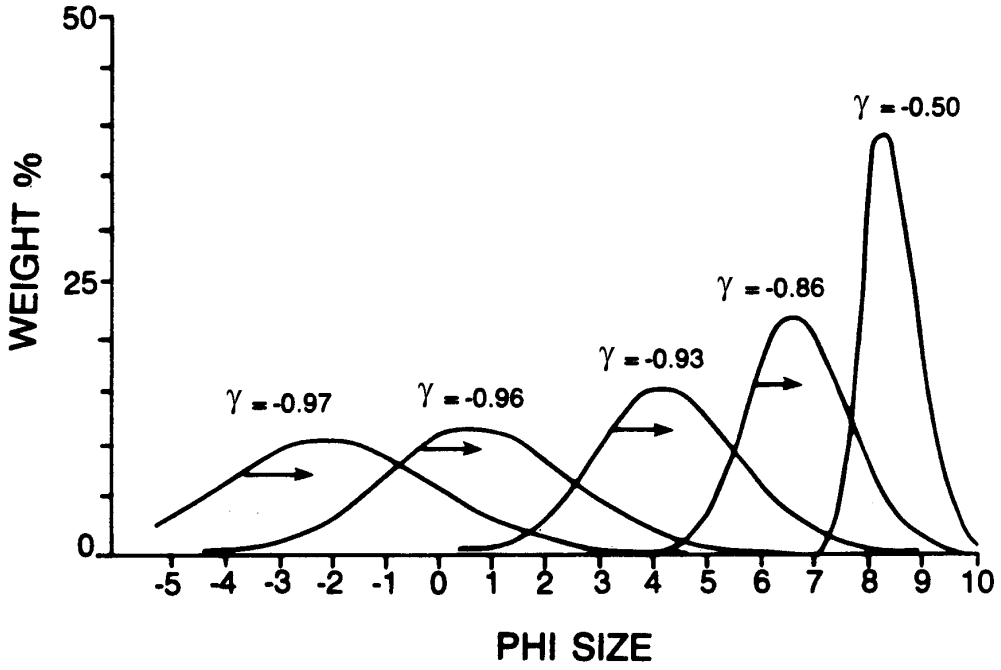

Fig. A-2. An illustration of the effect of the SFT γ parameter. For γ near -1.0 (little fragmentation) the distribution is coarse and broad, but with more developed fragmentation γ increases, making for a finer and narrower (better sorted) distribution (Wohletz et al. 1989).

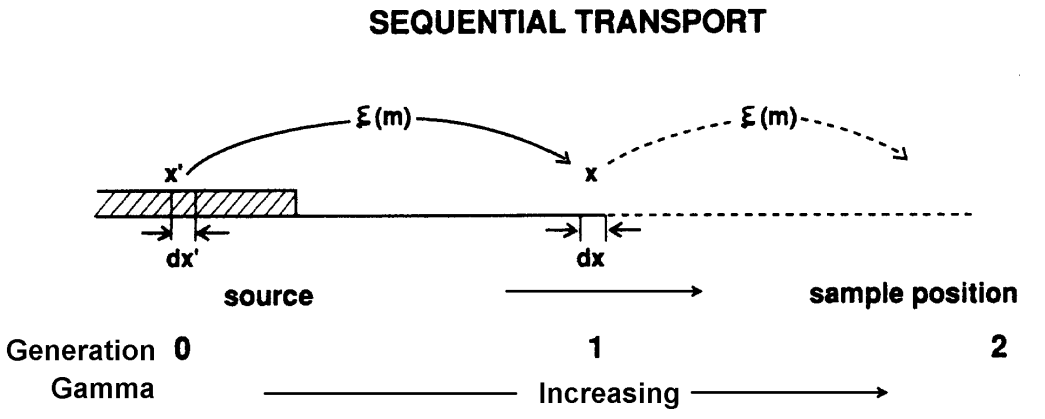

Fig. A-3. Schematic illustration of sequential transport for which generation 0 denotes the parental or source of fragments at location *x'* that are subsequently transported to new locations *x* by a sequence of transportation mechanisms while gamma increases.